MOLECULAR AND FUNCTIONAL IDENTIFICATION OF TWO MUCIN SECRETORY PATHWAYS

A Dissertation

by

ANA MARIA JARAMILLO HERNANDEZ

Submitted to the Office of Graduate and Professional Studies of
Texas A&M University
in partial fulfillment of the requirements for the degree of

DOCTOR OF PHILOSOPHY

Chair of Committee,	Magnus Hook
Co-Chair of Committee,	Burton Dickey
Committee Members,	Michael Tuvim
	James McNew
	David Reiner
	Margie Moczygemba
Head of Program,	Warren Zimmer

December 2018

Major Subject: Medical Sciences

ABSTRACT

In airways, secreted mucins absorb large volumes of water to form viscoelastic mucus, which is then propelled proximally by ciliary beating and swallowed. Mucins are secreted both at a low baseline rate and a high agonist-stimulated rate; baseline secretion is primarily responsible for clearance of inhaled particles and pathogens, while stimulated secretion can induce airway obstruction protectively to trap helminths traversing the lungs or pathologically in asthma.

Exocytosis requires a SNARE complex acting in concert with a Munc18 scaffolding protein. We previously found that Munc18b has the major scaffolding role in stimulated mucin secretion using heterozygous knockout mice. Here, we sought to identify the Munc18 protein mediating baseline secretion, and to test the hypothesis that selective impairment of stimulated secretion can protect against airway mucus obstruction.

Using conditional airway epithelial deletant mice, we found that Munc18a has the major role in baseline mucin secretion, Munc18b has the major role in stimulated mucin secretion, and Munc18c does not function in mucin secretion. In an allergic asthma model, Munc18b deletion reduced airway mucus occlusion and airflow resistance. In a cystic fibrosis model, Munc18b deletion reduced airway mucus occlusion and emphysema. Munc18b deficiency in the airway epithelium did not result in any abnormalities of lung structure, particle clearance, inflammation, or bacterial infection. Our results show that regulated secretion in a polarized epithelial cell may involve more

than one exocytic machine at the apical plasma membrane, and that the protective roles of mucin secretion can be preserved while therapeutically targeting its pathologic roles.

ACKNOWLEDGEMENTS

This work was possible due to the extensive support of mentors, co-workers, friends and family. I am deeply grateful to every individual that has provided mentorship and encouragement throughout these past five years.

First and foremost, I thank my graduate mentor Dr. Burton Dickey for his investment in my training. Dr. Dickey is a remarkable scientist who puts his students before him. He has negotiated for my authorship on collaborations ahead of his own and recommended me for speaking at conferences instead of himself. I am deeply indebted to him for his rigorous training, which has prepared me for a successful scientific career.

I sincerely thank my co-mentor Dr. Michael Tuvim, who played a crucial role in these past years. Through Dr. Tuvim training, my skills have significantly increased through experimental design and how to conduct hypothesis-driven experimental research. He has also guided me through new experimental techniques, troubleshooting, and how to aptly interpret results. Without his unyielding support and guidance, I wouldn't have the confidence to be the independent researcher I am today.

I extend my deep gratitude to the outstanding members of my thesis committee, Drs. Magnus Hook, David Reiner, James McNew, and Margie Moczygemba for their scientific input and scholastic support. I would like to thank Dr. McNew for giving me insightful feedback on my project and for his helpful advice on choosing a postdoc; Dr. Hook for challenging me to thoroughly flesh out my experimental design; Dr. Moczygemba for her knowledge and continuous mentoring; and in particular, Dr. Reiner

for motivating me to genuinely think about my future and providing insights to excel further my career.

I am also grateful to my current and past lab mates, graduate school classmates, and friends who have been key sources of support over the years; the faculty and co-workers in my department for their valuable intellectual input; Javier Navarro, for encouraging and helping me to get out of my comfort zone and start a PhD; Danielle Little, for her amazing help with the editing of this dissertation; Carlus McKenzie and Cindy Lewis for their excellent administrative assistance; the staff of IBT building for their excitement of life and keeping the workplace fun; the animal facility for all their hard work; my family for their support and encouragement; and Marco, thank you for all your love and support.

CONTRIBUTORS AND FUNDING SOURCES

This work was supervised by a dissertation committee consisting of Dr. Burton Dickey and Dr. Michael Tuvim of MD Anderson Cancer Center, Dr. Magnus Hook, Dr. David Reiner, and Dr. Margie Moczygemba of Texas A&M Health Science Center, and Dr. James McNew of Rice University.

The ENaC-18b data in Chapter II was conducted by Dr. Silvia Kreda of University of North Carolina-Chapell Hill. The immunofluorescence in Chapter III was conducted by Dr. Manfred Frick of the University of Ulm. The mucin Western blot in Chapter III was done by Dr. John Dickinson of University of Nebraska.

All other work conducted for the dissertation was completed by the student independently.

This work was supported by grants from the National Institutes of Health (R01 HL129795, and R41 HL136057) and from the Cystic Fibrosis Foundation (DICKEY18G0). Graduate study was supported for the first six months by the IBT graduate program.

TABLE OF CONTENTS

Page

LIST OF FIGURES

Page

CHAPTER I

INTRODUCTION AND LITERATURE REVIEW

1.1 Mucin biology: an overview

1.1.1 Mucin structural organization

1.1.1.1 Secretory cells

The conducting airways of the lung are lined by a pseudostratified columnar epithelium that consists of two principal cell types — ciliated and secretory (Fig. 1.1) (*1*). Both cell types are present in similar numbers, intermixed throughout the epithelium.

Secretory cells are responsible for producing and secreting gel-forming mucins into the airway lumen (Fig. 1.1). They can be further divided into club, goblet, mucous and serous cells based on their appearance under a microscope (*2*). Club and goblet cells are found in the airway surface epithelium while mucous and serous cells are found in submucosal glands. Club, goblet and mucous cells produce and secrete mucins while serous cells do not secrete mucins, but liquid and antimicrobial peptides. Goblet cells show a typical accumulation of intracellular mucin. These intracellular mucins granules can be detected by Periodic Acid/Schiff (PAS) staining, or by its fluorescent version (PAFS) as we will see later in this document. In the PAS or PAFS reaction, mucins are stained when the sugar residues present on the mucin core undergo a periodate oxidation of their hydroxyl groups. The resulting aldehyde groups then react with Schiff's reagent to produce the purple color for PAS or the red fluorescence for PAFS.

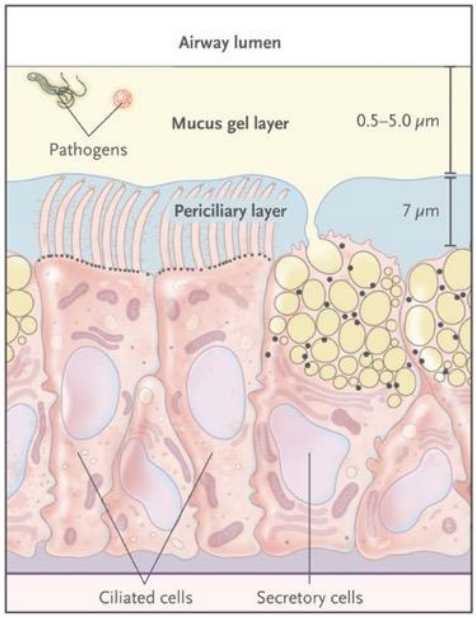

Figure 1.1. Composition of the surface epithelium. Ciliated cells express approximately 200 cilia. Secretory cells show small, black apical granules containing proteins and large yellow granules containing mucins. The mucus layer moves over an immobile periciliary layer that is approximately 7 µm deep. Reprinted from (*2*).

Ciliated cells possess approximately 300 ~7 µm long cilia across the apical cell surface that sweep the mucus layer out of the lungs by beating. Ciliated cells originate from secretory cells and are considered terminally differentiated, as they do not further differentiate or proliferate after epithelial injury (*3*).

1.1.1.2 Mucus composition

Mucus plays an important role in providing an essential barrier that constitutes the first line of defense from inhaled particles and pathogens. These toxicants are trapped in the mucus layer and swept out of the lungs by ciliary action into the pharynx where they are swallowed, constituting a process called mucociliary clearance (*2*). Clearance of recruited leukocytes, dead cells, and endogenous debris is also carried out

by mucociliary clearance. Mucus has physical characteristics on the border between a viscous fluid and a soft elastic solid, which is essential to allow ciliary beating and proper clearance out of the lungs. These characteristics are conferred by a dilute network of polymerized mucins in water. In healthy airway mucus, water accounts for ~98% of the mass, while salts, mucins and non-mucin macromolecules for the other ~2%. The dense glycosylation of secreted mucins gives them the ability to interact with such large volumes of water, which can reach more than 100-fold their mass of water.

The mucus layer sits on top of a dense periciliary layer (Fig. 1.1). Its dense property is a result of the presence of membrane-tethered glyconjugates, including glycosaminoglycans and membrane-anchored mucins that prevent the penetration of the mucus layer but also provide hydration to the periciliary layer through bound water (*4*). The periciliary layer is 7 μm deep and its depth is controlled by the concentrations of ATP, UTP and adenosine. Ciliated cells sense mechanical stress during ventilation and secrete ATP, and secretory cells release uridine conjugates. In response to extracellular concentrations of ATP and uridine conjugates, $P2Y_2$ receptors are activated, which stimulates chloride release and inhibits sodium absorption, resulting in water moving into the airway lumen (*5, 6*). The cystic fibrosis transmembrane conductance regulator (CFTR) also plays a crucial role in fluid homeostasis. Elevation of cAMP leads to protein kinase A mediated phosphorylation of CFTR, opening the channel and allowing for efflux of chloride and bicarbonate (*7*).

1.1.1.3 Mucin glycoproteins

Mucins are extremely large, heavily glycosylated proteins that are the major macromolecular components of mucus. Mucins are encoded by the *MUC* (*MUC* refers to human genes and *Muc* to murine) genes. There are 21 *MUC* genes identified, and their products are mainly classified into two groups, secreted mucins and membrane-associated mucins. Secreted mucins are packaged and secreted into the airway lumen via secretory granules, whereas membrane-bound mucins are anchored into the plasma membrane via a transmembrane domain. Of the 21 mucins, seven are highly expressed in the airway (*8*). Among those seven, two are gel-forming secreted polymeric mucins (*MUC5B, MUC5AC*), four are membrane-associated mucins (*MUC1, MUC4, MUC16, MUC20*), and one is a secreted, non-gel forming mucin (*MUC7*) (*9*).

MUC5B is produced in secretory cells of the surface epithelium and of submucosal glands, while MUC5AC is produced in proximal airways by goblet cells of the surface epithelium. MUC7 is expressed in submucosal glands. MUC4 is expressed on the cilia of ciliated cells. MUC1 is expressed on the cell surface and microvilli of both secretory and ciliated cells. While MUC1 is smaller than MUC4, it has a cytoplasmic tail that can generate a cascade of intracellular signaling that is active in pathogen defense. MUC16, which is the largest mucin, is present in both secretory and ciliated cells and possesses a transmembrane domain that is able to be cleaved to become part of the mobile mucus layer (*4, 10*).

1.1.1.4 Mucin structure

The length of mucin apoproteins ranges from 1000 to over 5000 amino acids (or 300-500 kDa). Muc5b and Muc5ac monomers are around 500 nm long and they form homotypic polymers that reach at lengths up to hundreds of micrometers (*11, 12*). Both mucins contain glycosylated domains rich in proline, threonine, and serine residues (PTS domains), in addition to von Willebrand factor D (vWD)-like domains and cysteine-rich domains (CysD) (Fig. 1.2) (*13*).

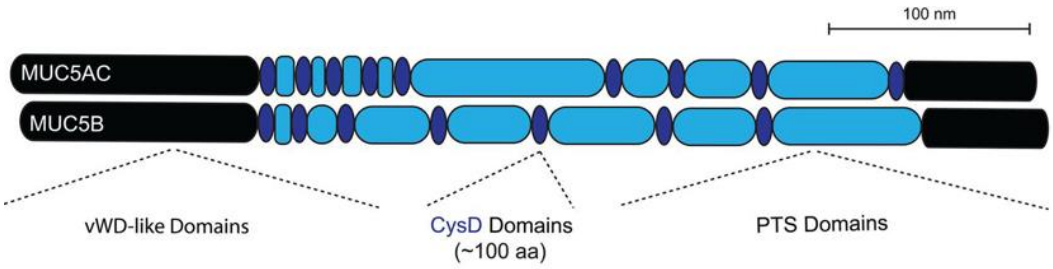

Figure 1.2. MUC5AC/MUC5B structural domains. MUC5AC and MUC5B apoproteins contain PTS domains (light blue ovals) interspersed with CysD (dark blue ovals), capped with vWD-like domains (black ovals). Reprinted from (*14*).

PTS domains are present in all mucins. They are centrally located in the mucin apoprotein, found in tandem repeats, and serve as sites for mucin glycosylation (more specifically, O-glycosylation, see below). Mucins consist of 50-90% carbohydrates — this property allows glycosylation modifications to increase the mass of mucins up to 5-fold (*13*). PTS domains vary in length, from 7 amino acids in Muc19 to 375 in Muc3a, and frequency, from 10 to 500 repeats between different mucins (*15*). The specific sequences of PTS domains vary significantly among homologous mucin genes and

among different species, which provides unique characteristics to each mucin, such as different number of carbohydrate side chains or different crosslinking patterns (*16*).

Mucin polymerization is mediated by vWD-like domains. These cysteine rich domains are located at the N-terminus and C-terminus of secreted mucin proteins that allows for the creation of disulfide bonds and resulting dimerization. Muc5b and Muc5ac form homodimers in the endoplasmic reticulum (ER) via C-terminal-to-C-terminal disulfide bonds (Fig. 1.3). Homodimers are then polymerized in the Golgi via N-terminal-to-N-terminal linkage, resulting in a linear conformation or in a tetrad-like structure (*17*).

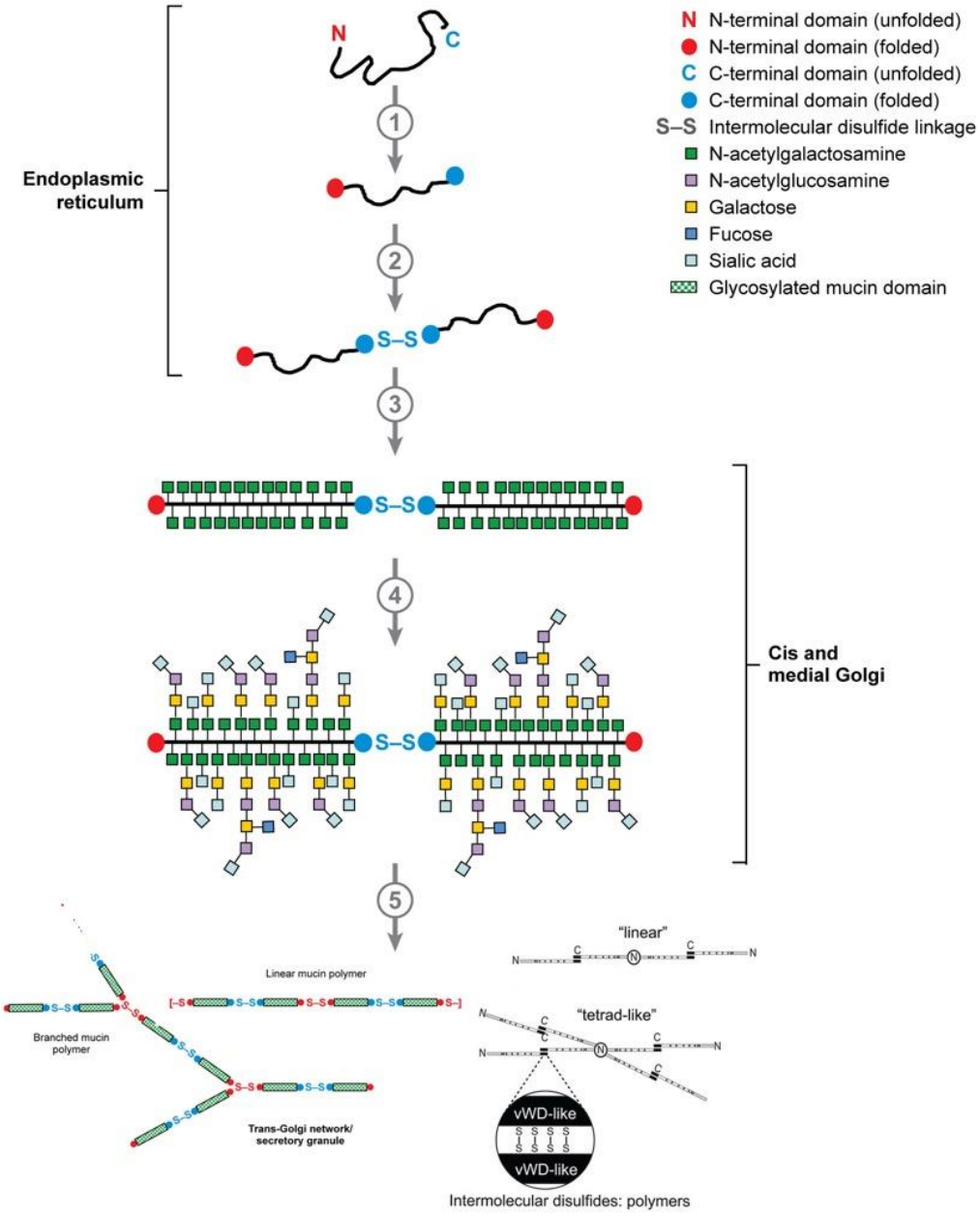

Figure 1.3. Intracellular assembly of polymeric mucins. (1) In the endoplasmic reticulum, mucin protein undergoes intramolecular disulfide bond formation in their N- and C- termini as well as in their internal CysD domains. (2) Disulfide bonds form between C-terminal domains forming homodimers. (3) In the cis Golgi, GalNAc is added to the PTS domains. (4) Further glycosylation occurs as mucins travel through the Golgi. (5) Mucin dimers polymerize through intermolecular disulfide bonds, giving rise to linear or branched structures (left, old model), or linear or tetrad-like structures (right, new model). Adapted from (*13*, *14*).

CysD domains function as additional sites for mucin glycosylation and are located interspersed among PTS domains (*18*). The position of these domains may also confer flexibility, allowing mucin polymerization. A more specific type of glycosylation is attributed to the CysD domains, mannosylation. Muc5b has seven potential mannosylation sites and Muc5ac has nine. Mannosylation may have a role in intracellular trafficking, protein folding and protein localization. It is known that mannosylation is essential for the maturation of Muc5b and Muc5ac since mutations in the mannosylation sites arrest mucins in the ER and prevent their proper folding (*19*).

1.1.1.5 Mucin glycosylation

Mucin O-glycosylation occurs in the Golgi and can be separated into three steps — initiation, elongations and termination. During initiation, N-acetylgalactosamine (GalNAc)-transferase transfers a single GalNAc to the hydroxyl side group of serines and threonines within the PTS domains (Fig. 1.4) (*20*). There are around 20 GalNAc-transferases, and some are only able to function with unglycosylated proteins, while others need a glycosylated protein as substrate. Once the first GalNAc is placed, neutral sugars can be attached constitutively, making up the 4 "core" structures. Core 1 structure is formed by the addition of galactose (Gal) to the GalNAc-O-Ser/Thr. Core 2 structure is formed by the addition of N-acetylglucosamine (GlcNAc) to the core 1 structure. Core 3 structure is formed by the addition of GlcNAc to the GalNAc-O-Ser/Thr, and core 4 structure is formed by the branching of a core 3 structure and the addition of a second GlcNAc to the GalNAc-O-Ser/Thr. After core formation, elongation continues by sequential addition of Gals and GlcNAcs to form long strands in the case of cores 1 and

3, or bi-antennary structures in the case of cores 2 and 4 (*21*). These bi-antennary structures can further branch to become tri- or tetra-antennary. Glycans can also be modified by the addition of fucose, a common glycan in Muc5ac. For the termination step, these glycosylated structures end in Gal or GlcNAc, referred to as the uncapped glycoproteins, or they can be capped by sialic acid or sulfate. The resulting combination of glycans is highly variable; therefore, it is possible for the same mucin protein to have different glycosylation patterns even when expressed in the same tissue. For example, a study found over 100 different O-linked oligosaccharides structures in a single MUC2 protein (*22*). Different glycosylation patterns provide different physical properties to each mucin. For example, sialic acid and sulfates confer negative charges to the strands, which makes glycosylated side chains repel each other and mucin glycoproteins more rigid. These properties end up affecting the viscosity of the mucus layer, as they can regulate the number of water molecules each mucin interacts with (*14*).

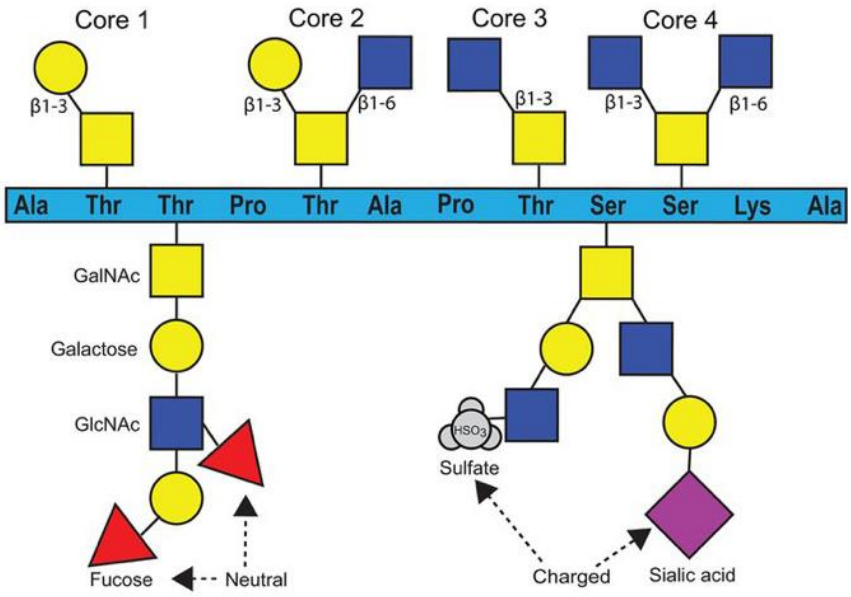

Figure 1.4. PTS domains showing the four core glycosylation structures. GalNAc (yellow squares) is attached to serine or threonine residues in all four core structures. This is followed by galactose (yellow circles) to form core 1, addition of both a galactose and a GlcNAc (blue squares) to form core 2, GlcNAc to form core 3, or addition of two GlcNAc to form core 4. These cores can be further elongated by the addition of extra sugars such as fucose (red triangles) to form long strands or bi-antennary structures, or capped by SO_4 (gray circles) or sialic acid (purple diamonds). Reprinted from (*14*).

1.1.2 Mucin production and function

1.1.2.1 Muc5b

Muc5b is the predominant polymeric mucin in airway mucus in healthy conditions. It is produced both by the surface epithelium and submucosal glands (*2*). By immunohistochemistry, Muc5b is visible throughout the surface epithelium from the trachea distally to (but not including) terminal bronchioles (*23*). With exposure to inflammatory stimuli, such as IL-1β, mucin production can go up several fold. The transcriptional mechanisms that regulate *MUC5B/Muc5b* expression are not yet well

understood. Some studies have shown that the transcription factor Nkx2.1 inhibits *Muc5b* gene expression (*24*), while other studies have shown that GATA6 may activate *Muc5b* expression (*25*).

Deletion of the major constitutively-expressed airway mucin, Muc5b, results in a severe defect in mucociliary clearance of particles and pathogens in mice, and in 50% mortality by 6 months of age (*26*). Partial reductions in Muc5b result in corresponding reductions in particle clearance and may be a factor in the increased susceptibility to lung infection with ageing (*27*). Protection against lung infection is likely to have driven selection of an allele of the MUC5B enhancer in Caucasians that results in ~20-fold overexpression in the airways (*28*). The 12% allele frequency in Caucasians is similar to the 15% frequency of the sickle hemoglobin allele in areas of hyperendemic malaria, consistent with strong positive selection (*29*). However, constitutive overexpression of MUC5B comes at a price because it is a major risk factor for development of interstitial lung disease late in life. This is possibly due to epithelial progenitor cell depletion from the proteostasis stress of producing large amounts of mucin (*30*).

1.1.2.2 Muc5ac

In healthy humans but not in mice, MUC5AC is produced constitutively in proximal airway epithelial cells. In the distal airways of humans and all of the airways of mice, which resemble human distal airways, almost no Muc5ac is detectable (*2*). Upon inflammatory stimuli, such as IL-13, Muc5ac expression in surface epithelial cells goes up 40-fold (*31*). Since Muc5ac is present in many mucoobstructive diseases such as asthma, cystic fibrosis and chronic obstructive pulmonary disease, the underlying

transcriptional mechanisms leading to its expression better understood. Epidermal growth factor receptor (EGFR) signaling have been shown to activate *Muc5ac* expression (*32*, *33*), while forkhead box a2 (FOXA2) suppresses *Muc5ac* expression (*34*). IL-13 is a potent inflammatory cytokine that drives *Muc5ac* expression in pathologies with type 2 inflammation, such as asthma and allergy. Both IL-13 and EGFR induce *Muc5ac* expression via hypoxia inducible factor-1 (HIF-1) binding at the mucin's promoter. Furthermore, IL-13 induces SAM-pointed domain-containing ETS transcription factor (SPDEF) that in turn inhibits FOXA2, leading to up-regulation of Muc5ac expression (*35*).

Muc2 is constitutively expressed in the gut, but induced Muc5ac expression contributes importantly to helminth defense in the gut (*36*) and there is now evidence that it may help trap helminths migrating through the lungs. It is possible this pathogen defense mechanism goes awry in allergic asthma, where inhaled substances such as pollens, chitin in insect exoskeletons and fungi, and allergenic proteases falsely signal the presence of helminths, resulting in the release of IL-13 from leukocytes (*37*). Thus, an adaptive mechanism that probably evolved to selectively close a limited number of airways to protect against helminth migration becomes maladaptive when multiple airways close simultaneously in response to inhaled stimuli. Deletion of Muc5ac abolishes airway hyperresponsiveness and reduces airway mucus plugging in an allergic mouse model, with no impact in mucociliary clearance (*38*). This suggests that deleting Muc5ac could bring relief to mucoobstructive diseases without the detrimental effects of failing to clear particles and toxicants.

1.2 Mucin exocytosis

1.2.1 Baseline and stimulated secretion

1.2.1.1 Baseline secretion

Mucin is secreted in the airways at a slow baseline rate and at a high stimulated rate. In surface epithelial cells of all intrapulmonary airways of mice and the distal bronchi and bronchioles of humans, the rate of baseline mucin secretion matches the rate of synthesis in naïve (uninflamed) airways such that there is only minimal intracellular mucin (Fig. 1.5, left column) (*31*). This low level of mucin is difficult to detect, with only highly sensitive immunohistochemical stains detecting the mentioned intracellular Muc5b throughout the surface epithelium from distal trachea to terminal bronchioles (*23*). With exposure to inflammatory stimuli, mucin production in surface epithelial cells can increase 10 to 100-fold but the rate of secretion is not increased, resulting in the accumulation of mucins intracellularly (Fig. 1.5, middle column).

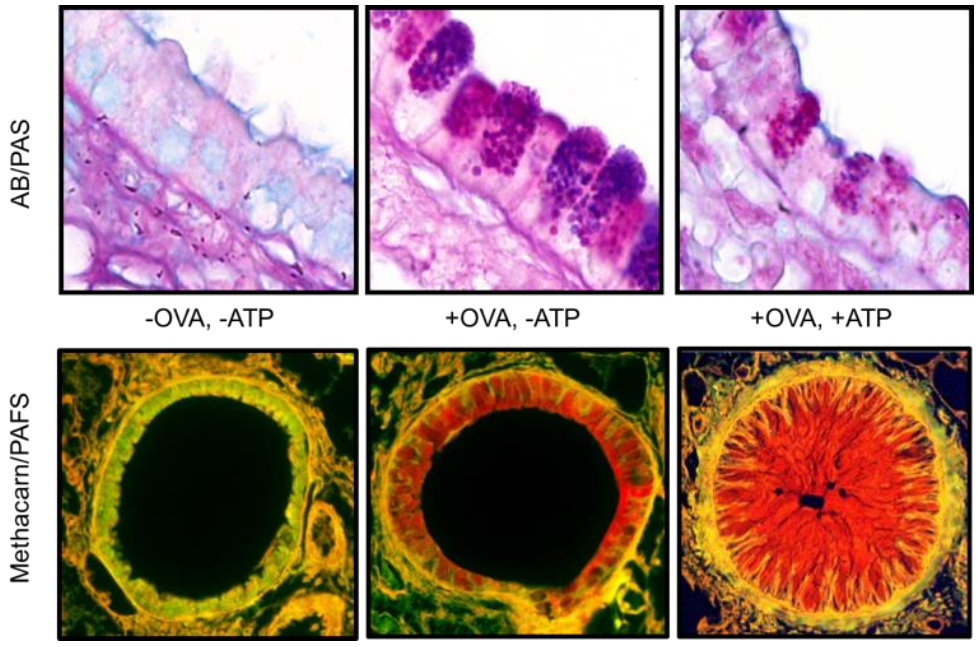

Figure 1.5. Mucins are secreted both at a low baseline rate and a high agonist-stimulated rate. The baseline rate of mucin production matches the rate of secretion so that intracellular mucin is not visible by histochemical staining (first column). During mucous metaplasia, the rate of production exceeds the rate of the baseline secretion such that histochemically visible mucin accumulates (second column). The rate of secretion can be stimulated by agonists, resulting in the rapid release of stored mucins (third column).

1.2.1.2 Stimulated secretion

Upon stimulation by high levels of extracellular agonists such as ATP, acetylcholine, or histamine, the rate of airway mucin secretion can be increased thousands-fold, resulting in intracellular mucin being released into the airway lumen (Fig. 1.5, right column). Davis and colleagues measured this effect using high-speed video microscopy in canine airways, finding a 1,760-fold increase in rate of mucin secretion after the addition of ATP to the perfusate (*39*). Similar observations were made using the epithelium of normal and cystic fibrosis subjects (*40*). Individual mucin

granules have been observed to release their contents in ~1/10 second, and the released mucins absorb several hundred-fold their mass of water to generate mucus in ~1 second (*41*), so the transition from intracellular mucin to extracellular mucus is very rapid after stimulation. While the initial burst of stimulated secretion exceeds the baseline rate by almost 2,000-fold, it lasts only ~10 seconds. During this initial phase, ~1/2 of the total granules that are ultimately released in response to high levels of ATP from naïve canine airways are released. The remaining granules are released during a ~2-minute plateau phase that is ~38-fold higher than baseline rate. In other words, the stimulation of secretion in an inflamed airway that has large amounts of intracellular mucin stored leads to the rapid release and swelling of mucin. This rapid release and expansion of mucins in inflamed airways leads to occlusion of airways in diseases such as asthma, cystic fibrosis and chronic obstructive pulmonary disease (Fig. 1.5, right column).

1.2.2 Steps of exocytosis

1.2.2.1 Trafficking

All cells have a constitutive secretory pathway, and some specialized cells have a regulated one. The constitutive secretory pathway functions continuously and is necessary for cell viability. The regulated secretory pathway is only found in specialized secretory cells.

Secretory granules need to be transported from the Golgi along actin filaments or microtubules to the apical surface where they are tethered to the membrane to be exocytosed. Rab GTPases regulate these functions. They belong to the small monomeric

Ras-like GTPase superfamily, and are the largest family with over 60 members identified in mammals and 11 in yeast (*42*). Rabs associate with each secretory granule in order to regulate formation, transport, tethering, docking and fusion with the plasma membrane, and do it by recruiting specific effectors along the vesicle trafficking pathway. Rab8, -10 and -14 regulate vesicle trafficking from the trans-Golgi network to the plasma membrane for the constitutive secretory pathway, while Rab3 and -27 are present in the regulated secretory pathway.

Rab effectors vary greatly and one Rab can have the ability to bind several different effectors. Two microtubule-based motor effectors are kinesin and dynein that help transport vesicles towards the plus-end or the minus-end of microtubules (*43*). Other effectors can be tethering proteins that will be explained below, but briefly, they help draw the vesicle towards a target membrane. Rabs can change the identity of an organelle, for example, a Rab5 containing vesicle belongs to the early endosome compartment, while a Rab7 containing vesicle is a late endosome organelle, and the exchange of Rab5 for Rab7 promotes the change of organelle identity. The way Rab proteins are sequentially recruited and interchanged is a well studied process called the Rab cascade.

1.2.2.2 Tethering

Tethering factors for secretory granules can be divided into two main groups, homodimeric long coiled-coil proteins and multisubunit tethering complexes (MTC). Coiled-coil tethers are large homodimers that can interact with vesicles 200 nm apart. MTCs are composed of three to ten subunits and can only reach vesicles up to 30 nm

apart (*44*). It is thought that coiled-coil tethers function in the initial steps of tethering because of their ability to form transient, low-affinity interactions, while the MTCs may function at a later stage and interact with the soluble N-ethylmaleimide-sensitive factor attachment protein receptor (SNARE) machinery, the set of proteins necessary for vesicle fusion, because of their ability to bind with different components at the same time due to their different subunits (*45*).

1.2.2.3 Docking

Docking is generally defined as a stage in which vesicles are located at a minimal distance from the plasma membrane. While its mechanism is not fully understood, it is thought that the SM (Sec1/Munc18) protein Munc18a is involved, as deletion of Munc18a results in a reduced number of docked dense core vesicles in chromaffin cells (*46*). Studies using heterozygous mice and overexpression of the protein confirmed these findings. Rab proteins have also been suggested as participating in the docking process as mutations in their GTP binding site result in accumulation of vesicles in the cytoplasm (*47*).

1.2.2.4 Priming

Once the vesicle is docked to the plasma membrane, the SNARE proteins start partially pairing in preparation for fusion. This process is well studied in neurons where upon stimulation, the speed of neurotransmitter release was too fast for the multistep SNARE fusion process to occur. For regulated exocytosis, regulatory proteins such as complexin and synaptotagmin appear to hold in place the partially paired SNARE

complex, until intracellular signaling releases this clamp effect and fusion can occur (*48*).

1.2.2.5 Fusion

Fusion takes place once the lipid membranes are in close proximity to each other and the SNARE proteins are fully coiled; providing the energy necessary for the lipid membranes to fuse. This results in the intracellular vesicle membrane fusing with the plasma membrane and releasing its content into the extracellular space (*48*).

1.2.3 Exocytic machinery

1.2.3.1 SNAREs

SNARE proteins are required for all steps of intracellular vesicular traffic on the endocytic and exocytic pathway. They each share a ~65 residue SNARE motif capable of assembling with three other SNARE motifs to form a parallel four-helical complex (*49*). The assembly of SNAREs that are located on apposing membranes, forming a trans SNARE complex allows membrane fusion.

SNARE proteins are divided into two main groups, depending on whether they have an arginine (R-SNARE) or a glutamine (Q-SNARE) at the midpoint of their conserved polar layer, also referred to as the zero layer. These polar interactions at the center of the hydrophobic SNARE motif ensure that the four helix bundle is correctly assembled. SNAREs were originally classified as v-SNAREs and t-SNARES, based on whether they were localized to either the vesicle (v) or target membrane (t), but this classification becomes ambiguous for many fusion reactions. VAMPs (vesicle associated

membrane proteins) belong to the family of R-SNAREs/v-SNAREs and, as their name states, they are located on the vesicle membrane. They contribute to the four helix bundle with one SNARE domain. The Syntaxin and SNAP-23 families comprise the Q-SNAREs/t-SNAREs that are located on the plasma membrane and contribute with one and two SNARE helices, respectively, completing the four helix bundle. The authors of early in vitro studies suggested that the SNARE proteins constitute the minimal membrane fusion machinery. However, these studies did not demonstrate full content mixing at a physiological speed, which is indicative of a complete exocytic event along with full lipid mixing (*50-52*).

1.2.3.2 SM proteins

SM proteins are necessary for all types of intracellular vesicular traffic that requires SNARE proteins. This evolutionary conserved family of proteins, with sizes around 60-70 kDa, drive membrane fusion by interacting with their cognate SNARE partners. There are seven isoforms present in mammals (Munc18a, Munc18b, Munc18c, Vps33a, Vps33b, Vps45 and Sly1) and four in yeast (Sec1, Vps33, Vps45 and Sly1). Munc18a, b, and c are the three mammalian isoforms to have been shown to have a role in secretion. Munc18a is expressed in neurons, endothelial cells and endocrine pancreas; Munc18b is expressed apically in secretory epithelia and immune cells; and Munc18c is ubiquitously expressed. Besides driving vesicle fusion, SM proteins are also responsible for chaperoning their cognate Syntaxin to the plasma membrane. In fact, the first report of a mammalian SM protein was of Munc18a bound to Syntaxin-1 (Fig. 1.6) (*53*). Each Munc18 protein has higher affinities for specific Syntaxin proteins. These high affinity

interactions with Syntaxins allow SM proteins to negatively regulate vesicle fusion as they hold their cognate Syntaxin in a closed conformation and prevent further binding to the other SNARE proteins prior to priming (*54*).

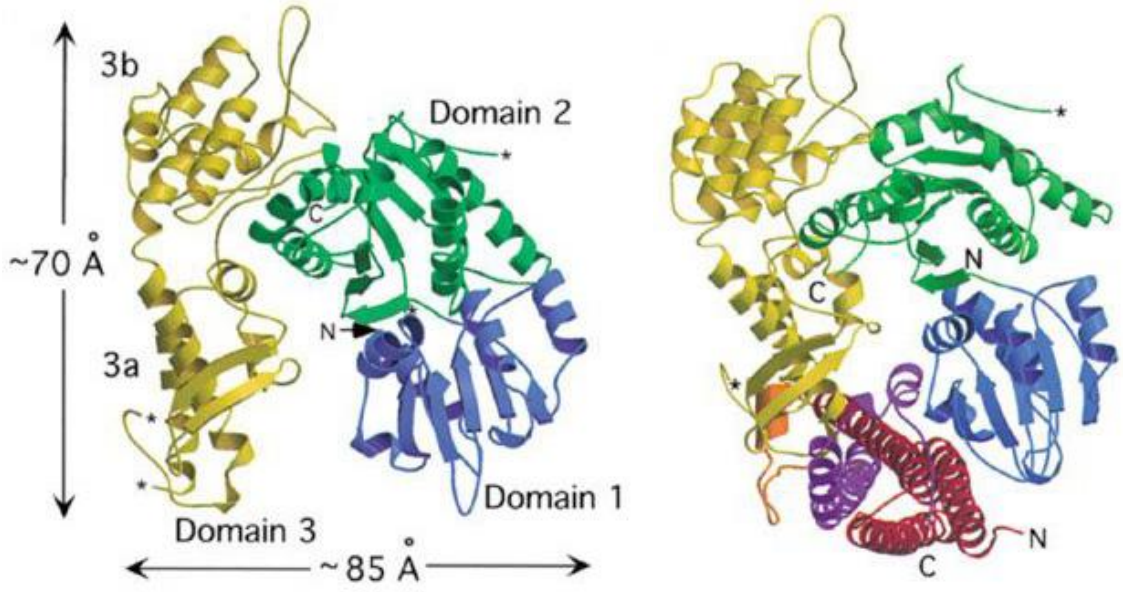

Figure 1.6. Structure of Munc18a. Left: Structure of Munc18a. Domain 1 is shown in blue, domain 2 in green and domain 3 in yellow. Asterisks indicate breaks in the structure. Right: Structure of Munc18a-Syntaxin1a complex. Syntaxin1a SNARE domain is shown in purple, Habc domain is shown in red. Reprinted from (*55*).

Crystal structure analysis revealed that SM proteins contain three domains that form an arch shape with a central cavity. Domains 1 and 2 form one arm of the arch while the third domain, divided into domains 3a and 3b, completes the other arm (Fig.

1.6) (*55*). Domains 1 and 3a provide a binding site for Syntaxin. A recent study generating x-ray structures of the yeast SM protein, Vps33, found that SM proteins can also bind the trans-SNARE partner, VAMP, through a groove in domain 3a (Fig. 1.7). This means that SM proteins not only function prior to priming and at the last step of SNARE complex formation, but rather that SM proteins guide the whole process (*56*).

The importance of the SM proteins has been recognized in different organisms. Unc-18 was the first SM protein to be identified through a genetic screen in *C. elegans*. Deletion of this protein resulted in a paralyzed phenotype due to severe locomotor defects (Uncoordinated) (*57*). Sec1, the yeast orthologue, was later identified through genetic screening for temperature sensitive secretion-defective mutants. Deletion of Sec1 at the non-permissive temperature resulted in accumulation of intracellular vesicles, visible by electron microscopy, indicating a defect in secretion (*58*). Similarly, mutation of the SM orthologue Rop in *Drosophila melanogaster* results in a secretion defect (*59*). In mammals, deletion of Munc18-1 in mice completely abolished neurotransmitter release (*60*). Together with the SNARE complex, SM proteins constitute the core exocytic machinery.

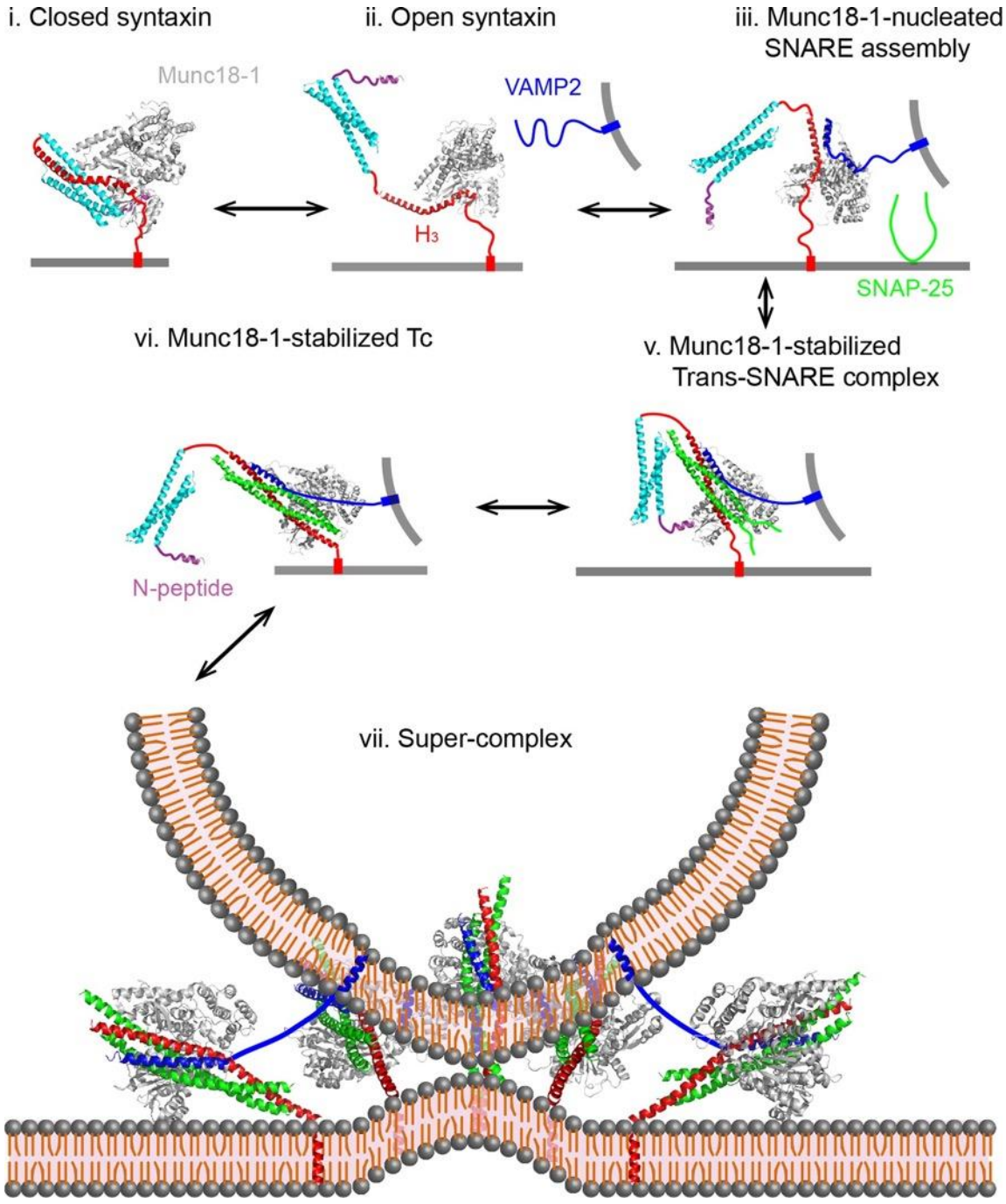

Figure 1.7. Working model of exocytosis. The neuronal exocytic machinery is depicted here. Munc18, with the help of Munc13 (not shown), undergoes a conformation transition to open Syntaxin (from states i to ii). VAMP, the v-SNARE, binds Munc18 (state iii), and the remainder t-SNARE from the SNAP-25 family joins to form the four helix bundle (state v). Full zippering of the SNARE complex leads to membrane fusion (states vi and vii). Reprinted from (*61*).

1.2.3.3 Regulatory proteins

Besides the core exocytic machinery, there are regulatory proteins that function at different steps of exocytosis. The Munc13 family is comprised of five proteins that contain a MUN, C1 and C2 domains. The MUN domain aids the transition of Syntaxin from a closed conformation to an open conformation and also promotes the assembly of the SNARE complex (*62*). C2 domains bind calcium, phospholipids, and other proteins that help in priming, for example. C1 domains bind diacylglycerol and are present in all Munc13 proteins except Munc13-4.

Synaptotagmins constitute a family of sixteen proteins that function as calcium sensors. They contain an N-terminal transmembrane domain, a variable linker, and two cytoplasmic C2 domains termed C2A and C2B. The C2 domains are responsible for binding calcium and curved membranes, which facilitates vesicles and plasma membrane interactions (*62*).

1.2.4 Exocytic machinery in mucin secretion

1.2.4.1 SNAREs

The exocytic machinery responsible for mucin secretion in the airway epithelium has not been well defined. The v-SNARE residing in the mucin secretory granule has been identified by a group at the University of North Carolina-Chapel Hill as VAMP8 (Fig. 1.8) (*63*). We should remember at this point that there are two rates of mucin secretion, a slow baseline continuous rate and a high stimulated one. It appears that VAMP8 only carries a role in stimulated mucin secretion, but not in baseline secretion.

The other SNAREs, the t-SNAREs are still being investigated. Our laboratory identified SNAP23 as being one of the t-SNAREs containing two SNARE helices and participating in both baseline and stimulated mucin secretion (*64*). The remaining t-SNARE belongs to the Syntaxin family and has not been yet identified.

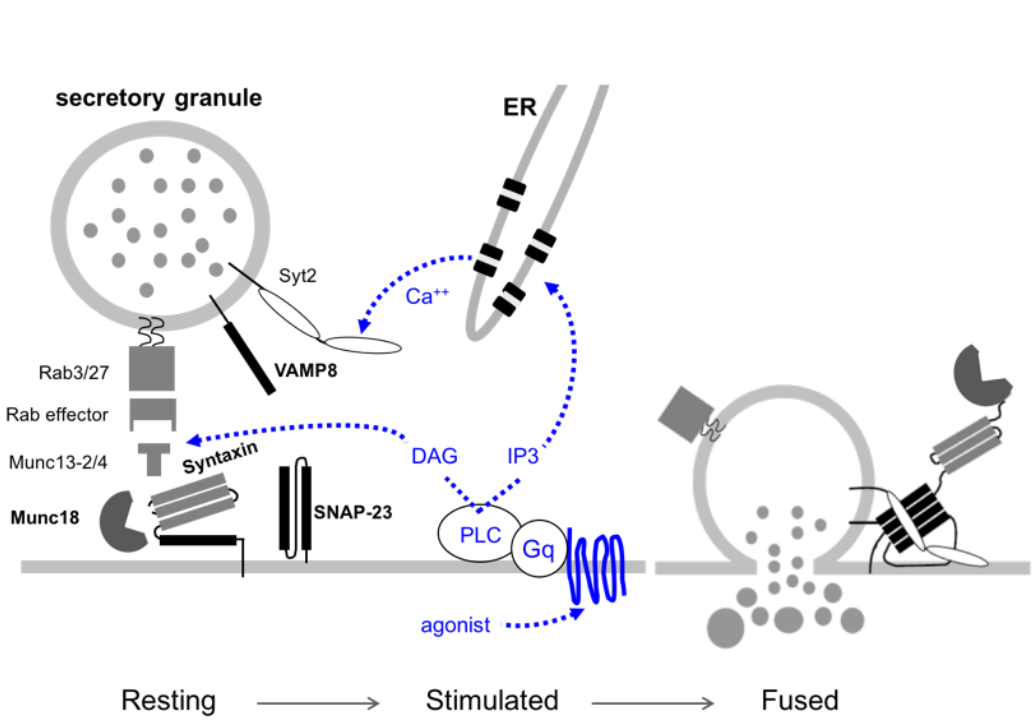

Figure 1.8. The Secretory Machinery. The SNARE complex is a four helix bundle, shown in black, with one helix present on the granule (VAMP), and three present on the plasma membrane (SNAP23 and Syntaxin). Munc18 serves as a scaffold for SNARE complex assembly. Some components are conserved between baseline and stimulated mucin secretion (SNAP23) while others participate only in one (Synaptotagmin 2 in stimulated mucin secretion). Other proteins are regulatory (Rab, Munc13). The blue component illustrates the signal transduction pathway that activates secretion.

1.2.4.2 SM proteins

The determination of the SM proteins responsible for mucin secretion in the airway epithelium constituted the core of my research in the past years and will be

described thoroughly in Chapter II. Briefly, our lab identified Munc18b as being largely responsible for stimulated mucin secretion using a heterozygous mutant mouse (*65*). Munc18a was later identified by me as the principal mediator of baseline mucin secretion using a conditional deletant mouse (Chapter II).

1.2.4.3 Regulatory proteins

One of the first proteins that was identified in the mucin secretory field was the priming protein Munc13-2. Munc13-2 knock-out (KO) mice revealed a severe but partial defect in both baseline and stimulated mucin secretion (*23*). The use of a double Munc13-2/Munc13-4 KO mouse showed a greater defect in baseline mucin secretion and an almost complete defect in stimulated mucin secretion. This suggests that both Munc13 proteins have a role in both rates of mucin secretion, with Munc13-2 having a predominant one in both rates (unpublished data, Dickey laboratory).

The calcium sensor that mediates stimulated mucin secretion in the airway epithelium is Synaptotagmin 2 (Syt2), a fast, low affinity calcium sensor (*66*). Syt2 has no apparent role in baseline mucin secretion, and KO mice showed a complete defect in stimulated secretion. The calcium sensor mediating baseline mucin secretion is still unknown. Other sensors such as Syt7 and Doc2b have been tested but have yielded negative results (unpublished data).

1.3 Mucus dysfunction in disease

1.3.1 Allergic asthma

1.3.1.1 Cell biology of asthma

Asthma is a complex disease affecting approximately 300 million people worldwide. It is mainly characterized by a type 2 (T2) immunological response. Airway type 2 responses are mediated by eosinophils, mast cells, basophils, Th2 cells, innate lymphoid cells 2 (ILC2s) and IgE-producing B cells (*67*). The three hallmarks of allergic asthma are eosinophilic inflammation, airway hyperresponsiveness (AHR) and airway epithelial mucous metaplasia.

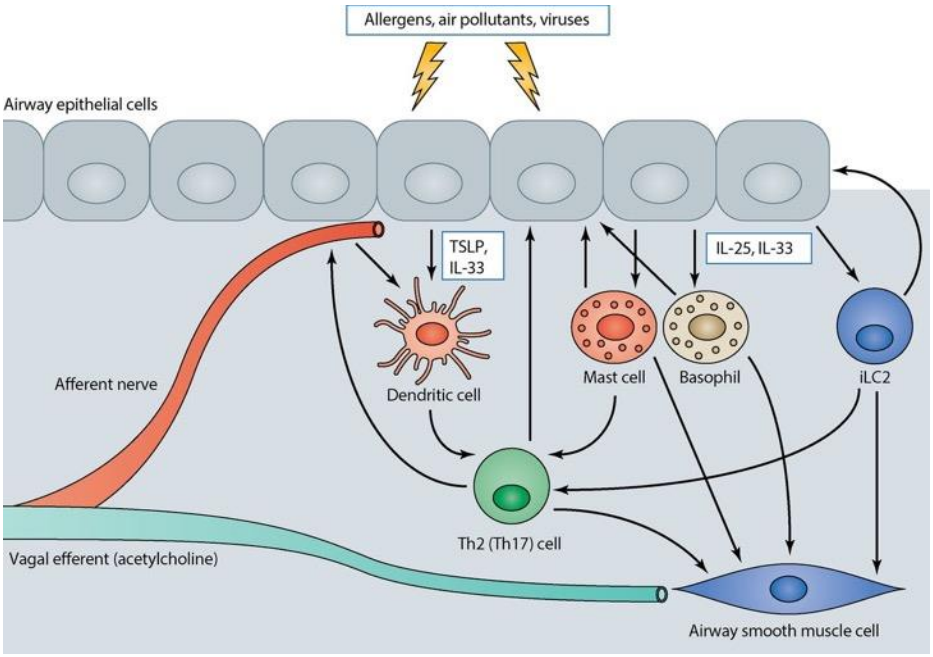

Figure 1.9. Cell-cell communication in airway epithelium in asthma. Environmental triggers act on airway epithelial cells to initiate responses in multiple cell types that result in mucous metaplasia and airway smooth muscle contraction. Reprinted from (*68*).

The airway epithelium serves as the first barrier for inhaled allergens and pathogens. In addition to the mucus protective layer generated by secretory cells, the airway epithelium expresses several types of pattern recognition receptors that serve for immunological surveillance. Activation of Toll-like receptors (TLRs), such as TLR4, has been widely studied and is thought to be one of the key mediators in triggering an allergic inflammatory response (*69*). Stimulation of TLR4 triggers activation of the cytoplasmic adaptor proteins myeloid differentiation primary response 88 (MyD88) and Toll-interleukin 1 receptor domain-containing adaptor protein (TIRAP) that then leads to the release of inflammatory cytokines and chemokines through the nuclear factor kappa-light-chain-enhancer of activated B cells (NF-kB) pathway and the interferon beta (IFN-β)/interferon regulatory transcription factor 3 (IRF3) pathway. Key cytokines released by the airway epithelium in allergic inflammation are IL-25, IL-33 and thymic stromal lymphopoietin (TSLP) (Fig. 1.9). These, in turn, activate the local network of dendritic cells (DCs), mast cells, basophils and ILC2s that produce type 2 cytokines such as IL-13 and IL-5 (*70*). IL-13, produced by ILC2s, acts on the airway epithelium by promoting mucous metaplasia. Specifically, IL-13 receptor binding leads to Janus kinase (JAK) activation and translocation of signal transducer and activator of transcription 6 (STAT6) to the nucleus. Once there, STAT6 promotes transcription of the calcium-activated chloride channel regulator 3 (CLCA3) and Serpin. CLCA3 then, through autocrine signaling, activates the mitogen-activated protein kinase (MAPK) cascade, ending in the upregulation of Muc5ac (*71*). Other receptors present in the airway epithelium include C-type lectins that recognize sugar motifs present in allergens, nucleotide-binding

oligomerization domain (NOD)-like receptors which contribute to NF-kB pathway activation, and protease-activated receptors (PARs) that respond to protease allergens (*72*). Thus the airway epithelium plays an important role in the development of asthma.

Mast cells are one of the triggering cells of the inflammatory response in asthma. They are activated by cross-linking of IgE receptors and secrete proinflammatory mediators such as histamine, leukotriene C4, prostaglandin D2, IL-5 and IL-13. These, in turn, promote bronchoconstriction and vasodilation, while IL-13 promotes mucous metaplasia.

Eosinophils, which are highly characteristic of T2 inflammation, secrete mediators such as leukotrienes, major basic protein (MBP) and eosinophil peroxidase (EPO). Eosinophils secrete cytokines such as IL-13 that promote mucous metaplasia and AHR, and growth factors such as TGF-β which induces basement membrane thickening. It is important to note that eosinophils are elevated only in a sub-population of patients with asthma, and treatments such as inhaled corticosteroids will only work in patients with eosinophilic asthma (*73*).

Dendritic cells are antigen-presenting cells that are able to stretch their dendrites across the epithelium into the airway lumen to sample inhaled air for antigens. Once activated, they migrate to lymph nodes through chemokine signaling, to present antigens to naïve T cells. DCs drive T cell differentiation to achieve a Th2 response that is a common feature of allergic inflammation. It was initially thought that DCs were able to become activated on their own, but studies have shown that they require activation of the TLR4 pathway from epithelial cells (*74*). The now-activated T cells, along with ILC2s,

produce IL-13 that acts on secretory cells of the airway epithelium and on airway smooth muscle.

Another key cell type present in asthma is the T cell. As I have mentioned above, Th2 cells release IL-13 that drives mucous metaplasia. They also secrete IL-4, that along with IL-13, activates B cells that then produce IgE, one of the major immunoglobulins responsible for an allergic response, activating mast cells and basophils. T cells also release IL-5 that is crucial for eosinophil survival and maturation. IL-5 is also responsible for eosinophil stimulation, which drives the eosinophilia observed in the lungs. These three cytokines also act on airway smooth muscle, stimulating hyperresponsiveness to constrictor stimuli, a feature that interacts with mucus plugging and narrow airways. Another important subset of T cells is Th17. These cells predominantly produce IL-17 that mainly effects neutrophils as well as airway smooth muscle, leading to an increase in airway contractility and priming it for airway hyperresponsiveness, but can also stimulate mucin production.

Recently, considerable attention has been given to ILC2s and their role in asthma. Their role was recognized when mice deficient in RAG (recombinase activated gene), which lack mature T cells or B cells, nonetheless generated T2 cytokines and eosinophilia upon allergic challenge. ILC2s behave similarly to Th2 cells although they are part of the innate immune system and lack T cell receptors. They respond to cytokines produced from the airway epithelium, IL-25, IL-33 and TSLP, producing the key cytokines of a type 2 profile: IL-13, IL-5 and IL-9 (Fig. 1.9) (*75*). These cytokines promote the recruitment of eosinophils and mucous metaplasia. One recent study

showed that ILC2s can represent more than half of the cell population that produces T2 cytokines, emphasizing their importance in promotion of airway inflammation (*76*).

1.3.1.2 The role of mucus in asthma

In asthma, the leading cause of death is asphyxiation from airway mucus occlusion (Fig. 1.10) (*77*). As mentioned above, *MUC5AC/Muc5ac* expression goes up, and in some humans, *MUC5B* expression goes down while *Muc5b* expression in several murine models appears to go up slightly. The upregulation of mucins is mainly due to the inflammatory cytokine IL-13, which is upregulated in more than 50% of patients with asthma (*71*). An increase in EGFR levels detected in asthma patients correlates with disease severity (*78*), and EGFR signaling supports *MUC5AC/Muc5ac* expression (*33*).

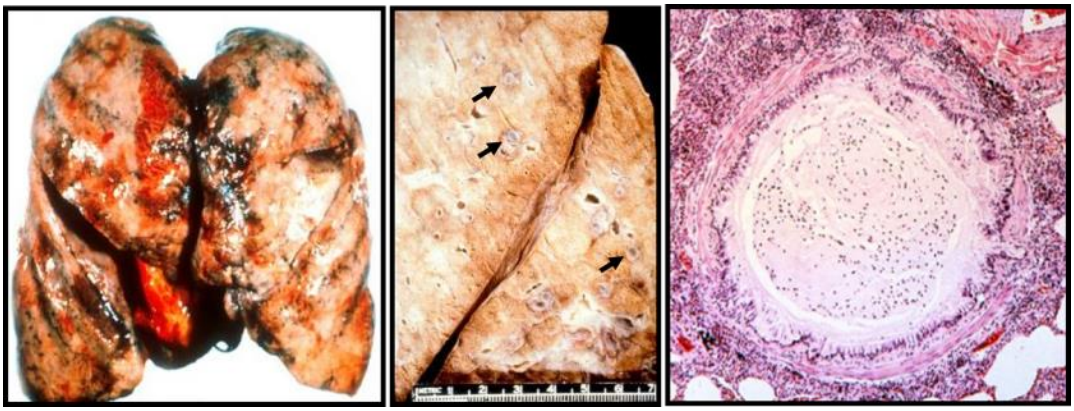

Figure 1.10. Airway mucus occlusion in a human lung from an asthmatic patient. Left: Human lung from an asthmatic patient who died from an asthma exacerbation. Airway mucus occlusion, airway hyperresponsiveness and inflammation are characteristic of acute asthma exacerbations. Center: Lung section with arrows showing mucus plugging the airways. Right: Histologic cross section of an airway with its lumen completely obstructed by mucus. Reprinted from (*79*).

Besides changes in expression levels, modifications in glycosylation patterns in MUC5B have also been observed. These changes may affect the gel-forming capabilities of mucins and the interactions with pathogens or other defense molecules (*80*). Rheological measurements of sputum from patients with asthma showed an increased elastic response, indicating increased crosslinking of mucin polymers. Other components such as DNA, albumin, and a decrease in protease activity, have been also found in the sputum of patients that may contribute to the increased viscoelasticity of mucus (*81*). These abnormalities make it difficult for mucus to be cleared via mucociliary clearance, creating airway mucus occlusion. In addition, a recent paper by Bonser and colleagues found that when MUC5AC was secreted, it further impaired mucociliary clearance by remaining tethered to epithelial secretory cells (*82*).

1.3.1.3 Therapeutics

Inhaled corticosteroids and β-adrenergic agonists are the two most common therapies used in asthma patients. Although they do not target mucus *per se*, corticosteroids aim to reduce the chronic inflammatory component. Their effectiveness has been seen as reduced exacerbations, death, and symptoms; improved lung function; and decreased eosinophil counts. Despite some efficacy with inhaled corticosteroids, there is a small group of patients that show no response to this treatment. Steroid-resistant patients often have severe disease, but they also demonstrate the heterogeneity of asthma. β-adrenergic agonists do not target mucus either as they primarily inhibit airway smooth muscle contraction, but they are also required for development of the asthma phenotype in a murine model (*83*). Corticosteroids can inhibit mucous

metaplasia after an IL-13 stimulation in human bronchial epithelial cells and that the addition of β-adrenergic agonists potentiates this effect (*84, 85*).

To target mucus itself, there are two main treatments available currently. One is the mucolytic reducing agent N-acetylcysteine, but it is generally not used anymore due to its very low efficacy at the tolerable dosage (*86*). The other treatment is hypertonic saline solution, which works by osmotically drawing water into the airway and reducing mucus viscosity, making it easier for mucociliary clearance to transport the mucus layer (*87*).

1.3.2 Cystic Fibrosis

1.3.2.1 Cell biology of cystic fibrosis

Cystic fibrosis (CF) is the most common fatal genetic disease in North America with a frequency of 1 out of every 2500 people (*88*). It occurs as a result of mutations in the cystic fibrosis transmembrane conductance regulator (*CFTR*) gene. The *CFTR* gene encodes a cyclic adenosine monophosphate (cAMP) regulated chloride channel with expression in the apical membrane of epithelia in the pancreas, intestine, lungs and reproductive tract (*89*). By regulating chloride transport across the plasma membrane, CFTR controls the movement of water through the epithelium in order to maintain homeostasis (Fig. 1.11). Besides regulating chloride transport across the plasma membrane, CFTR also controls bicarbonate secretion. Both of these functions are important for mucous membranes, since CFTR dysfunction leads to a dense mucus gel with abnormal biophysical properties as a consequence of epithelial surface dehydration

and a lowered pH (*90*). People with CF have an increased risk for lung infections due to this thick dense mucus that builds up in the lungs. Accumulation of mucus in the pancreas also prevents food and nutrient absorption, and mucus can occlude the bile duct in the liver. CFTR mutations are divided into defects in protein synthesis (class I), maturation/trafficking (class II), channel gating (class III), altered conductance (class IV), and decreased CFTR abundance (class V) (*91*). The most common mutation belongs to class II, commonly known as ΔF508, carried in almost 90% of the patients on at least one allele.

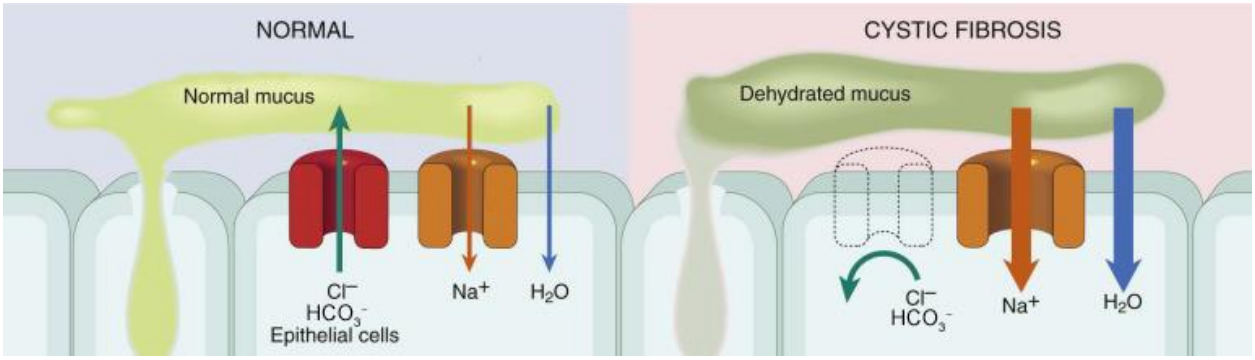

Figure 1.11. CFTR deficiency in the airway epithelium leads to dehydrated mucus. Left: In a normal airway, CFTR transports chloride and bicarbonate to the airway lumen and helps maintain the balance of water. Right: A CFTR dysfunction leads to impairment of chloride and bicarbonate transport leading to increased sodium and water reabsorption. This results in dehydration of the mucus layer, defective mucociliary action, and airway mucus occlusion. Adapted from (*92*).

Mouse models with a CFTR mutation or complete KOs are not good models for lung disease due to the mild phenotype resulting from expression of additional chloride channels in murine lung epithelium. To overcome that, a mouse model was developed

that overexpresses the β subunit of the sodium channel (β-ENaC) in the epithelium of the lungs increases airway surface dehydration, resulting in a CF-like phenotype (*93*). This CF-like phenotype exhibits periciliary layer collapse, a slowed mucociliary clearance rate, airway mucus occlusion, and neutrophilic inflammation. With bacterial infection, β-ENaC-overexpressing animals exhibit a temporary rise in bacterial burden upon birth that is resolved when reaching adulthood (*94*).

1.3.2.2 The role of mucus in CF

Although CF affects several organs, pulmonary complications are the major cause of mortality in these patients. With the airway dehydration in CF, there is an increase in mucus concentration and a reduction in mucociliary clearance. Since there is an increase in mucin concentration in the mucus layer, water is drawn from the periciliary layer leading to compression and reduction in ciliary activity. Thus, the mucus layer adheres to the cell surface of the epithelium, and mucociliary clearance eventually stops completely. Mucus stasis progresses into airway mucus occlusion, chronic bacterial infection, inflammation and airway tissue damage (*90*). In addition, the lack of bicarbonate in the airway lumen prevents the sequestration of calcium, which impedes the mucin from unfolding and hydrating properly (*95*).

Studies looking at CF sputum mucin content demonstrate that both MUC5B and MUC5AC were increased, with MUC5B being the predominant mucin (*96*). These findings were supported by further immunohistochemical analysis of airway mucus occlusion (*97*) and by another study where Muc5b was found to be the main contributor of the phenotypes shown by a CF mouse model (*98*).

1.3.2.3 Therapeutics

There are two types of strategy used to target CF. One is to try to correct the CFTR dysfunction itself, and the second one is to attack the abnormal physical properties of mucus. For the first strategy, a drug developed by Vertex Pharmaceuticals, ivacaftor, has shown very promising results. This drug increases the time the channel remains open in cell lines expressing a G551D mutation in *CFTR*, therefore increasing CFTR's chloride and bicarbonate transport. Patients with this mutation treated with ivacaftor had reduced pulmonary exacerbations and improved mucociliary clearance (*99*) This class III mutation is only expressed by ~5% of CF patients, but this served as an example of how targeting CFTR dysfunction could be effective for treating CF patients (*100*). More recently, ivacaftor has been combined with lumacaftor that corrects CFTR misprocessing and increases the number of CFTR proteins that are trafficked to the cell surface in ΔF508 mutations. Treatment with this combination is now being used in most CF patients (*101*).

To target mucus properties for treatment of CF, mucolytics and hydration therapy have been tried, as for asthma. NAC, the reducing agent, shows very little efficacy. However, to reduce viscoelasticity contributed by DNA released from inflammatory cells, DNase is now used routinely (*102*). The use of hypertonic saline has been surprisingly effective at rehydrating the mucus layer and improving mucociliary clearance (*103*).

CHAPTER II

DISTINCT MUNC18 PROTEINS MEDIATE BASELINE AND STIMULATED AIRWAY MUCIN SECRETION

2.1 Rationale

The following chapter contains the manuscript that summarizes my work on the role of Munc18 proteins in airway mucin secretion. The are several reasons for choosing to study Munc18. First, as discussed above, Munc18 belongs to the family of SM proteins, and together with the SNARE proteins, they constitute the core exocytic machinery, which we thought should be well characterized before analyzing the roles of regulatory proteins. Among the SNARE proteins, SNAP23 was being studied in our laboratory (see chapter III) but was found to have roles in both baseline and stimulated mucin secretion, so did not provide a pathway to dissect baseline and stimulated secretion. VAMP8 was partially studied in another laboratory (*104*), showing a role in stimulated secretion, but its baseline role was not tested. The remaining SNARE, Syntaxin, was completely unknown. From previous work in our laboratory, it was known that Munc18b had a major role in stimulated mucin secretion, but little or none in baseline. Identifying the SM protein responsible for baseline secretion would be the first example of a selective machinery in baseline secretion.

2.2 Introduction

In mammalian conducting airways, mucus forms a critical barrier that protects the lungs from inhaled particles, pathogens and toxicants (*2*). These foreign substances are trapped by mucus, which is swept out of the lungs by ciliary beating into the pharynx where it is swallowed. Secreted polymeric mucins, the principal macromolecular components of mucus, are large, highly glycosylated proteins that polymerize into linear chains and networks (*13, 41*). Mucins are packaged dehydrated in secretory granules, and after exocytosis they interact with several hundred-fold their mass of water to expand and generate viscoelastic, gel-like mucus.

Two polymeric secreted mucins are expressed in the airway epithelium—Muc5b and Muc5ac. Mouse Muc5b is expressed constitutively in superficial epithelial cells and submucosal glands, and is primarily responsible for mucociliary clearance. Deletion of the gene encoding Muc5b in mice results in death from bacterial infection and airway obstruction (*26*). Heterozygous gene deletion results in ~50% reduction in polystyrene bead clearance (*27*), showing that Muc5b is limiting for mucociliary clearance. Conversely, an overexpressing allele of human *MUC5B* is highly prevalent in Caucasians and shows evidence of positive selection, probably for its value in protection against lung infection even though it is a risk factor for pulmonary fibrosis late in life (*28, 105*). Muc5ac is expressed only at low levels in all airways of naïve (uninflamed) mice and in distal airways of humans (*2*). However, *Muc5ac* expression rises ~40-fold during allergic inflammation (*106, 107*). Induced *Muc5ac* expression contributes importantly to helminth defense in the gut (*36*), and may help trap helminths migrating

through the lungs (*37*). In allergic asthma, overexpressed and rapidly secreted Muc5ac causes airway mucus occlusion and airflow obstruction (*38*).

Mucins are secreted at a low baseline rate and a high agonist-stimulated rate (*108, 109*). Both rates are regulated by the second messengers diacylglycerol and calcium acting on the exocytic sensor Munc13-2 (*23*). Important extracellular agonists promoting baseline secretion are ATP and its metabolite adenosine, released predominantly from ciliated cells sensing shear stress from airflow during ventilation (*109-111*). These agonists act on heptahelical receptors coupled by G-proteins of the Gq subtype to PLC-β that generates the second messengers diacylglycerol and inositol triphosphate, with the latter inducing the release of calcium from intracellular stores (*108*). Higher levels of the same agonists can stimulate high rates of mucin secretion (*39*), as can the neural and inflammatory mediators acetylcholine and histamine acting on the same pathway downstream of their cognate receptors (*38*). At high levels of intracellular calcium, the fast, low-affinity exocytic calcium sensor Synaptotagmin-2 promotes mucin secretion (*66*). Baseline secretion is thought to be primarily responsible for clearance of inhaled particles and pathogens, while stimulated secretion can induce airway obstruction protectively to trap helminths or pathologically in asthma (*37, 38*).

Defects in mucin secretion in SNAP23 and VAMP8 mutant mice implicate the highly conserved SNARE (soluble N-ethylmaleimide-sensitive factor attachment protein receptors) machinery in mucin exocytosis (*64, 104*). The SNARE complex is a four-helix bundle comprised of three helices attached to the target membrane (t-SNAREs) and one attached to the vesicle membrane (v-SNARE). Specific binding of these helices

confers accuracy and directionality on the fusion reaction, and full coiling provides the energy to fuse the lipid membranes. SNARE-dependent vesicle traffic universally involves SM (Sec1/Munc18) proteins that promote SNARE complex assembly and help prevent off-target interactions (*112*). Yeast contain four SM proteins, among which the exocytic protein Sec1 has evolved into three exocytic Munc18 isoforms in metazoans. We previously found, using heterozygous hypomorphic mutant mice (*65*), that Munc18b has a role in stimulated mucin secretion, but were unable to identify a role in baseline secretion. Here, by performing a comprehensive analysis of airway epithelial deletants of all three Munc18 isoforms in mice, we sought to identify the Munc18 protein(s) mediating baseline secretion, to fully characterize the role of Munc18b in stimulated mucin secretion, and to test the hypothesis that selective impairment of stimulated secretion can protect against airway mucus obstruction in pathophysiologic models.

2.3 Results

2.3.1 Generation of airway epithelial Munc18 deletant mice

We had previously found that homozygous mutant Munc18b mice are not viable postnatally (*65*), and others found that homozygous Munc18a (*60*) and Munc18c (*113*) knockout mice are similarly not viable. Therefore we assembled a panel of conditional mutant Munc18 mice by generating a conditional allele of Munc18b that is described here (Fig. 2.1 A and 2.2), generating a conditional allele of Munc18c that is described elsewhere (*114*), and obtaining from others a conditional allele of Munc18a (*115*). Crossing conditional Munc18b mice with Zp3-Cre transgenic mice to generate whole

animal knockout mice did not yield any Munc18b$^{-/-}$ pups, confirming that Munc18b is an essential gene in mice. Munc18b$^{-/-}$ embryos grown in vitro developed to E3.5 at a Mendelian ratio, but in vivo, Munc18b$^{-/-}$ embryos at E10.5 were present at less than a Mendelian ratio, and at E11.5 there were none (Fig. 2.1 B).

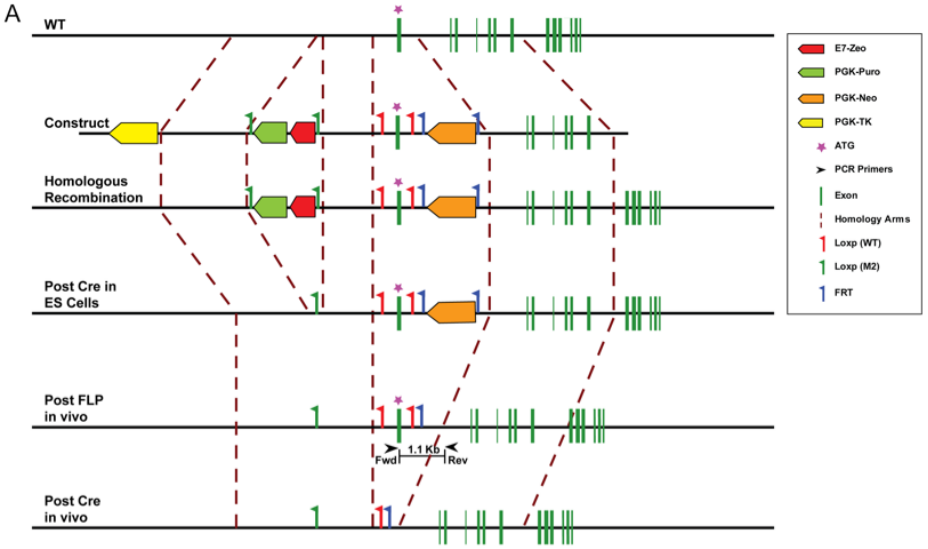

Stage	Total	+/+	+/–	–/–
E3.5*	42	8	22	12
E10.5	46	11	29	6
E11.5	49	16	33	0
E12.5	38	14	24	0
E13.5	16	6	10	0
E15.5	29	12	17	0

Figure 2.1. Generation of Munc18b conditional deletant mice. (A) Exon 1 of the Munc18b gene was flanked by two loxP sites (red flags) via homologous recombination. Herpes simplex virus thymidine kinase (yellow) was used for negative selection. Zeocin (red) and puromycin (green) resistance genes flanked by two loxP (M2) sites (green flags), removed by Cre in embryonic stem cells, and a neomycin resistance gene (orange) flanked by two FRT sites (blue flags), removed by Flp recombination, were used for positive selection. Exon 1 was removed by Cre recombination in mice. (B) Table showing embryos of different genotypes harvested at various days of embryonic (E) development after generating a full KO by crossing the mouse in (A) to a Zp3-Cre mouse. (C) Litter size after crossing floxed mouse in (A) to a CCSP^{iCre} mouse to generate a conditional deletant mouse specific for airway epithelium are compared to their floxed littermates (n=50-52 per group). (D) Weight at 3 weeks of age by Munc18b conditional deletants and their floxed littermates (n=50-52 per group).

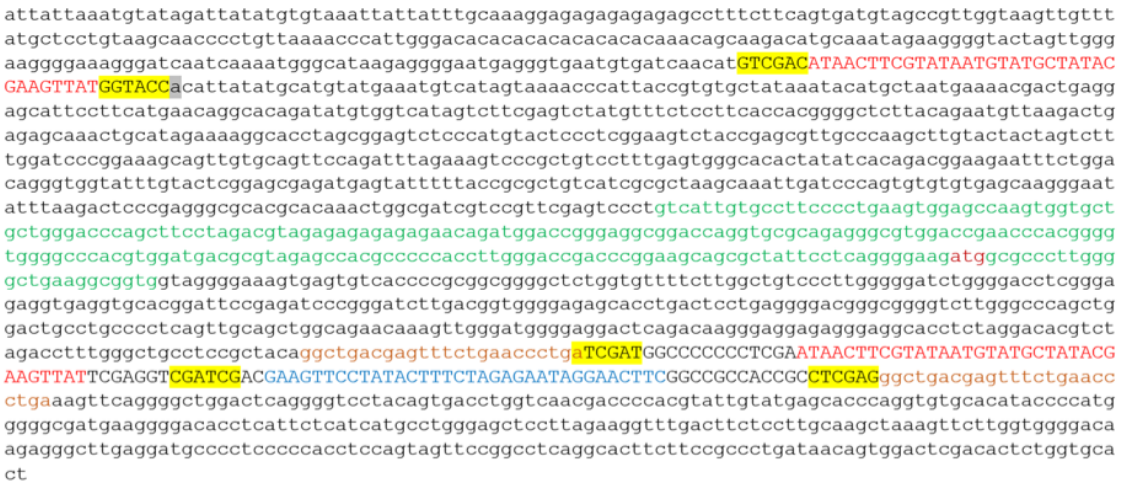

Figure 2.2. Sequence around exon 1 of the conditional deletant Munc18b gene. Sequencing result of 1788 bp around exon 1 (green) of the mouse shown in Figure 1, A after Flp recombination in vivo. Native sequence shown in lower case, introduced fragments shown in upper case. LoxP (red), FRT (blue), restriction sites used for cloning (yellow highlights), repeats (brown), lost base (grey highlight) and starting codon (red, lower case) are indicated.

Deletion of Munc18b in airway epithelial cells by crossing Munc18b$^{F/F}$ mice with CCSP^{iCre} mice (*116*) yielded Munc18b$^{CCSP\text{-}\Delta/\Delta}$ (hereafter Munc18b$^{\Delta/\Delta}$) mice with normal litter sizes and weight at 3 weeks compared to Munc18b$^{F/F}$ mice (Fig. 2.1 C and D). The efficiency of recombination of CCSP^{iCre} mice at the ROSA26 locus is >99% in both airway secretory and ciliated cells (Fig. 2.3 A and B), and occurs occasionally in alveolar type 2 secretory epithelial cells as well (Fig. 2.3 C). Histopathologically, the lungs of all floxed and single Munc18 isoform airway deletant mice were unremarkable by H&E staining, as were the lungs of Munc18a/b and Munc18b/c floxed mice, and Munc18a/b double deletant mice (Fig. 2.4 A and B). However, the airways of Munc18b/c double deletant mice showed a flattened epithelium with an almost complete

absence of airway secretory cells by immunohistochemical staining for club cell secretory protein (CCSP) (Fig. 2.4 C), and the lung alveolar regions showed emphysema (Fig. 2.4 D). To determine whether these abnormalities reflected dependency on Munc18b and Munc18c only during development, we used $CCSP^{CreER}$ mice to induce recombination during adulthood (*117*). Airway secretory cell viability was still impaired because CCSP expression was lost two weeks after recombination (Fig. 2.4 E), though emphysema was not present (Fig. 2.4 F).

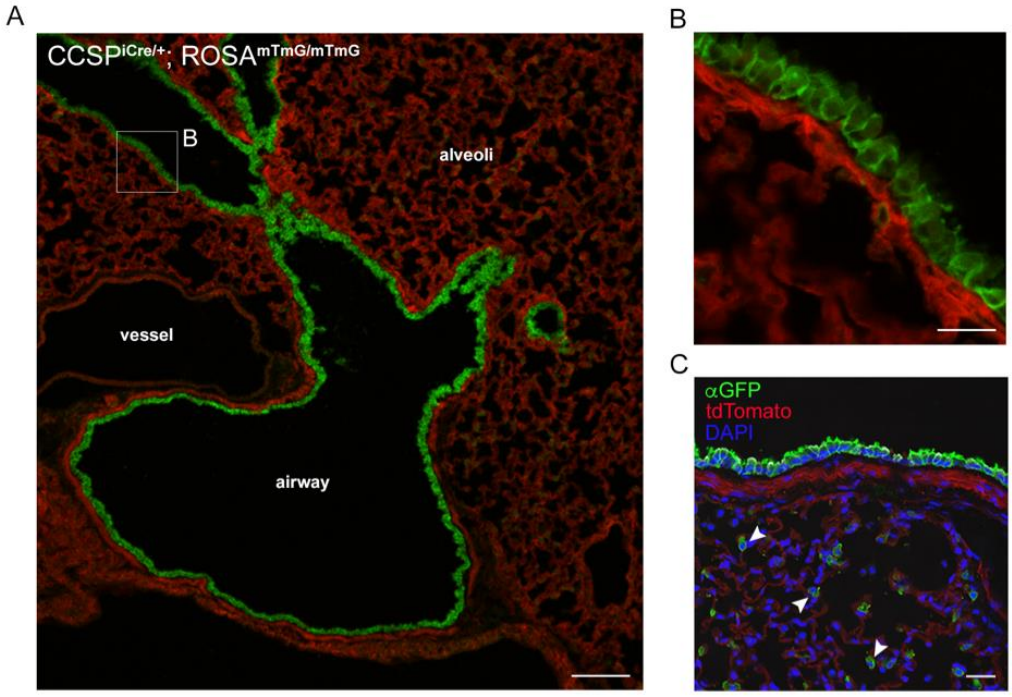

Figure 2.3. Efficiency of CCSPiCre recombination. (A) Confocal image of lung sections from $CCSP^{iCre}$; $ROSA^{mTmG/mTmG}$ mice. Lumens of an airway and a vessel, and region of alveoli, are indicated. Scale bar=100 μm. (B) High magnification image of lung section in (A), showing plasma membrane outline. Scale bar=50 μm. (C) Confocal image of immunostained lung section from same mouse as in (A) using GFP antibody to increase sensitivity of the detection of recombination. Arrowheads show type 2 alveolar cells. Scale bar=50 μm.

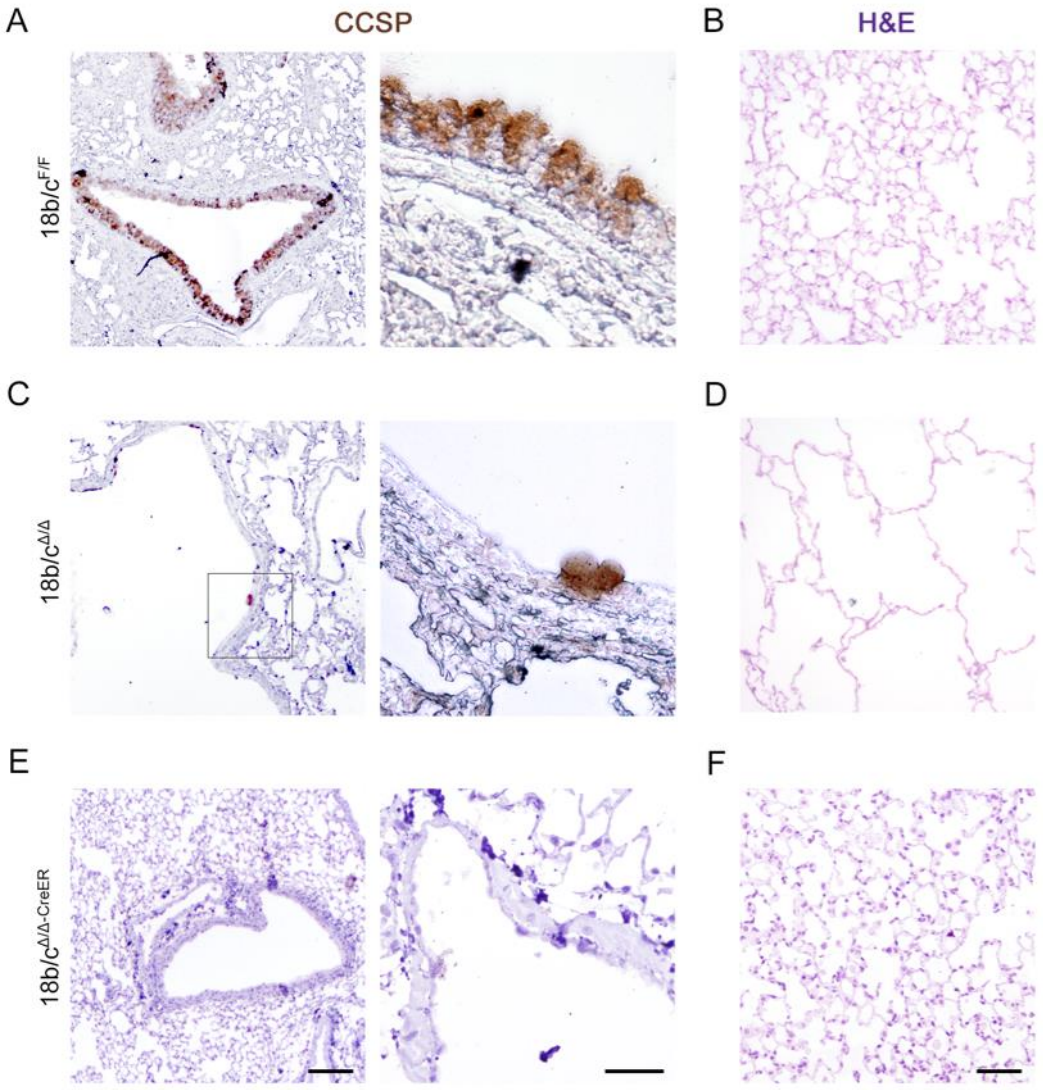

Figure 2.4 Double deletion of Munc18b and Munc18c in the airway epithelium. Representative lung sections of Munc18b/c$^{F/F}$ **(A, B)**, Munc18b/c$^{\Delta/\Delta}$ **(C, D)** and Munc18b/c$^{\Delta/\Delta\text{-CreER}}$ **(E, F)** mice. A, C and E show airways immunostained with CCSP at a low magnification (left column, scale bar=200 μm) and at a high magnification (right column, scale bar=25 μm). B, D and F show alveolar regions stained with hematoxylin and eosin. Scale bar=50 μm.

To determine the normal expression of Munc18 isoforms in the airway epithelium and confirm the efficiency of gene deletion, we performed quantitative *in situ* hybridization with riboprobes. Munc18a and Munc18b transcripts were expressed in secretory cells at levels several-fold higher than in ciliated cells (Fig. 2.5 A and B), whereas Munc18c transcripts were expressed in both cell types at similar levels (Fig. 2.5 C). All three Munc18 conditional deletant mice showed no significant expression of cognate transcripts (Fig. 2.5), and there was no significant difference in transcript expression between any of the floxed mice and WT (not shown).

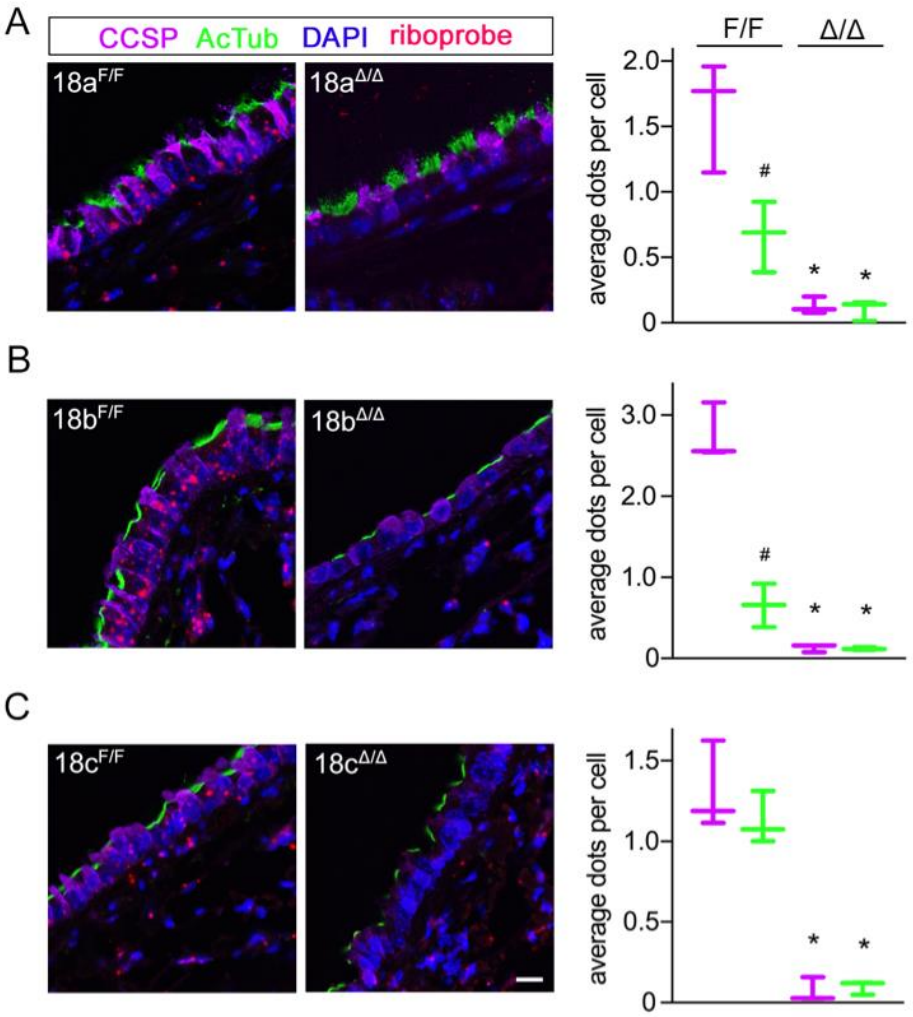

Figure 2.5. In situ hybridization of Munc18 isoforms. Representative images of in situ hybridization with fluorescent-labeled riboprobes (shown in red), specific for murine Munc18a (A), Munc18b (B) and Munc18c (C). Sections are from naïve (uninflamed) lungs of floxed and conditional deletant mice. CCSP was used as a secretory cell marker (purple) and acetylated tubulin as a ciliated cell marker (green). Graphs show quantification of dots per cell type, per genotype, for each probe. Scale bar=30 μm. (n=3 mice per group). (A) Secretory vs ciliated ($18a^{F/F}$), P=0.03; secretory ($18a^{F/F}$) vs secretory ($18a^{\Delta/\Delta}$), P=0.0038; ciliated ($18a^{F/F}$) vs ciliated ($18a^{\Delta/\Delta}$), P=0.0254. (B) Secretory vs ciliated ($18b^{F/F}$), P=0.0012; secretory ($18b^{F/F}$) vs secretory ($18b^{\Delta/\Delta}$), P=0.0002; ciliated ($18b^{F/F}$) vs ciliated ($18b^{\Delta/\Delta}$), P=0.0253. (C) Secretory ($18c^{F/F}$) vs secretory ($18c^{\Delta/\Delta}$), P=0.0017; ciliated ($18c^{F/F}$) vs ciliated ($18c^{\Delta/\Delta}$), P=0.0004, Student's two-tailed *t* test. #, P<0.05 between cell types; *, P<0.05 within cell type.

2.3.2 Munc18b predominates in stimulated mucin secretion

Our previous study using heterozygous mutant mice indicated that Munc18b has a major role in stimulated mucin secretion (*65*). To comprehensively analyze Munc18 function in stimulated secretion, mucin production was first increased (mucous metaplasia) in all mutant mice using ovalbumin sensitization and challenge to induce allergic inflammation, and then mice were stimulated with the secretagogue ATP to induce secretion acutely (Fig. 2.6 A). None of the Munc18 floxed mice showed a phenotype in mucous metaplasia or in mucin secretion in this or any subsequent experiments. All three Munc18 single conditional deletants had mucin content similar to WT mice after the ovalbumin challenge, but the Munc18a/b double deletant had significantly higher mucin content (Fig. 2.6 A and B), suggesting a defect in baseline secretion that results in mucin accumulation (see below). After ATP exposure, the predominant role of Munc18b was confirmed because the conditional deletant secreted only ~26% of intracellular mucin (mean value) compared to Munc18b floxed mice that secreted ~60% or WT mice that secreted ~52% (Fig. 2.6 C). Munc18a and Munc18c deletants secreted as efficiently as their cognate floxed mice or WT mice, while the Munc18a/b double deletant secreted ~31%, comparable to the Munc18b single deletant (Fig. 2.6 C).

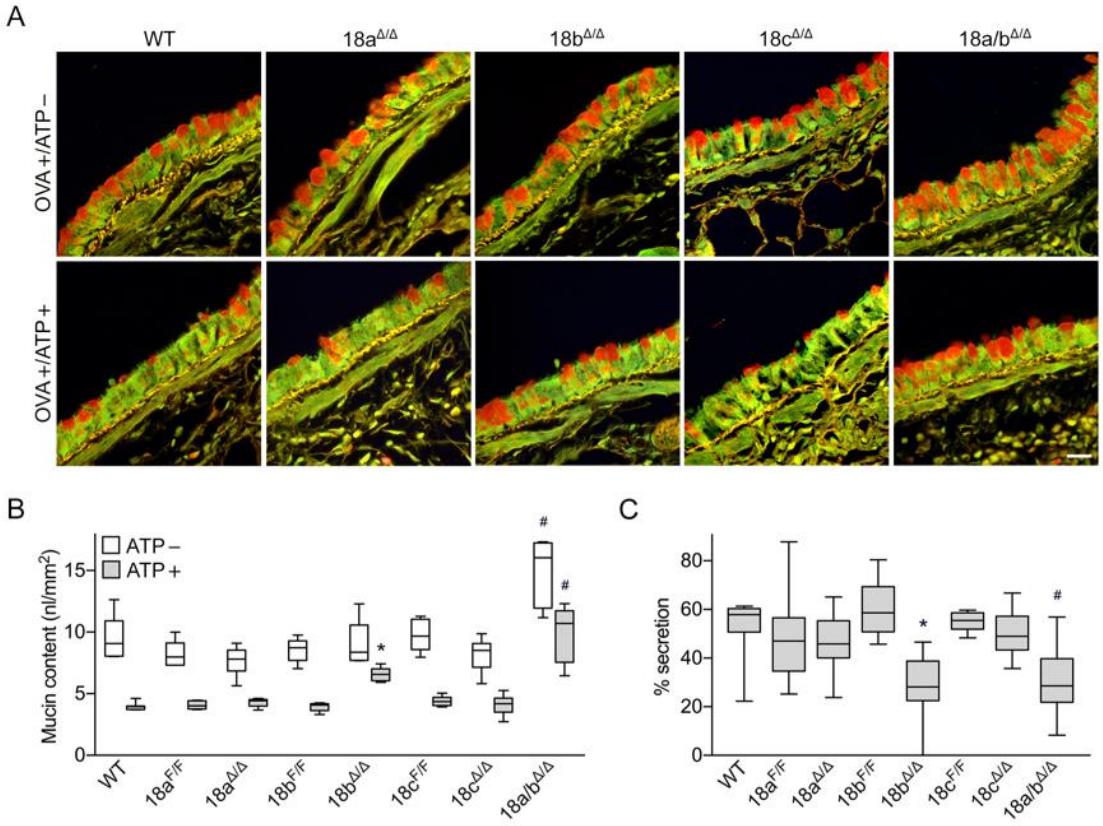

Figure 2.6. Stimulated mucin secretion measured by residual intracellular mucin content. (A) High-magnification views of representative fields of PAFS-stained bronchial airways from mice sensitized and challenged with ovalbumin to increase mucin production (OVA+/ATP-, top row), then exposed to aerosolized 100 mM ATP to stimulate mucin secretion (OVA+/ATP+, bottom row). Scale bar=20 μm. (B) Quantification of the volume density (expressed as nl mucin per mm^2 basement membrane) of intracellular mucin in mice with or without ATP stimulation as in (A) (representative experiment of three separate experiments with all genotypes, n=5-8 mice per group). 18a/b$^{\Delta/\Delta}$ (ATP-) vs WT (ATP-), P<0.0001, vs 18a$^{F/F}$ (ATP-), P<0.0001, vs 18b$^{F/F}$ (ATP-), P<0.0001, Tukey test. 18b$^{\Delta/\Delta}$ (ATP+) vs 18b$^{F/F}$ (ATP+), P<0.0001; 18a/b$^{\Delta/\Delta}$ (ATP+) vs WT (ATP+), P<0.0001, vs 18a$^{F/F}$ (ATP+), P=0.0001, vs 18b$^{F/F}$ (ATP+), P<0.0001, Student's two-tailed *t* test. (C) The percentage of mucin released for each genotype (three independent experiments like those in (B), combined). 18b$^{\Delta/\Delta}$ vs 18b$^{F/F}$, P<0.0001; 18a/b$^{\Delta/\Delta}$ vs WT, P=0.001, vs 18a$^{F/F}$, P<0.0001, vs 18b$^{F/F}$, P<0.0001, Mann-Whitney test. Box plots, line=median; box=25th-75th percentile; whiskers=5th-95th percentile for this and all subsequent figures. *, P<0.05 vs floxed littermate; #, P<0.05 vs WT.

2.3.3 Munc18a predominates in baseline mucin secretion

No defect in baseline mucin secretion had been observed in Munc18b heterozygous mutant mice (*65*). This could be due either to the lack of a role of Munc18b or to the lack of an obvious phenotype with just a 50% reduction in protein expression. To further study baseline mucin secretion, all Munc18 airway deletants were examined.

In naïve (uninflamed) WT mice, the rate of mucin secretion closely matches the rate of mucin production such that intracellular mucin does not accumulate and is not visible by PAFS histochemical staining. Hence, a defect in baseline mucin secretion can be detected as spontaneous mucin accumulation (*23, 118*). Munc18a deletant mice showed significant spontaneous mucin accumulation, indicating a role of Munc18a in baseline secretion (Fig. 2.7 A and B). Munc18b and Munc18c deletants showed no mucin accumulation. However, Munc18a/b double deletant mice showed a higher level of mucin accumulation than Munc18a single deletant mice, indicating an additive effect of Munc18a and Munc18b in baseline mucin secretion. Spontaneous mucin accumulation was further analyzed by quantitative immunoblotting for Muc5b, which is expressed in the airways of naïve mice (*23, 26, 85, 106*). This confirmed significant mucin accumulation in Munc18a deletant mice, a trend towards a small increase in Munc18b deletant mice (P=0.09), and an additive effect in Munc18a/b double deletant mice (Fig. 2.7 C; Fig. 2.8). Muc5ac is not expressed significantly in the airways of naïve mice (*26, 85, 106*), and was not detected in immunoblots of the lungs of any naïve Munc18 deletant mice (not shown).

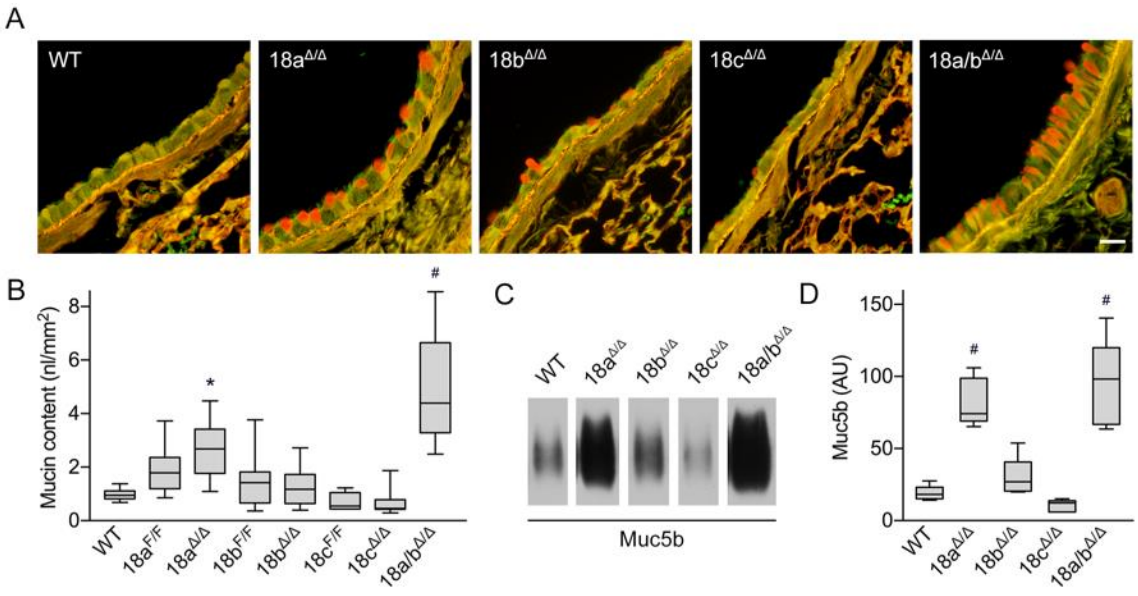

Figure 2.7. Baseline mucin secretion measured by spontaneous intracellular mucin accumulation. (A) High-magnification views of representative fields of PAFS-stained bronchial airways from naïve mice. Scale bar=20 μm. (B) Quantification of the volume density of spontaneous intracellular mucin accumulation (n=5-18 mice per group, three independent experiments combined). 18a$^{\Delta/\Delta}$ vs 18a$^{F/F}$, P=0.0243; 18a/b$^{\Delta/\Delta}$ vs WT, P<0.0001, vs 18a$^{\Delta/\Delta}$, P=0.0008, Student's two-tailed *t* test. (C) Representative immunoblot of 50 μg of whole lung lysates from naïve mice probed for Muc5b. (D) Densitometric analysis of immunoblot shown in (C) derived from standard curve (Fig. S4) (AU, arbitrary units) (n=5-7 mice per group). 18a$^{\Delta/\Delta}$ vs WT, P=0.0079; 18a/b$^{\Delta/\Delta}$ vs WT, P=0.0025, Mann-Whitney test. *, P<0.05 vs floxed littermate; #, P<0.05 vs WT.

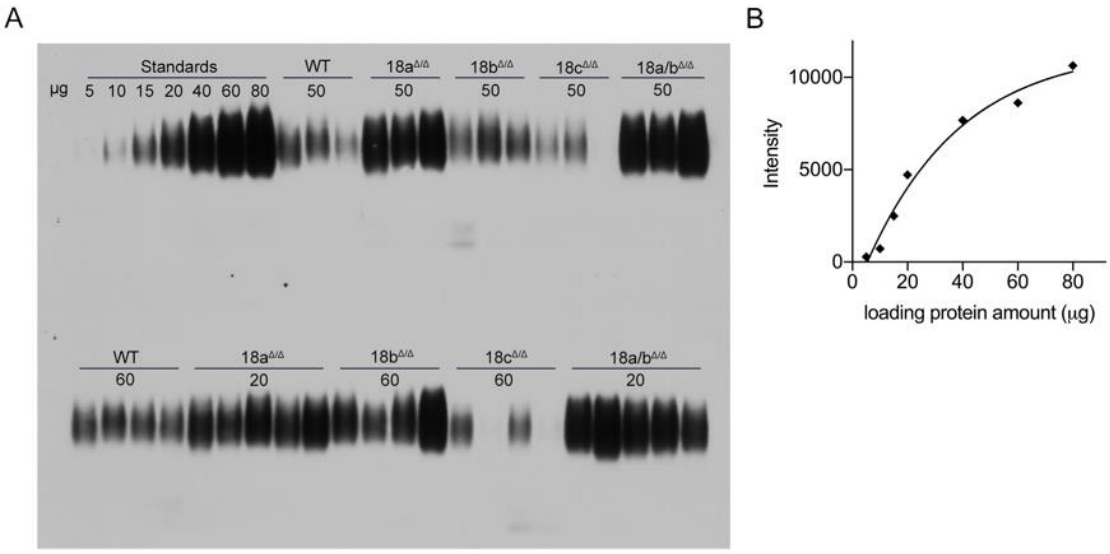

Figure 2.8. Muc5b immunoblot of naïve Munc18 conditional deletant mice excerpted in Figure 2.7. (A) Agarose gel electrophoresis and PVDF membrane transfer developed with ECL and imaged using X-ray film of lung lysates from naïve WT and Munc18 conditional deletant mice probed for Muc5b. Labels on gel show genotype and protein amount loaded. Standard lanes come from a Munc18a$^{\Delta/\Delta}$ lung homogenate. (B) Band intensity was determined for a range of standard loading amounts and the curve was fitted using a 4-parameter logistic curve.

To examine granule morphology by electron microscopy and stereological analysis, mice were lightly stimulated with IL-13 so that mucin granules were readily visible in WT mice (Fig. 2.9 A). Munc18a/b double deletant mice showed an increase in surface-to-volume density of granules (Sv, Fig. 2.9 B), indicating smaller granules with a lower ratio of surface area to volume. However, there was no change in volume density of granules per volume density of cells (Vv, Fig. 2.9 C). Together, these findings indicate that the cells from Munc18a/b double deletant mice had an increased number of

smaller granules. In addition, mucin granules in Munc18a/b double deletant mice were also found to be more electron-dense (Fig. 2.9 D).

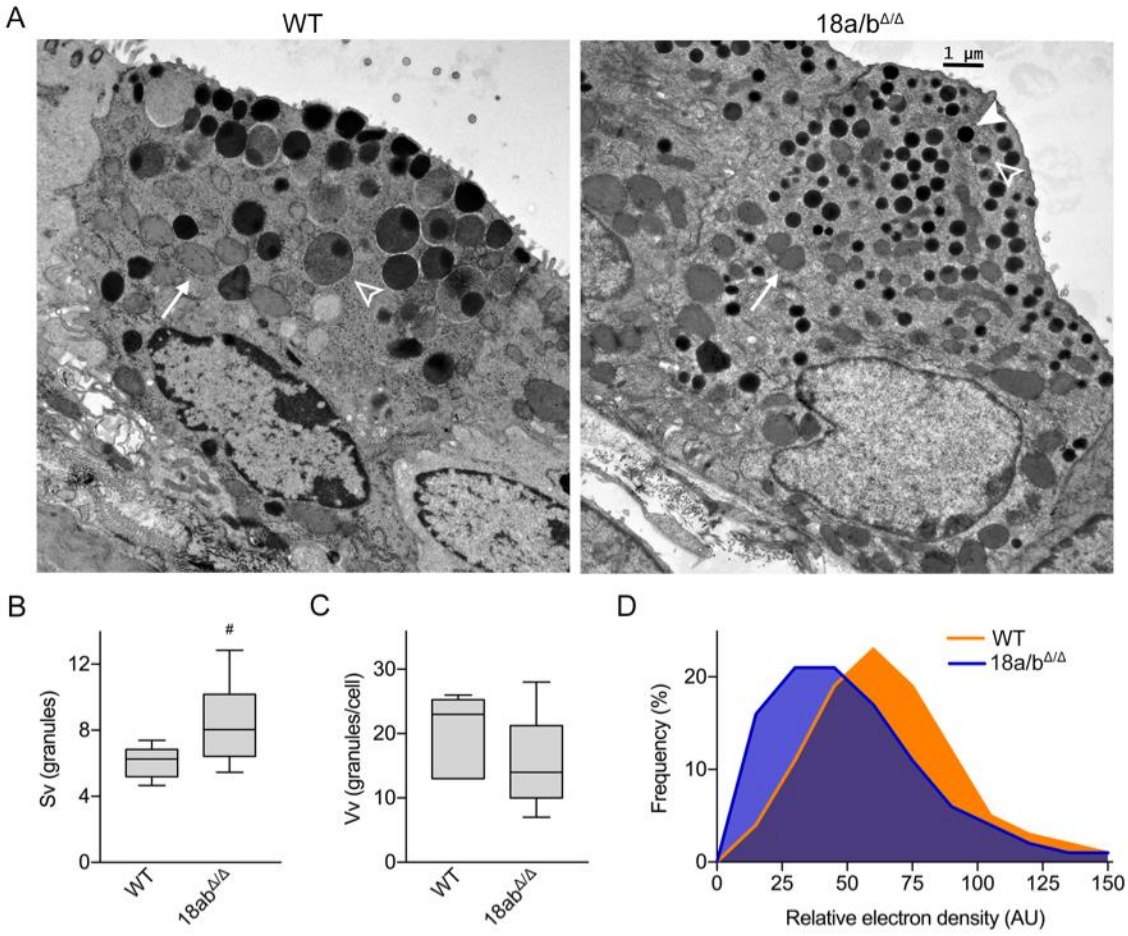

Figure 2.9. Assessment of granule size, number and density by electron microscopy. (A) Representative EM images of secretory cells of WT and Munc18a/b$^{\Delta/\Delta}$ mice treated with a low dose (0.2 µg) of IL-13. Arrow – atypical mitochondrion (*31*); open arrowhead – lucent mucin granule with dense core; filled arrowhead – condensed mucin granule with dense core. Scale bar=1 µm. (B) Sv (surface density related to volume density) of granules measured by stereology, with greater Sv indicating smaller size. WT vs 18a/b$^{\Delta/\Delta}$, P<0.0001, Student's two-tailed *t* test. (C) Vv (volume density of granules related to volume density of cells). (D) Frequency distribution of electron density of mucin granules based on a 0 to 255 relative scale (only values between 0-150 are shown). WT vs 18a/b$^{\Delta/\Delta}$, P<0.0001, Kolmogorov-Smirnov test. #, P<0.05 vs WT.

2.3.4 Deletion of Munc18a or Munc18b does not impair mucociliary clearance

To rule out the possibility that spontaneous mucin accumulation was due to an increase in mucin expression resulting from an inflammatory response in any of the deletants, mRNA expression was analyzed by qRT-PCR in Munc18a and Munc18 single deletant mice and Munc18a/b double deletants. There was no significant increase in expression of *Muc5ac* or *Muc5b* in any of the conditional deletants (Fig. 2.10 A). This absence suggested that mucociliary clearance function was preserved, preventing lung infection and inflammation that might induce mucin gene upregulation. To further test these inferences, several additional studies were performed. First, lung lavage fluid was obtained for measurement of leukocytes, which is a sensitive indicator of inflammatory status. There was no difference in total cell number or fractional representation of any leukocyte subset in either of the Munc18a or Munc18b single deletant mice compared to WT or floxed littermate mice (Fig. 2.10 B). However, the double deletant mice showed a small but significant increase in neutrophil number. Next, polystyrene beads were instilled into the lungs to measure their clearance by mucociliary transport. There was no difference in the fraction of beads cleared by Munc18a or Munc18b deletant mice compared to WT (Fig. 2.10 C). Last, the lung microbiome was interrogated by qPCR and sequencing of 16S ribosomal RNA. There was no significant difference in the quantity (Fig. 2.10 D) or composition (Fig. 2.10 E) of bacteria present in the lungs of Munc18 single or double deletant mice compared to WT or floxed littermate mice.

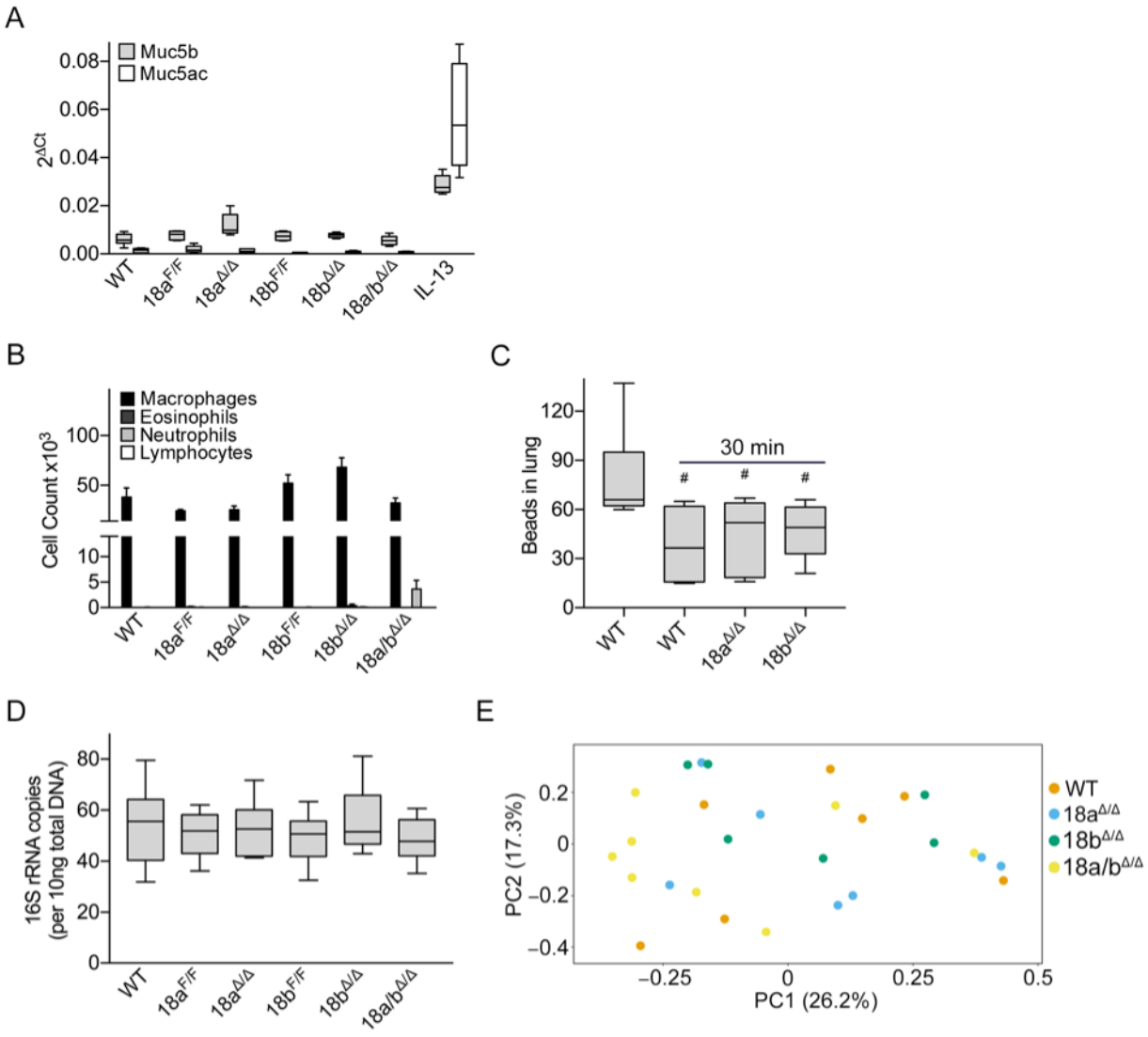

Figure 2.10. Assessment of mucin gene expression, inflammation, mucociliary clearance function and bacterial infection in Munc18 conditional deletant mice. (A) qRT-PCR of lung tissue for Muc5b and Muc5ac relative to β-actin (n=5 mice per group). Mice treated with IL-13 are plotted for comparison. (B) Total inflammatory cell numbers from the lung lavage fluid of naïve mice (n=5-9 mice per group). (C) Fluorescent 4 μm polystyrene microspheres were instilled into the lungs, and microspheres present in the lungs were counted at the time of instillation and after 30 min (n=5-8 mice per group). WT (0 min) vs WT (30 min), P=0.0127, vs $18a^{\Delta/\Delta}$ (30 min), P=0.0295, vs $18b^{\Delta/\Delta}$ (30 min), P=0.0087, Mann-Whitney test. (D) qPCR of lung tissue for copies of bacterial 16S per 10 ng of total DNA (n=7 per group) (E) Principal components analysis of bacterial communities using ribosome gene 16S rDNA gene sequencing (n=7 per group). #, P<0.05 vs WT.

2.3.5 Deletion of Munc18b protects mice against airway obstruction in a model of allergic asthma

Increased mucin production followed by stimulated secretion causes airway lumenal mucus occlusion and airflow obstruction in asthma (*2, 38*). We hypothesized that deletion of Munc18b in airway secretory cells would protect against this pathophysiology. To test this, we first performed a pilot study in a WT mouse with IL-13 instilled intrapharyngeally to induce mucous metaplasia and then exposed to a methacholine aerosol to stimulate mucin secretion. We measured the occlusion of airways throughout the lungs at 500 μm intervals as a fraction of cross-sectional airway area, and found that the right caudal lobe had the highest fractional occlusion (Fig. 2.11 A). We next compared fractional occlusion in the right caudal lobe between Munc18b floxed and deletant mice and found a significant reduction (~50%, mean values) in the deletant mice (Fig. 2.11 B). We then performed a definitive study comparing the sum of the area of lumenal mucus in the right caudal lobe at 1 mm intervals together with measurement of lung mechanics (Fig. 2.12). Munc18b deletant mice showed a ~62% reduction (mean values) in lumenal mucus area compared to Munc18b floxed mice, similar to the ~37% reduction in Muc5ac knockout mice, whereas Munc18a deletant mice showed no reduction (Fig. 2.12 B).

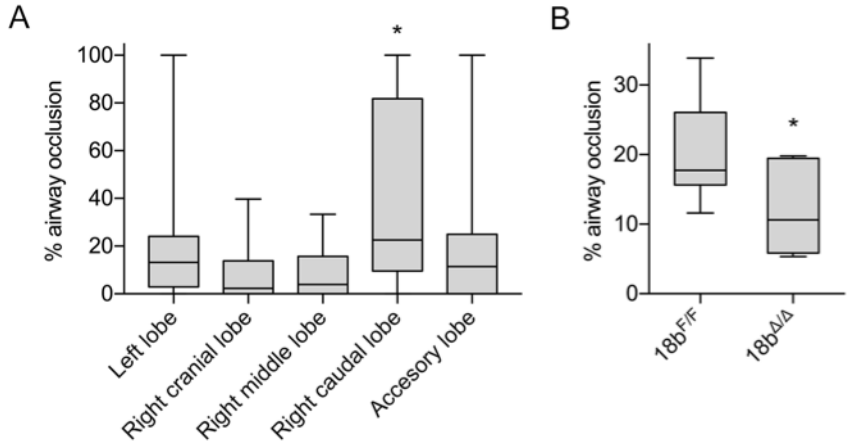

Figure 2.11. Assessment of airway mucus occlusion. (A) Distribution of airway mucus occlusion throughout the lung lobes. A WT mouse was treated with IL-13 (2 μg daily for 4 days) to induce mucin production, and then stimulated with aerosolized 150 mM (30 mg/ml) MCh to stimulate mucin secretion. Lobes were sectioned every 500 μm, stained with PAFS, and a ratio of the area of mucus to the area of lumen (fractional occlusion) was obtained. Right caudal lobe vs left lobe, P=0.0043, vs right cranial lobe, P=0.0002, vs right middle lobe, P=0.0008, vs accessory lobe, P=0.0025, Tukey test. (B) Munc18 deletant and floxed littermate mice were treated as in (A), and fractional occlusion in the right caudal lobe was determined. (n=7-8 mice). $18b^{\Delta/\Delta}$ vs $18b^{F/F}$, P=0.0336, Student's two-tailed *t* test. *, P<0.05.

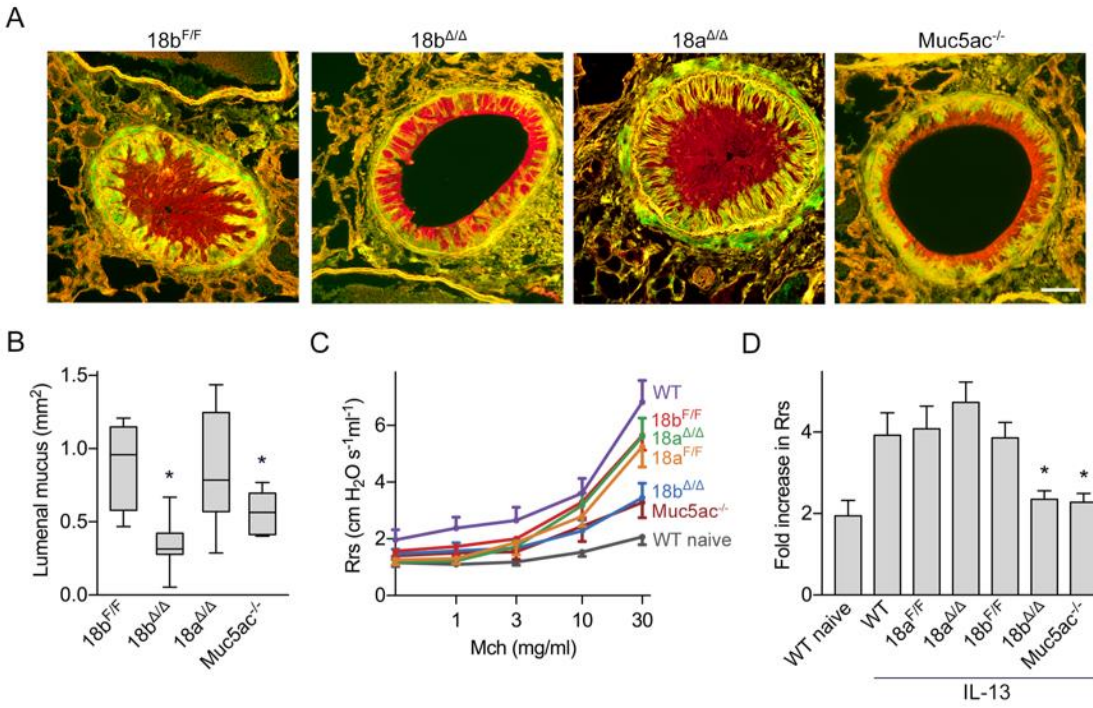

Figure 2.12. Airway mucus occlusion and airway hyperreactivity of Munc18b conditional deletant mice in an allergic asthma model. (A) Representative cross-sections of airways fixed with methacarn to preserve mucus volume and stained with PAFS. Mice were treated with IL-13 to induce mucin production and then stimulated with aerosolized 150 mM methacholine (MCh) to stimulate mucin secretion and smooth muscle contraction. Scale bar=50 μm. (B) Cross-sectional area of lumenal mucus in the right caudal lobe measured at 1000 μm intervals. (n=5-9 mice per group, representative experiment, >100 airways per group quantified). 18b$^{\Delta/\Delta}$ vs 18b$^{F/F}$, P=0.0002; Muc5ac$^{-/-}$ vs 18b$^{F/F}$, P=0.0378, Student's two-tailed *t* test. (C) Total respiratory system resistance (Rrs) at increasing doses of nebulized MCh in mice treated with or without IL-13 (n=6-14 per group, three independent experiments combined). Line, mean; error bar, SEM. (D) Fold-change Rrs at the highest dose of nebulized MCh (30 mg/ml) from (C). Each genotype is normalized to its own baseline measured with nebulized saline. 18b$^{\Delta/\Delta}$ vs 18b$^{F/F}$, P=0.0018; Muc5ac$^{-/-}$ vs 18b$^{F/F}$, P=0.0044, Student's two-tailed *t* test. *, P<0.05 vs floxed littermate. Bar, mean; error bar, SEM.

Exposure to methacholine induces resistance to airflow due to a combination of smooth muscle contraction (bronchoconstriction) and mucus obstruction (*38*). An augmented response to methacholine (airway hyperresponsiveness) is a sensitive

indicator of asthmatic airway dysfunction. WT mice with mucous metaplasia induced by IL-13 and exposed to increasing concentrations of aerosolized methacholine showed increased respiratory system resistance compared to naïve WT mice (Fig. 2.12 C and D). Munc18a$^{F/F}$, Munc18b$^{F/F}$, and Munc18a$^{\Delta/\Delta}$ mice with mucous metaplasia were similar to WT mice, but Munc18b$^{\Delta/\Delta}$ and Muc5ac$^{-/-}$ mice with mucous metaplasia were highly protected from airway hyperresponsiveness to methacholine (Fig. 2.12 C and D).

2.3.6 Deletion of Munc18b protects mice against airway mucus occlusion and parenchymal emphysema in a model of cystic fibrosis

In cystic fibrosis, an inherited defect in transepithelial anion and water transport causes the formation of mucus that is excessively concentrated, viscoelastic and adhesive (*119-121*). Mucus accumulates because its excessive viscoelasticity impedes clearance by ciliary beating and its adhesivity results in the formation of airway mucus plaques. These in turn, lead to infection and inflammation that cause progressive lung disease. In mice, deletion of the anion transporter, CFTR, does not result in lung disease because of the presence of alternative mechanisms of anion transport, but transgenic overexpression of the beta subunit of the epithelial Na^+ channel (ENaC) results in concentrated mucus leading to lung disease that resembles human cystic fibrosis (*93*).

To test whether stimulated mucin secretion contributes to pathophysiology in this model, we crossed Munc18b deletant mice with βENaC-Tg mice (Fig. 2.13 A). Mucus occlusion in βENaC-Tg mice was reduced by ~66% (mean values) by deletion of Munc18b in the airway (Fig. 2.13 B). Emphysema measured as equivalent mean

diameter (D_2) was increased ~86% in βENaC-Tg-Munc18b$^{F/F}$ mice compared to Munc18$^{F/F}$ mice as previously described for the βENaC-Tg (*93*) (Fig. 2.13 C). This increase was attenuated by ~22% by deletion of Munc18b in the airway (Fig. 2.13 C). However, lung neutrophilic and eosinophilic inflammation present in βENaC-Tg-Munc18b$^{F/F}$ was not reduced by Munc18b deletion (Fig. 2.13 D).

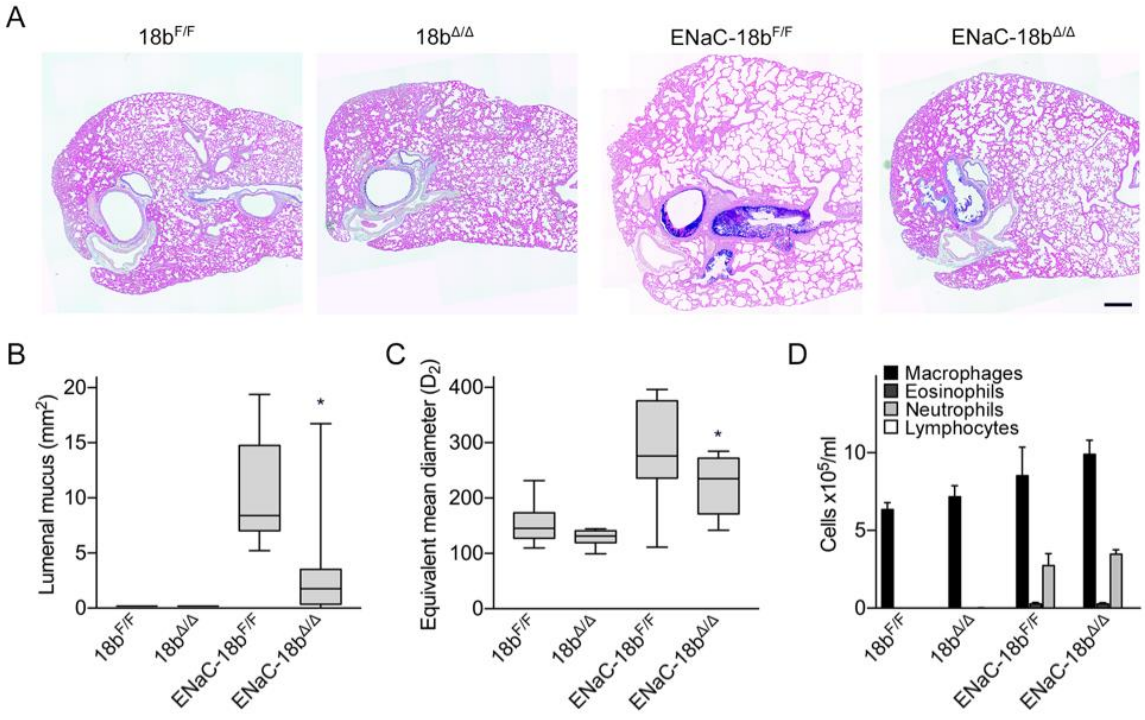

Figure 2.13. Airway mucus occlusion and emphysema of Munc18b conditional deletant mice in a cystic fibrosis-like model. Munc18b$^{F/F}$ and Munc18b$^{\Delta/\Delta}$ mice were crossed or not to β-ENaC-overexpressing transgenic (ENaC) mice. (A) Representative transverse left lung sections stained with AB-PAS. Scale bar=300 μm. (B) Cross-sectional area of lumenal mucus was quantified. (n=8-16 mice per group). ENaC-18b$^{\Delta/\Delta}$ vs ENaC-18b$^{F/F}$, P=0.0013, Mann-Whitney test. (C) Emphysema was assessed as the equivalent mean diameter, D_2. (n=8-16 mice per group). ENaC-18b$^{\Delta/\Delta}$ vs ENaC-18b$^{F/F}$, P=0.0009, Student's two-tailed *t* test. (D) Total inflammatory cell numbers from lung lavage fluid (n=8-16 mice per group). *, P<0.05 vs floxed littermate.

2.4 Discussion

Here, we have performed a comprehensive analysis of the function of Munc18 proteins in a polarized epithelial cell specialized for apically directed regulated secretion. Our central finding is that baseline and stimulated secretion are predominantly mediated by different Munc18 proteins, with Munc18a having the major role in baseline secretion, Munc18b having the major role in stimulated secretion, and Munc18c having no apparent role. This finding has implications for understanding the cell biology of regulated secretion in polarized cells and for manipulating the exocytic machinery of the airway epithelium therapeutically to alleviate mucus dysfunction.

Regarding cell biology, Munc18b has been described previously by us and others as mediating apical secretion in polarized epithelial cells (*65, 122, 123*). Munc18a has been studied primarily for its role in synaptic vesicle release from neurons (*60, 124, 125*), but other regulated exocytic systems where Munc18a has been reported to function include vascular endothelial cells (*126*) and acrosomal exocytosis in spermatozoa (*127*). In airway epithelium, Munc18a was reported to modulate the conductance of the apical anion channel CFTR (*128*), but a role in vesicular transport was not described. Munc18a and Munc18b have been reported to cooperate in regulated exocytosis of insulin-containing granules of pancreatic islet cells (*129, 130*) and cytolytic granules of natural killer cells (*131*) in response to different signaling pathways. Prior reports that Munc18a and Munc18b both participate in mast cell degranulation appear to have been in error, with Munc18b having an exclusive role as we recently described (*114*). Thus, the current

work is the first report, of which we are aware, of two different Munc18 proteins mediating different rates of secretion in response to the same signaling pathway.

Munc18c has been proposed to mediate basolateral secretion in polarized epithelial cells (*132, 133*), consistent with the lack of effect of Munc18c deletion in apical regulated secretion in our system (Fig. 2.6 and 2.7). A role for Munc18c in stimulated exocytosis has been described in non-polarized cells, such as translocation of glucose transporters in adipocytes (*134*), but not in in polarized epithelia. The cellular lethality induced by simultaneous deletion of both Munc18b and Munc18c in airway epithelial cells (Fig. 2.4) suggests that the predominant function of Munc18c is in constitutive secretion because that is an essential cellular function. We hypothesize that Munc18c function is rescued in the single airway deletant mouse by ectopic function of Munc18b. This hypothesis is consistent with the cellular viability of airway epithelial cells in double Munc18a/b mice (Fig. 2.6 and 2.7) because regulated secretion is not a cell-autonomous essential function. Whether Munc18c mediates constitutive secretion at both the apical and basolateral surfaces in airway epithelial cells or functions exclusively at the basolateral surface is not known.

Since Munc18 proteins partner with specific Syntaxins t-SNAREs (*65*), our findings here suggest that the exocytic SM-SNARE machinery is mostly different between baseline and stimulated mucin secretion. This inference is supported by the role of the v-SNARE VAMP8 predominantly in stimulated secretion (*104*), even though SNAP23 functions in both processes (*64*). What might be the adaptive value of utilizing different exocytic machines for baseline and stimulated secretion rather than utilizing a

single machine capable of running at different rates? In view of the differing roles of baseline and stimulated mucin secretion in mucociliary clearance and airway occlusion (*38*), and the differing roles of Muc5ac and Muc5b in helminthic and microbial defense (*26, 36*), several plausible possibilities exist. These include different exocytic machines acting on small immature granules in baseline secretion to minimize the chance of airway occlusion, and on large mature granules in stimulated secretion to maximize the chance of occlusion. This might occur by exchanging VAMP proteins during granule maturation, by analogy with Rab conversion during progression from early to late endosomes (*135*). Another possibility is that Muc5ac and Muc5b are packaged separately during exit from the trans-Golgi network (*136*), with different exocytic machines acting on secretory granules containing either secreted mucin. This last possibility is supported by the apparent segregation of MUC5AC and MUC5B extracellularly and intracellularly in human asthmatic airways (*82*). Further studies colocalizing vesicular components of the exocytic machinery such as VAMPs and Synaptotagmins with different secreted mucins will be required to resolve these questions. The fact that secretory granules visualized by EM in Munc18a/b double deletant mice are smaller and denser than granules in WT mice (Fig. 2.9) suggests that these SM proteins also mediate homotypic fusion between granules during post-Golgi maturation, and that mucins decondense to some degree during granule maturation.

Importantly, the existence of two different exocytic machines in airway secretory cells affords the possibility to molecularly target the pathologic consequences of stimulated mucin secretion without compromising the critical protective clearance

function of baseline mucin secretion. While the fundamental pathophysiologic processes in allergic asthma and cystic fibrosis are mucin hyperproduction and impaired anion transport, respectively, stimulated mucin secretion contributes to airway occlusion in both diseases as indicated by our prior (*38*) and current studies in mouse models of allergic asthma (Fig. 2.12) and cystic fibrosis (Fig. 2.13). To fully appreciate the contribution of stimulated secretion to airway mucus occlusion, it is important to recognize several features of mucin biology. First, the production of mucins, particularly of Muc5ac, can be greatly increased by inflammatory signaling, resulting in the filling of airway epithelial secretory cells with large amounts of mucin contained within secretory granules (Fig. 2.6). If secretion is not stimulated, the stored mucins are slowly released and cause only minimal mucus occlusion (*38*). Second, stimulated secretion can result in the explosive exocytic release of mucin granule contents within seconds (*39*), and the massive extracellular swelling of the released mucins by absorbing several hundred-fold their mass of water occurs in less than a second (*41, 137*). Thus, the area of the airway cross-section occupied by intracellular mucin is only a small fraction of that occupied by fully hydrated extracellular mucus, and the extracellular expansion of mucin volume within such a short time frame are key determinants of pathophysiology. In large proximal airways, rapid release of stored mucins from surface epithelial cells is unlikely to completely occlude the airway lumen, and may have adaptive value in promoting the trapping of particles and pathogens for clearance, as described for submucosal glands (*138, 139*). However, in small distal airways, rapid massive mucin release can overwhelm clearance mechanisms, resulting in airway lumenal occlusion (*38*) (Fig. 2.12

and 2.13). The adaptive value of small airway occlusion in the stimulated secretion of metaplastic epithelial cells may be to trap helminths migrating through lungs (*37*), a hypothesis being tested by us and others. In allergic asthma, IL-13 plays a central role in increased mucin production, as it does in helminth infection, and rapid secretion can be induced by acute inflammatory mediators such as acetylcholine and histamine (*37, 38*). In cystic fibrosis, increased mucin production is more modest (*119*), and the role of secretagogues in small distal airways is less well studied. However, the stimulation of secretion from submucosal glands is critical to mucus dysfunction in a pig model of cystic fibrosis (*119*), and the stimulation of mucin secretion from surface epithelial cell by acetylcholine from neurons or ATP from leukocytes or epithelial cells could contribute to mucus occlusion in small airways.

Mucus occlusion was significantly reduced by deletion of Munc18b in airway epithelial cells in both of the mouse models of airway disease we tested. In the allergic asthma model, reduction of mucus occlusion was shown to result in improvement of lung mechanics (Fig. 2.12 C and D). In the cystic fibrosis model, while the emphysema that occurs secondary to mucus occlusion was also mitigated (Fig. 2.13 A and C), neutrophilic and eosinophilic inflammation was not reduced (Fig. 2.13 D), similar to what occurred upon treatment with aerosolized hypertonic saline solution in that model (*140*). Deletion of Munc18b in airway epithelium did not result in any abnormalities of lung structure, particle clearance, inflammation, or bacterial infection (Fig. 2.10). Therefore, targeting the stimulated exocytic machine with small molecules or RNA silencing technologies in human subjects might be free of intrinsic adverse

consequences. Whether the trapping of helminths during migration through the lungs might be impaired by Munc18b deletion is an area of our active investigation, but helminth infestation is not a common problem in developed countries.

2.5 Methods

2.5.1 Mice

C57BL/6J (catalog no. 000664), C57BL/6-Tg(Zp3-cre)93Knw/J (catalog no. 003651), Gt(ROSA)26Sor$^{tm4(ACTB-tdTomato,-EGFP)Luo}$/J (catalog no. 007576) and B6N.129S6(Cg)-Scgb1a1$^{tm1(cre/ERT)Blh/}$/J (catalog no. 016225) mice were purchased from The Jackson Laboratory. We obtained Munc18a conditional deletant mice from Dr. Matthijs Verhage (U. Amsterdam) (*115*), Munc18c conditional deletant mice from Dr. Roberto Adachi (U. Texas MD Anderson Cancer Center) (*114*) and CCSP^{iCre} (Scgb1a1$^{tm1(icre)Fjd}$) mice from Dr. Francisco DeMayo (NIEHS) (*116*). β-ENaC-C57BL/6-Tg mice (*93*) were crossed to Munc18b conditional deletant mice at the University of North Carolina at Chapel Hill.

In the Munc18a conditional deletant, exon 2 of the gene is flanked by two loxP sites and Cre recombination induces a frameshift resulting in a nonsense codon and absence of protein (*115*). In the Munc18c conditional deletant, exon 1 is flanked by two loxP sites and Cre recombination removes the start codon (*114*). To generate Munc18b conditional deletant mice, we built a targeting vector to insert two loxP sites to flank exon 1 (Figure S1) by homologous recombination. Upstream of exon 1, the zeocin and puromycin resistance genes flanked by two loxP sites (M2) were inserted, and

downstream of exon 1, the phosphoglucokinase promoter-neomycin resistance gene (PGK-neo) resistance gene flanked by two Flp recognition target (FRT) sites was inserted. The herpes simplex virus thymidine kinase gene was introduced outside the homology arms for negative selection. This vector was electroporated into 129S6:B6 embryonic stem cells; after 24 h cells were selected using (1-(2-deoxy-2-fluoro-1-D-arabinofuranosyl)-5-iodouracil), puromycin and G418. Of 84 surviving clones, one correctly targeted clone was chosen for subsequent manipulation. The puromycin resistance gene was removed in vitro by electroporation of a circular CMV-Cre plasmid into the positive clone. Cells were plated at low density (2.5×10^5 to 2.0×10^4 cells/ml), and individual clones were transferred to 96-well plates. Duplicate plates were prepared, and one plate selected on puromycin. Of the 19 subclones that did not survive puromycin selection, one clone was shown to have correct targeting to remove the puromycin resistance gene by PCR. This clone was used for injection into B6(Cg)-Tyrc-2J/J blastocysts. The 8 chimeric males generated were crossed to B6(Cg)-Tyrc-Gt(ROSA)26Sor$^{tm1(FLP1)Dym}$/RainJ (The Jackson Laboratory, catalog no. 009086) to remove PGK-Neo and establish our floxed line. We then crossed the Munc18b floxed mouse with C57BL/6-Tg(Zp3-cre)93Knw/J (catalog no. 003651) to generate full animal KOs (Figure 1, B) or with CCSP^{iCre} mice for specific deletion in the airway epithelium. All our lines were crossed with C57BL/6J mice for 10 generations.

Genotypes of Munc18b mutant mice were determined by PCR of genomic DNA with primers #7 (AAGGCGGTGGTAGGGAAAGT) and #64 (CAGTTGGTCAAATTCAAGTGCTC) to differentiate between the conditional (F;

1075 bp) and WT (+; 931 bp) alleles. Munc18a and Munc18c were genotyped as previously described (*114*). The presence of Zp3-cre was determined by PCR with primers ZpCre 5' (GCGGTCTGGCAGTAAAAACTTC); ZpCre 3' (GTGAAACAGCATTGCTGTCACTT); IntControl 5' (CTAGGCCACAGAATTGAATTGAAAGATCT); IntControl 3' (GTAGGTGGAAATTCTAGCATCATCC), that give a 324 bp internal control band and a 100 bp band from the transgene. The presence of conditional $CCSP^{iCre}$ was determined by PCR with primers CC10-iCreR (GAGATGTCCTTCACTCTGATTC); CC10-iCreF (TCTGATGAAGTCAGGAAGAACC); FJD13 (TGCCAGAGATTGTTCTAGAAAACAA) and FJD14 (GGCACAATGATGTTAATGACGTAAA), that give a 1 kbp internal control band and a 0.5 kbp band from the transgene. Genotyping for the β-ENaC-Tg mice was performed as previously described (*93*).

For CreER induction, five doses of 6 mg of tamoxifen (T5648, MilliporeSigma) dissolved in corn oil (C8267, MilliporeSigma) were injected into adult mice every other day intraperitoneally (i.p.). Mice were harvested two days after the last dose. Mice of both sexes were used in all experiments, ranging from 6-32 weeks of age.

2.5.2 Immunohistochemistry

Lungs were inflated and fixed with 10% neutral buffered formalin (NBF) for 24 h at 4°C and then embedded in paraffin. Lung sections were cut into 5-μm transverse sections, deparaffinized, exposed for 10 min to 3% H_2O_2 in 90% methanol and then

heated for 10 min in 10 mM sodium citrate, pH 6.0, for antigen retrieval. Tissue sections were blocked with 5% donkey serum (017-000-121, Jackson ImmunoResearch) for 1 h at room temperature and then incubated with goat anti-CCSP (a gift from Dr. Barry Stripp, Cedars-Sinai, 1:2000) diluted in blocking solution at 4°C overnight. Secondary antibody-horseradish peroxidase (HRP)-labeled donkey anti-goat (705-035-003, Jackson ImmunoResearch, 1:500) was incubated for 1 h at room temperature. Tissue sections were then washed with PBS, dehydrated and mounted with VectaMount (Vector Laboratories).

2.5.3 In situ hybridization and immunofluorescence

In situ RNA detection was performed using the RNAscope detection kit (Advanced Cell Diagnostics, Hayward, CA) according to the manufacturer's instructions. Briefly, lungs were inflated and fixed with 10% NBF for 30 h at room temperature and then embedded in paraffin. Tissue blocks were cut into 5-μm sections, deparaffinized, and pretreated with heat and protease before hybridization with the target oligonucleotide probes: murine Munc18a (Probe-Mm-Stxbp1, 521961), Munc18b (Probe-Mm-Stxbp2, 536201) and Munc18c (Probe-Mm-Stxbp3, 536191). The positive control probe was Ppib (peptidylprolyl isomerase B, 313911) and the negative control probe was DapB (4-hydroxy-tetrahydrodipicolinate reductase from *Bacillus subtilis*, 310043). Preamplifier, amplifier and fluorescent-labeled oligonucleotides were then hybrized sequentially. RNAscope signal was imaged at the axial bronchus, between lateral branches 1 and 2 (*118*). Images were acquired using a confocal microscope

(A1plus, Nikon) with a 40× NA 1.3 objective lens. For analysis, the number of dots per secretory or ciliated cell were counted using ImageJ (*141*). Since dot intensity represents transcript amount, brighter and/or bigger dots were counted twice. More than 70% of the dots were scored as singlets. Scoring all the doublets as singlets can only result in a 4% error.

Immunofluorescence was performed using antibodies against goat CCSP (1:2000) and mouse acetylated tubulin (T6793 MilliporeSigma, 1:2000). Secondary antibodies were species-specific donkey anti-IgG coupled with Alexa Fluor 488 (A21202) and Alexa Fluor 647 (A21447) (1:1000, Invitrogen).

2.5.4 Airway epithelial mucin content by PAFS staining and image analysis

Mucous metaplasia was induced in the airways of mice by sensitizing mice to ovalbumin (OVA) (20 μg OVA Grade V, 2.25 mg alum in 0.9% saline, pH 7.4; MilliporeSigma) administered by i.p. injection once weekly, for 3 weeks. Sensitized mice were exposed for 20 min to an aerosol challenge of 2.5% (wt/vol) OVA in 0.9% saline supplemented with 0.02% (vol/vol) antifoam A silicon polymer (MilliporeSigma) daily for five days via an Aerotech II compressed gas nebulizer (Biodex, New York) in the presence of room air supplemented with 5% CO_2. Three days after the last OVA aerosol exposure, half of the mice in each group were exposed for 10 min to an aerosol of 100 mM ATP (MilliporeSigma) in 0.9% NaCl to induce mucin secretion, then sacrificed after 20 min. Lungs were harvested, inflated and fixed in 10% NBF, embedded in paraffin and sectioned into a single transverse 5 μm cut of the axial airway

of the left lung, between the lateral branches 1 and 2 (*118*). Sections were deparaffinized, rehydrated, and then stained with periodic acid fluorescent Schiff reagent (PAFS). Images were acquired using an upright microscope (Olympus BX 60) with a 40× NA 0.75 objective lens and intracellular mucin was measured around all the circumferential section of the axial bronchus using ImagePro (Media Cybernetics, Bethesda, MD). Data are presented as the epithelial mucin volume density, signifying the measured volume of mucin overlying a unit area of epithelial basal lamina, derived as described (*31*). Images were analyzed by investigators blinded to mouse genotype and treatment.

2.5.5 Agarose gel Western blot for mucin

Lungs were perfused by intracardiac injection of 2 ml PBS until blanched, then homogenized in 1 ml of 6 M guanidinium buffer containing protease inhibitors and incubated for two days at 4°C. Lysates were centrifuged at 19,000 g and the supernatants were then dialyzed overnight at 4°C against PBS in Slide-A-Lyzer 2K MWCO 3 ml cassettes (Thermo Fisher Scientific). Protein concentrations were determined using a bicinchoninic acid protein assay kit (Thermo Fisher Scientific) and then the samples were incubated with 20 Kunitz DNase (LS002139, Worthington) for 15 min at 37°C and reduced with 10 mM DTT (MilliporeSigma) for 10 min at 95°C in loading buffer (5% glycerol, 0.1% SDS, 0.0025% bromophenol blue, 0.6 M urea, 10 mM Tris-HCl, 0.5 mM EDTA, pH 8). Samples were electrophoresed through a 0.8% agarose/0.1% SDS hydrogel, and the gel was then soaked in 10 mM DTT for 20 min, then the samples were

transferred by vacuum onto a PVDF membrane. Membranes were washed in PBS and blocked with 5% nonfat milk in PBS/0.05% Tween before probing with lectin UEA-1 conjugated to HRP (1:1000, L8146, MilliporeSigma) in blocking solution to detect fucosylated Muc5ac (*118*), or with monoclonal antibody MDA-3E1 raised by us against peptide TTCQPQCQWTKWIDVDYPSS in blocking solution (1:1500) to detect Muc5b (*64*). Secondary antibody for Muc5b was goat anti-mouse conjugated to HRP (1:5000, Thermo Fisher Scientific), and the chemiluminescence signal was detected with ECL Western Blotting Substrate (Thermo Fisher Scientific). Relative protein amounts were determined for each sample using ImageJ (NIH) against a standard curve run for each gel (Figure S4).

2.5.6 Electron microscopy and stereology

Slight mucous metaplasia was induced in mice with one dose of 0.2 μg of IL-13 instilled intrapharyngeally on day 1 of the experiment in order to achieve optimal visualization of mucin granules. Mice were then anesthetized and sacrificed on day 5. Lungs were excised, fixed in 2.5% glutaraldehyde in 0.1 M sodium cacodylate buffer (pH 7.2), containing 20 mM calcium chloride for 2 h, followed by a 1 h post-fixation in buffered 1% osmium tetroxide. The fixed left lung was then sectioned into a single transverse cut of the axial airway between lateral branches 1 and 2 and embedded in Embed 812 epoxy resin (14120 EMS). Sections of 100 nm thickness were stained with uranyl acetate and lead citrate and were viewed at 8200× magnification in a Tecnai 12 transmission electron microscopy. Secretory cells were randomly selected and imaged,

and at least 19 images were used per mouse. Vv and Sv were obtained with randomly placed dot and line grids (line pairs, 64 tiles) on the cell profiles (*142*). To measure the relative electron lucency of mucin granules, a cycloid stereological grid with circles of 30 pixels in diameter was randomly superimposed on the images. At least 5 circles that fell on nuclear heterochromatin and electron-lucent extracellular space were selected, and their grayscale value (0–255) was recorded. These values were used to set a linear scale for each image. Then at least 30 random circles that fell on granules were recorded using that scale. These data were recorded and the appropriate bin range and histogram distribution was calculated.

2.5.7 Mucin transcript quantitative RT-PCR analysis

Total RNA was extracted from whole lung (RNeasy mini kit; Qiagen) and reverse-transcribed (iSCRIPT, Bio-Rad). Quantitative PCR was carried out for each cDNA sample in triplicates with qPCR master mix (Quanta Biosciences) and 6-carboxyfluorescein-labeled probes for Muc5b (Mm00466391_m1), Muc5ac (Mm01276725_g1) and β-actin (Mm02619580_g1; all from Thermo Fisher Scientific) on a ViiA 7 RT PCR System (Applied Biosystems). Results were expressed as ΔCt (normalized for β-actin) (*143*).

2.5.8 Lung lavage

This was performed by instilling and collecting 1 ml of PBS through a tracheostomy (20-gauge cannula). Total leukocyte count was determined using a

hemocytometer, and differential count by cytocentrifugation of 200 μl of lavage fluid at 300 g for 5 min. Cytospins were stained by Wright-Giemsa for microscopic morphologic cell identification and counting.

2.5.9 Mucociliary clearance

Mucociliary clearance was measured as the elimination of fluorescent microspheres from the lungs over time. Mice were anesthetized with urethane (2 mg/g, i.p.) and tracheostomized with a blunt beveled 18 gauge Luer stub adapter (Becton, Dickinson). Using a microsprayer (Penn-Century), 25 μl of PBS/0.1% Tween containing $7.43x10^4$ of 4.19 μm fluorescent microspheres (Bangs Laboratories) were loaded at the lung carina through the tracheostomy. Lungs were harvested either immediately (time 0) or mice were mechanically ventilated with a flexiVent (Scireq, Canada) to guarantee uniform ventilation. Lungs were harvested after 30 min, homogenized with 1.5 g of 1.3 mm chrome steel beads (BioSpec) and 1 ml of PBS/0.1% Tween using a Mini-Bead Beater (BioSpec) at 4800 rpm for 3 min. Fluorescent microspheres were then manually counted using a hemocytometer.

2.5.10 Total bacterial 16S rDNA qPCR

Lungs were harvested and bacterial genomic DNA was extracted and analyzed at Baylor College of Medicine by methods developed for the NIH-Human Microbiome Project (*144, 145*). Briefly, bacterial genomic DNA was extracted using a PowerSoil DNA Isolation Kit (MO BIO Laboratories, California) following the manufacturer's

instructions. Extracted DNA concentrations were measured by Qubit (Life Technologies) for subsequent normalization of quantitative PCR results (qPCR). qPCR sample analysis was performed in a 7500 Fast Real-Time PCR System. The qPCR primers (1369F-1492R) target regions flanking V9 of the 16S rRNA gene (*146*). A standard curve was made using a serially diluted plasmid that contains nucleotides 1369 to 1492 of an *E. coli* 16S rRNA gene, and concentrations of the samples were calculated from C_T values using the equation generated from plotting the standard curve. All samples were run in triplicate, including the standard curve, a set of non-template controls (NTC), and inhibitor controls (known positives + unknown DNA).

2.5.11 16S rRNA gene compositional analysis

The 16S rDNA V4 region was amplified by PCR and sequenced in the MiSeq platform (Illumina) using the 2x250 bp paired-end protocol yielding pair-end reads that overlap almost completely. The primers used for amplification contain adapters for MiSeq sequencing and dual-index barcodes so that the PCR products may be pooled and sequenced directly (*147*), targeting at least 10,000 reads per sample. The read pairs are demultiplexed based on the unique molecular barcodes, and reads are merged using USEARCH v7.0.1001 (*148*) allowing zero mismatches and a minimum overlap of 50 bases. Merged reads are trimmed at first base with Q5. In addition, a quality filter is applied to the resulting merged reads, and reads containing above 0.05 expected errors are discarded. 16S rRNA gene sequences were assigned into Operational Taxonomic Units (OTUs) or phylotypes at a similarity cutoff value of 97% using the

UPARSE algorithm. OTUs were then mapped to an optimized version of the SILVA Database (*149, 150*) containing only the 16S v4 region to determine taxonomies. Abundances were recovered by mapping the demultiplexed reads to the UPARSE OTUs.

2.5.12 Lumenal occlusion in an allergic asthma model

Airway mucus plugging was measured by modifications, as follows, of a method we have described previously (*38*). Lungs were fixed by immersion, to avoid displacement of lumenal mucus by inflation, in methanol-based Carnoy's solution (methacarn), to minimize changes in mucus volume, for 48 h at 4°C. Lungs were then excised, and the right caudal lobe (Figure 6, B and figure S6, B), or every lobe (Figure S6, A), was embedded in paraffin. For Figure S6, A and Figure S6, B, a 5 μm section was obtained every 500 μm starting from the most caudal point of the lobe. For Figure 6, B, a 5 μm section was obtained every 1 mm section of the right caudal lobe, yielding 4 sections per lung. Slides were then deparaffinized, rehydrated, and stained with PAFS. Images were acquired using an upright microscope (Olympus BX 60) with a 20× NA 0.5 lens objective. For quantification, the cross-sectional area of the lumenal mucus was traced (Figure 6, B), and the airway cross-sectional area was also traced to calculate the occlusion fraction (Figure S6, A and figure S6, B), using ImageJ (NIH).

2.5.13 Lung mechanics

Respiratory resistance was analyzed using a flexiVent system (Scireq). Mice were anaesthetized with urethane (3 mg/g by i.p. injection, a dose sufficient for 2 h of

sedation even though experiments last less than 30 min), and paralyzed with succinylcholine chloride (5 mg by i.p. injection followed by continuous i.p. infusion at 20 μg/g·min). Mice were tracheostomized with a blunt beveled 18-gauge Luer-Stub adapter and ventilated at 150 breaths/min, 10 μl/g, against 2-3 cm H_2O positive end-expiratory pressure. Respiratory resistance was assessed at baseline and in response to four incremental doses of methacholine (MCh) (1, 3, 10 and 30 mg/ml) administered by an in-line ultrasonic nebulizer (4-6 μm, Aerogen, Ireland). Total respiratory resistance was calculated by averaging eight values measured after each dose of MCh for each mouse.

2.5.14 Lumenal occlusion and emphysema in the β-ENaC-Tg model of cystic fibrosis

Lungs were fixed with 10% NBF and the left lobes were cut in transverse sections starting at the level of the hilum and then every 2 mm from rostral to caudal, yielding 2-4 slices. All slices were embedded in paraffin, and a 5 μm section was obtained from each slice. Sections were then stained with Alcian Blue-Periodic Acid Schiff (AB-PAS) (*63*). Whole lung section images were obtained in an Olympus BX61VS scanner with a BX81 stage and UPlanSApo 20× NA 0.75 objective lens; scanning conditions were kept constant among specimens. Lumenal occlusion was quantified as in Fig. 5, B from the first 2 sections of each mouse. Emphysema was measured using D_2, the equivalent mean diameter, computed from measurement of airspace area, and weighted for variance and for skewness towards large spaces (*151*), from 10 high magnification non-continuous images (1134 × 1134 pixels), equidistant

from the center of the section and excluding airways, selected from the sections used in Figure 6, B.

2.5.15 Statistics

All statistical analyses were performed using GraphPad Prism 7.0 with $P<0.05$ considered statistically significant. Exact P values and n values for each sample are included in each figure legend. Statistical analysis was performed using one-way ANOVA followed by Tukey's post hoc test for multiple pair-wise comparisons, and Student's t test or Mann-Whitney U test after determining normality of the data using D'Agostino-Pearson omnibus K2 test. A Kolmogorov-Smirnov test was used for Figure S5, D. Values that did not reach significance were not noted. After determining that the expression and secretory function of Munc18 proteins in floxed mice was equivalent to WT, the primary endpoint for studies of secretion, clearance and obstruction was of differences between airway deletant mice and their floxed littermates.

2.5.16 Study approval

All mice were kept in pathogen-free facilities and handled in accordance with the Institutional Animal Care and Use Committees of The University of Texas MD Anderson Cancer Center, The Texas A&M University Health Science Center Institute of Bioscience and Technology and The University of North Carolina.

2.5.17 Author contributions

M.J. Tuvim and B.F. Dickey conceived the study. A.M. Jaramillo performed most experiments and analyses. L. Piccotti, W. Velasco, A.S. Huerta, Z. Azzegagh, U. Nazeer, J. Farooq, J. Brenner and J. Parker-Thornburg conducted the remaining experiments. M.J. Tuvim and B.L. Scott generated the conditional Munc18b mouse. R. Adachi generated the conditional Munc18c mouse and helped with statistical and stereological analyses. C.M. Evans generated the Muc5ac knockout mouse and assisted with the analysis of mucus occlusion. S. M. Kreda and F. Chung performed the mouse crossing/breeding, the experimental procedures, and data analysis in the β-ENaC-Tg studies. A.R. Burns performed the electron microscopy. A.M. Jaramillo and B.F. Dickey wrote the manuscript. All authors contributed to discussion of the study.

2.5.18 Acknowledgments

We thank Mehmet Kesimer (UNC-CH) for advice with mucin immunoblots, David E. Ost for assistance with statistical methods, James P. Carson for facilitating use of the program for emphysema analysis, and the MD Anderson Genetically Engineered Mouse Facility (GEMF). For the β-ENaC-Tg studies, we thank the CF Center Molecular Biology Core (Dr. W O'Neal, UNC-CH) for the genotyping, Ms. C van Heusden (UNC-CH) for the BAL preparations, Ms. Kim Burns (UNC-CH) for the lung histology processing and Dr. Hong Dang for the statistical power analysis. A.M.J. thanks the members of her doctoral thesis committee, Magnus Hook, David Reiner, James McNew and Margie Moczygemba, for helpful advice. This work was supported by National

Institutes of Health grants R01HL129795, R41HL136057, NIDDK DK065988, R01HL080396, R01HL130938 and R21ES023384; by Cystic Fibrosis Foundation grants DICKEY15P0, DICKEY18G0, KREDA13G0, KREDA16XX0, and BOUCHER15R0 and by Department of Defense grant PR160247. The GEMF at MD Anderson is supported by the Cancer Center Support Grant NCI-CA016672(GEMF). B. L. Scott was supported by the MD Anderson Odyssey Fellowship Program.

CHAPTER III

OTHER WORK

During the course of my PhD, I have contributed to other projects that I will discuss briefly below.

3.1 SNAP23 is selectively expressed in airway secretory cells and mediates baseline and stimulated mucin secretion

SNAP23 is one of the family of t-SNAREs that, as we discovered, is present in airway secretory cells and is responsible for both baseline and stimulated mucin secretion (Fig. 3.1). I made a technical contribution to all aspects of the paper (*152*). This was the first project that I contributed to, and since I was new in the laboratory, it helped me learn techniques that I then used for my main project on Munc18 (Chapter II). This went from the very basic, such as to learning how to handle mice and manage a genetically modified mouse colony, to advanced techniques such as how to analyze respiratory resistance upon a methacholine challenge and how to measure mucin secretion by image analysis.

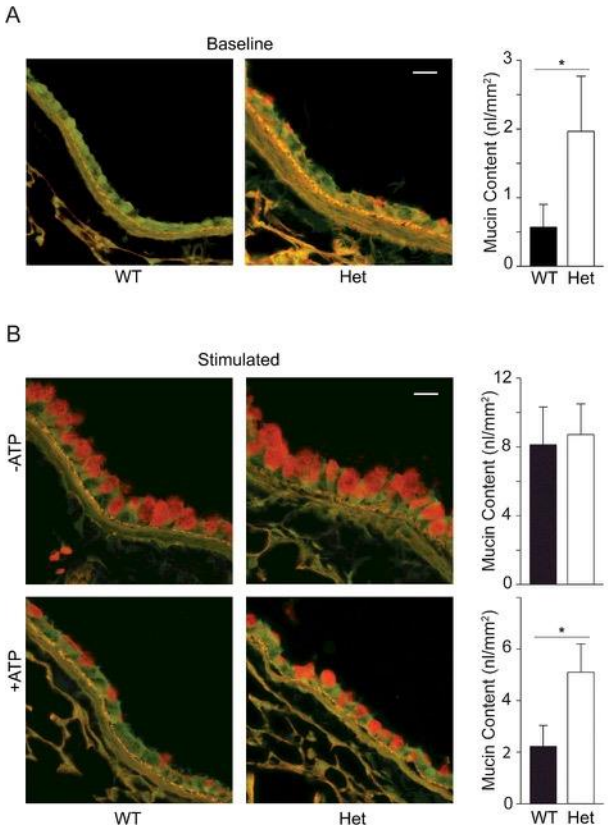

Figure 3.1. SNAP23 is responsible for baseline and stimulated mucin secretion. (A) PAFS images show spontaneous mucin accumulation in the airways of SNAP23 heterozygous mice and are quantified in the adjacent bar graph. (B) Stimulated secretion was examined by PAFS staining of airways of mice with mucous metaplasia (top row), then treated with an aerosol of ATP to induce acute mucin secretion (bottom row). Intracellular mucin content is quantified in the adjacent bar graphs. Reprinted from (*152*).

3.2 Aerosolized TLR agonists suppress acute Sendai virus lung infection and chronic asthma-like lung disease in mice

One of our laboratory side projects consists of stimulating innate immunity within the lungs to reduce the severity of a respiratory viral infection in the short term and the resulting severity of virus-induced asthma in the long term. My part in this

project started with the observation that lungs of mice infected with Sendai virus showed multiple yellow nodules on their surface 49 days after infection (long term phenotype). Histopathologic staining of the nodules showed alveolar accumulation of characteristic macrophages heavily laden with lipids leading to the hypothesis that mucus plugs were causing this accumulation, which is characteristic of chronic airway obstruction. I evaluated the post-infected lungs and indeed saw that mucus plugs were present, and that stimulating innate immunity before the viral infection reduced the presence of plugs (Fig. 3.2). The plugs were then probed with mucin antibodies which demonstrated that both Muc5ac and Muc5b were present. In addition to mucus plugging, respiratory viral infection caused mucous metaplasia in the long term, providing an explanation for the presence of plugs. The project resulted in a manuscript that is nearly ready for submission to Science Translational Medicine.

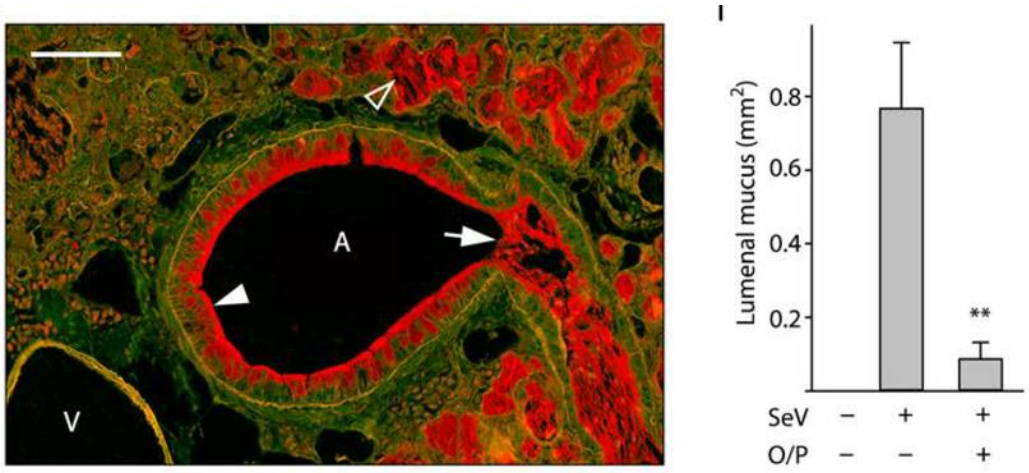

Figure 3.2. Lungs infected with Sendai virus display airway mucus occlusion. Cross-section of an infected lung stained with PAFS showing mucous metaplasia and airway mucous occlusion. Cross-sectional area of lumenal mucus was quantified and is shown in the adjacent bar graph.

3.3 Inflammation-induced upregulation of $P2X_4$ expression augments mucin secretion in airway epithelia

It is well established that ATP induces mucin secretion in the airway epithelium via metabotropic $P2Y_2$ purinoreceptors. However, the P2X family of ionotropic ATP receptors is less studied and their specific cell type expression has not been reported. Our collaborator, Manfred Frick from Ulm University, wanted to address this gap in knowledge and contacted us based on our ability to isolate airway secretory cells by fluorescence activated cell sorting (FACS). This technique, which is mentioned here for the first time in this document, has been developed over time in our laboratory. A key breakthrough was when I deciphered by immunofluorescence microscopy that the Cre we were using, $CCSP^{iCre}$, with the Cre recombinase improved for mammalian codon usage and knocked into the CCSP locus that is specific for secretory cells (*116*), was not in fact specifically expressed in airway secretory cells, but was active throughout the whole airway epithelium. This now makes sense since new studies have been published showing that ciliated cells develop from secretory club cells (*117*), so a CCSP-driven Cre recombinase must be expressed post-developmentally in order to only target secretory cells. Going back to the $P2X_4$ project, we needed to sort specifically for airway secretory cells and not ciliated cells, so we used an inducible Cre, one conjugated to a mutated estrogen receptor ($CCSP^{Cre\text{-}ER}$). This allowed for recombination in the mature adulthood epithelium only within airway secretory cells. For our cell sorting, we cross a double fluorescent reporter mouse (mT/mG) (*153*) with the mouse carrying the modified Cre necessary for our study.

The utilization of this method along with other techniques allowed Dr. Frick to demonstrate that $P2X_4$ receptors are expressed in the plasma membrane and in vesicular structures of airway secretory cells specifically distinct from mucin granules, and even upregulated under conditions of chronic inflammation that include mucous metaplasia (Fig. 3.3). $P2X_4$ receptors are ligand-gated calcium channels that are activated by extracellular ATP and allow for the increase of intracellular calcium concentrations. Activation of the receptors by extracellular ATP augments stimulated mucin secretion, whereas mucin secretion is dampened by inhibition of $P2X_4$ receptors. This work is under review as a resubmission to the American Journal of Physiology.

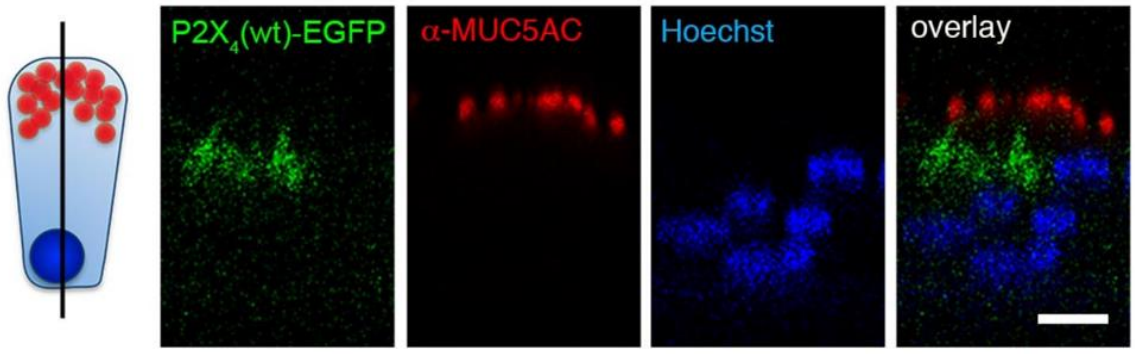

Figure 3.3. P2X4 is expressed in vesicular structures in goblet cell.
Immunofluorescence staining of human primary tracheal epithelial cells expressing wild-type $P2X_4$-EGFP (green), and stained for MUC5AC (red). Nuclei is shown in blue. Reprinted from (*154*).

3.4 Ascaris larval infection and lung invasion induces mucin production and airway mucus occlusion

Ascaris lumbricoides is the most common helminth infection globally and a cause of life-long morbidity. Our collaborator, Jill Weatherhead, from Baylor College of Medicine, was evaluating the immunological and histopathological changes during *Ascaris* infection in a mouse model. We established a collaboration to investigate the mucus response during and after the infection.

Our first question was to see if there was a mucus response and to characterize its extent. We analyzed lungs at day 8 of infection, since that is when the maximal number of worms are traversing the lungs. Mice are infected with eggs at day 0 by oral gavage, larvae hatch and penetrate the small intestine, then enter the liver through the portal system, enter the lungs via the systemic circulation, exit the lungs through the trachea, get swallowed, infect the intestinal lumen and are eliminated around day 14. By PAFS staining, we found that *Ascaris* infection induced mucous metaplasia and airway mucus occlusion, and to a similar extent as in our IL-13 allergic model (Fig. 3.4). To determine if Muc5b or Muc5ac were preferentially upregulated in this model, we probed the mucus plugs with antibodies against the two mucins. We found that both mucins were present and were being secreted into the airway lumen (Fig. 3.4).

Next, we wanted to see if studying one section of the lung, for example, the left lobe, would be a fair representation of what is happening throughout the whole lung, so other portions of the lungs could be used for other purposes in the future. In other words, we were wondering if worms preferentially migrated through the anterior or posterior

region, the right or left side, or the rostral or caudal region. We therefore examined the infected lungs rigorously through several transverse sections via PAFS staining and concluded that there was no differential mucin expression or secretion in any particular lung anatomic area other than the lung periphery, where there is a lack of mucin-producing airways. This work ended in an accepted publication in Infection and Immunity.

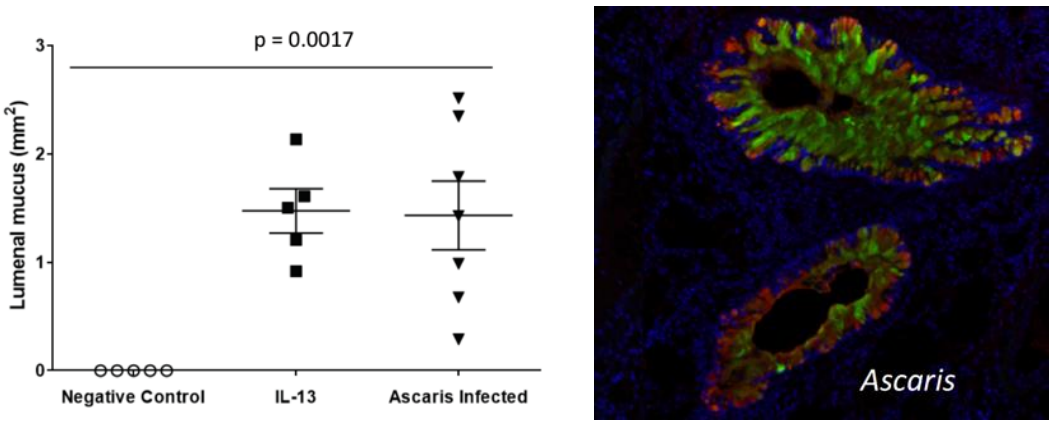

Figure 3.4. Airway mucus occlusion in lungs infected with Ascaris lumbricoides. Left: Cross-sectional area of lumenal mucus was quantified in lungs infected with Ascaris or stimulated with IL-13. Right: Immunofluorescence staining of a cross section of an airway mucus plug showing Muc5b in green and Muc5ac in red. Nuclei is shown in blue.

This project is ongoing and we are now investigating whether the trapping of helminths during migration through the lungs might be impaired by Munc18b deletion, building upon discoveries made in my main project (Chapter II).

3.5 MyD88 controls airway epithelial Muc5ac expression during TLR activation from agricultural organic dust exposure

Our collaborator, John Dickinson from the University of Nebraska, who has recently become an assistant professor, investigates how agricultural organic dust extract (ODE) induces airway inflammation and mucous metaplasia. His key endpoint was to quantify the mucus response to ODE in a MyD88 mutant mouse, since ODE is known to activate inflammation through TLR activation of MyD88. We helped him developed the techniques he needed to address his questions, such as immunofluorescence microscopy using mucin antibodies developed by our laboratory, and most importantly, Western blots for mucins using whole lung tissue which were developed in our laboratory too. Of note, prior work with mucin Western blots had generally started with extracellular mucus, such as that obtained from lung lavage fluid or cell culture supernatant. Mucins are notoriously difficult to study, since they are big proteins, heavily glycosylated and often entangled. To develop a reliable technique, I travelled to the University of North Carolina-Chapel Hill in 2017 to work with Mehmet Kesimer, a biophysicist. Building upon existing methods used in our laboratory (*118*), the key component to add to the sample is DNase to improved our electrophoretic resolution (see Methods section of Chapter II). With these techniques in hand, Dr. Dickinson found that deleting MyD88 paradoxically increases Muc5ac production after ODE exposure compared to WT mice (Fig. 3.5). He concluded that ODE is signaling mucous metaplasia through non-TLR pathways that could activate transcription factors that upregulate *Muc5ac* gene expression such as SPDEF, and that MyD88 inhibits this pathway. Thus, MyD88

promotes neutrophilic inflammation in response to ODE, but suppresses mucous metaplasia. This work is under review as a resubmission to the American Journal of Physiology.

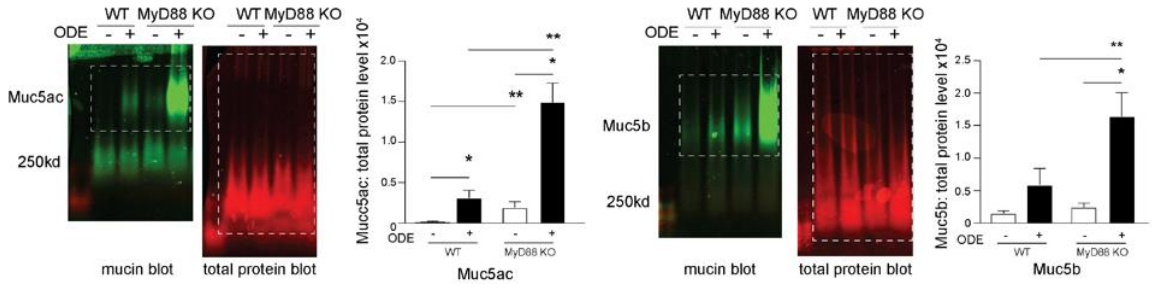

Figure 3.5. MyD88-deficient mice have increased mucin levels with ODE-mediated inflammation. Representative mucin Western blots from whole lung homogenates for Muc5ac (left) and Muc5b (right) with corresponding quantification of band densitometry. Reprinted from (*155*).

3.6 Airway mucin secretion

I wrote a review article with Dr. Dickey and other members of the laboratory that summarizes what we have learned about airway mucin secretion as a result of my studies and work by others. This article is in press in Annals of the American Thoracic Society, and some of the conclusions and future directions discussed below in Chapter IV are elaborated in this article.

CHAPTER IV

DISCUSSION AND CONCLUSIONS [1]

4.1 Discussion

After a comprehensive analysis, we have found that baseline and stimulated mucin secretion are predominantly mediated by different Munc18 proteins, with Munc18a having the major role in baseline secretion and Munc18b having the major role in stimulated secretion. Importantly, the existence of two different Munc18 proteins regulating different rates of mucin secretion allows the possibility to target the pathologic consequences of stimulated mucin secretion without impairing toxicant clearance.

Previously, when talking about mucin secretion, two mechanisms were plausible. One was that a single secretory machine was responsible for both rates of mucin secretion, baseline and stimulated, wherein a rise in intracellular calcium concentration would increase the rate of the one machine. The other possibility was the presence of two secretory machines. The project described in Chapter II unambiguously demonstrates the presence of two machines.

---

[1] Part of this chapter is reprinted with permission of the American Thoracic Society. Copyright © 2018 American Thoracic Society.
Jaramillo AM, Azzegagh Z, Tuvim MJ, Dickey BF/Airway Mucin Secretion by Annals of the American Thoracic Society is an official journal of the American Thoracic Society.

Since Munc18 proteins transport Syntaxins to the plasma membrane and hold them in a closed conformation to prevent nonspecific binding with other SNARE proteins, their interaction is specific. For example, Munc18a will bind Syntaxin-1 but Munc18b will not. This strongly suggests that different Syntaxins could mediate baseline and stimulated mucin secretion too. A recent study also found that Munc18 proteins bind to VAMPs before the complete SNARE complex is formed, docking the vesicle close to the plasma membrane and bringing the SNARE proteins together. This would then suggest that different VAMPs could mediate the different rates of mucin secretion. There is a study that shows that VAMP8 has a role in stimulated mucin secretion, but its role in baseline was not well defined (*104*). With the knowledge of the two machines that my project generated, new preliminary data in our laboratory using mutant mice suggests the presence of a different VAMP isoform in baseline secretion, VAMP3. This isoform is expressed in airway epithelial cells and has been shown to have a role in other secretory pathways, such as secretion of Weibel-Palade Bodies in endothelial cells and granule release in platelets (*156*, *157*).

A key open question is whether the baseline and stimulated mucin secretory machines interact selectively with Muc5ac, Muc5b, and other secretory products. Four possible models of interaction between the plasma membrane machines and secretory vesicles are illustrated in Figure 4.1. The first two of these are considered highly unlikely because there would be no apparent value to the existence of separate plasma membrane machines in these models (Fig. 4.1 A and B). In the third model (Fig. 4.1 C), the baseline exocytic machine is hypothesized to interact selectively with smaller

granules early in their maturation after leaving the trans-Golgi network. As the granules further mature and enlarge through lateral fusion, the baseline VAMP and Syt proteins would be removed and replaced by the stimulated machine components VAMP8 and Syt2. This model is reminiscent of the Rab conversion model that directs traffic from early to late endosomes (*135*). The possible utility of this model could be that baseline secretion of small granules would minimize the chance of airway occlusion during healthy conditions with its adverse consequences for airflow (*38*), while the stimulated secretion of large granules would maximize the chance of airway occlusion to trap migrating helminths during infection. In the fourth model (Fig. 4.1 D), the baseline exocytic machine is hypothesized to interact selectively with granules containing Muc5b, whereas the stimulated machine would interact selectively with granules containing Muc5ac. The possible utility of this model could be the selective release of Muc5b for baseline mucociliary clearance, consistent with its demonstrated functional role (*26*), and the selective explosive release of Muc5ac to trap helminths, again consistent with it demonstrated function (*36*). Muc5ac and Muc5b have been shown to occupy distinct domains in lumenal mucus (*10, 82, 139, 158*). With the help of deconvolution microscopy, preliminary data from our laboratory also show that they may be packaged in distinct granules, favoring the fourth model.

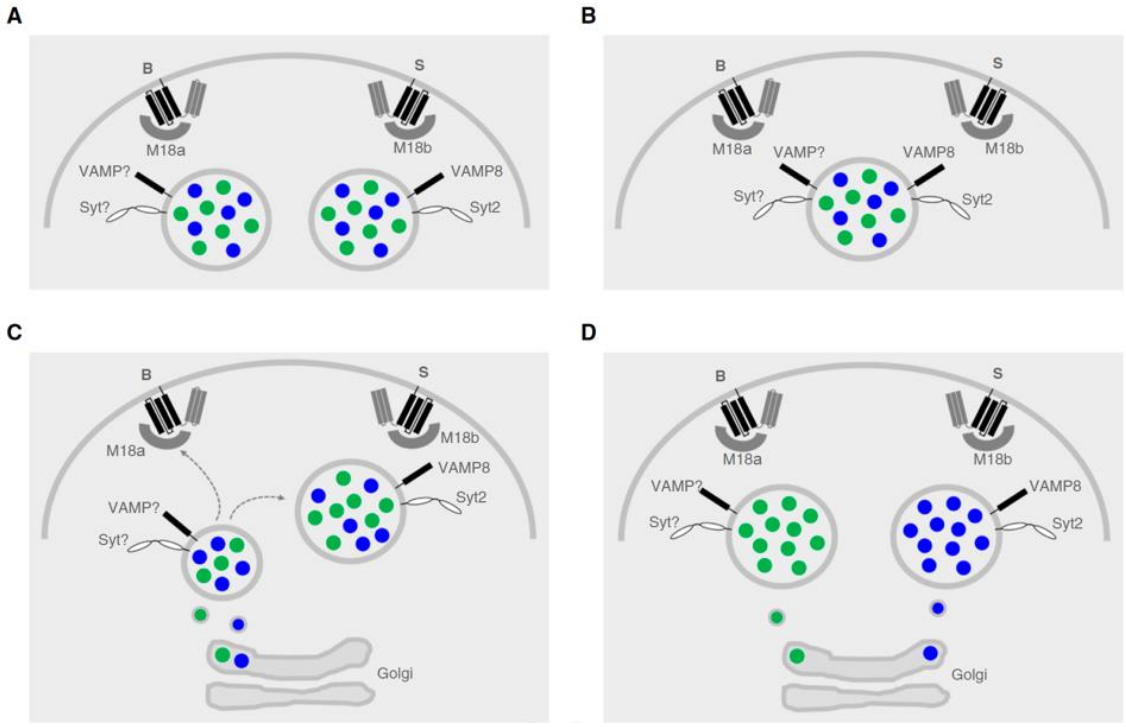

Figure 4.1. Models illustrating the possible interactions of the two regulated exocytic machines of airway secretory cells with mucin granules. In each model, B designates the baseline exocytic machine and S designates the stimulated machine. Green dots within the secretory granules designate Muc5ac, and blue dots designate Muc5b. Munc18 has been shortened to M18 to avoid clutter, and "?" is used to designate an unknown isoform of VAMP or Syt (synaptotagmin) proteins.

4.2 Conclusions

In summary, my principal work was to build upon prior studies in the Dickey laboratory to test whether or not a single core exocytic machine mediates all airway epithelial mucin secretion. My finding that two different Munc18 proteins mediate baseline and stimulated mucin secretion firmly establishes the presence of two machines. This finding is now serving as an anchor for the laboratory to identify additional components of the machines, analyze their regulation, and dissect the trafficking of

different cargo proteins. In side projects, I used my increasing expertise in mucin biochemistry and cell biology to contribute to work being done in other laboratories.

4.3 Future work

4.3.1 Identification of Syntaxins in baseline and stimulated mucin secretion

The remaining t-SNARE proteins in mucin secretion that belong to the Syntaxin family remain unknown. Identifying these proteins would be of importance as it would complete the molecular dissection of the core exocytic machinery responsible for mucin secretion. There are several hints that our previous research and research by others have provided. The first comes from the fact that there is a close and specific interaction between SM proteins and Syntaxins. This implies that, since we have two different Munc18s, one for baseline secretion and one for stimulated secretion, then there is a high probability that there are also two different Syntaxins present. The close interaction between these two proteins also provides us with clues as to which isoforms might be present, as some SM proteins have greater affinity for certain Syntaxins than others. Out of the 19 members of the Syntaxin family, we can already narrow it down to a handful of isoforms. For example, previous studies by us and others have shown that Munc18a interacts with Syntaxins 1, 2 and 3, whereas Munc18b interacts with Syntaxins 2, 3 and 11 (*65, 159-161*).

Syntaxin 11 was a particularly attractive candidate because it partners with Munc18b in cytolytic T cells and natural killer cells, as revealed by mutational analysis in familial hemophagocytic lymphohistiocytosis and confirmatory cellular studies (*160,*

162, 163). However, we have already obtained a conditional deletant mouse for Syntaxin 11 and have ruled out a role in baseline or stimulated mucin secretion. Syntaxin 3 is also an attractive candidate because it partners with Munc18b in apical secretion in other polarized epithelial systems (*122, 164-166*). We have also obtained a conditional deletant mouse for Syntaxin 3 but have not been able to study it since a complete deletion of the gene in the airway epithelium impairs mouse viability; and contrary to our Munc18b and SNAP23 mutant mice, deletion of one allele of the Syntaxin 3 gene in the airway epithelium does not provide a phenotype in either baseline or stimulated mucin secretion. Because of all these problems, the approach we are now taking is to induce recombination during adulthood using the tamoxifen-inducible CCSP-CreER construct to delete Syntaxin 3 gene from the airway epithelium. The remaining Syntaxin 3 protein left in the cell will degrade over time until levels become too low for the cell to be viable. Our plan is to study the role of Syntaxin 3 in mucin secretion just before cell death, in other words, when there is more than a 50% reduction in protein levels so as to detect a secretory phenotype but just enough for the cell to be viable. The temporal degradation of the protein would be established by Western blots of sorted secretory cells.

Assuming that Syntaxin 3 partners with Munc18b to function in stimulated mucin secretion, our leading candidate to study for baseline mucin secretion would be Syntaxin 1. Syntaxin 1 is a well studied protein and is a partner of Munc18a in neurotransmitter exocytosis. The difficulty with testing this candidate is that it is composed of two isoforms, Syntaxin 1a and 1b, and -1a complements -1b upon deletion.

Nevertheless, conditional deletants of both isoforms exist and are readily available. If Syntaxin 1 is not found to mediate baseline mucin secretion, then Syntaxin 2 is another candidate, and knockout mice are available (*167*).

4.3.2 Mucin granule identity

VAMP proteins belong to the v-SNARE group and are located in the granule membrane. The VAMP protein responsible for stimulated mucin secretion has been already identified by another group as being VAMP8 (*104*). Preliminary data from our laboratory using VAMP3 knockout mice indicates that VAMP3 is the one functioning in baseline mucin secretion. Based on our four models proposed in Figure 4.1, we also have some preliminary data that supports model 4, suggesting that Muc5b and Muc5ac are packaged in distinct granules. This leaves us the question of whether VAMP proteins are segregated into different granules too, having VAMP3 on Muc5b granules and VAMP8 on Muc5ac granules. Answers to this question should be achieved with immunofluorescence and deconvolution microscopy.

Cells may not also be exclusively selecting cargo to be sorted in different granules. The different packaging we are seeing in our preliminary results may be restricted to certain types of cells, or at least to different temporal stages of the cell after induction of mucous metaplasia by inflammatory cytokines. Moreover, upon deletion of important trafficking machinery such as VAMPs, cargo segregation may not be preserved anymore, prompting Muc5b and Muc5ac to be trafficked in the same granules. This problem then leads us to the next question, which is what happens to the cargo, i.e.

mucins, when VAMPs are deleted? Cargo sorting at the trans-Golgi network is still not well characterized for big proteins (jvb). VAMP proteins may exit the Golgi with the mucin granule but they may also be incorporated at a later stage. Thus, if VAMPs are required for cargo sorting, one problem arising upon deletion of VAMPs could be aggregation of mucins at the Golgi. What we also don't know is what other cargo is being packaged into mucin granules. Previous data from our lab suggests that CCSP partially colocalizes with mucins, but the identity of the mucin and the degree of the colocalization remains to be studied. What would happen to other cargo upon deletion of VAMPs? Is the secretory machinery important for granule biogenesis? These are several important questions that remain to be addressed and this will mainly be the focus of the laboratory for the next years.

4.3.3 Development of Munc18b as a therapeutic target

The generation of a Munc18b-targeted therapy would be of great interest as mucus dysfunction contributes to the symptoms and pathophysiology of many common diseases. There are several ways to target this protein. First, direct deletion of the gene in airway epithelium with the use of CRISPR/Cas9 (Clustered Regularly interspaced Short Palindromic Repeats/CRISPR-associated protein 9) or targeting of the transcripts using siRNAs. Gene silencing by siRNA is already in the clinic, and is being pursued in airway epithelium by several companies. The Dickey laboratory is collaborating with Arrowhead Pharmaceuticals to target Munc18b using their siRNA technology. CRISPR/Cas9 gene therapy in airway epithelium is being actively pursued for correction

of mutations in cystic fibrosis, and if this technology is developed successfully, it could be used to target Munc18b.

At the protein level, Munc18b can be targeted with the use of stapled peptides. These stapled peptides are designed to have a 3D configuration that allows them to bind a protein of interest while retaining conformation and resisting degradation. Specifically for Munc18b, a good targeting region would be its interacting pocket with Syntaxin, or the interacting region with VAMP. This would impede Munc18b-SNARE complex formation inhibiting stimulated mucin secretion. One caveat with targeting Munc18b is that it may disrupt Syntaxin localization in the plasma membrane. As we already know our secretory cells are not viable without Syntaxin 3, if Syntaxin 3 is the isoform responsible for stimulated mucin secretion, then it would be better to target other functions of Munc18b and not its Syntaxin interaction region. This strategy is being pursued by the Dickey laboratory in collaboration with Dr. Phil Jones of the MD Anderson Institute for Applied Cancer Science and Dr. Axel Brunger, a structural biologist at Stanford University.

4.3.4 Summary

Further work on molecular mechanisms of baseline and stimulated airway mucin secretion is likely to lead to new cell biological insights, and possibly to further understanding of disease mechanisms and avenues for therapeutic intervention.

REFERENCES

1. P. K. Jeffery, D. Li, Airway mucosa: secretory cells, mucus and mucin genes. *Eur Respir J* **10**, 1655-1662 (1997).
2. J. V. Fahy, B. F. Dickey, Airway mucus function and dysfunction. *N Engl J Med* **363**, 2233-2247 (2010).
3. E. L. Rawlins, L. E. Ostrowski, S. H. Randell, B. L. Hogan, Lung development and repair: contribution of the ciliated lineage. *Proc Natl Acad Sci U S A* **104**, 410-417 (2007).
4. C. L. Hattrup, S. J. Gendler, Structure and function of the cell surface (tethered) mucins. *Annu Rev Physiol* **70**, 431-457 (2008).
5. C. W. Davis, E. Lazarowski, Coupling of airway ciliary activity and mucin secretion to mechanical stresses by purinergic signaling. *Respir Physiol Neurobiol* **163**, 208-213 (2008).
6. S. F. Okada, R. A. Nicholas, S. M. Kreda, E. R. Lazarowski, R. C. Boucher, Physiological regulation of ATP release at the apical surface of human airway epithelia. *J Biol Chem* **281**, 22992-23002 (2006).
7. S. Monterisi *et al.*, CFTR regulation in human airway epithelial cells requires integrity of the actin cytoskeleton and compartmentalized cAMP and PKA activity. *J Cell Sci* **125**, 1106-1117 (2012).
8. M. C. Rose, J. A. Voynow, Respiratory tract mucin genes and mucin glycoproteins in health and disease. *Physiol Rev* **86**, 245-278 (2006).

9. J. Ma, B. K. Rubin, J. A. Voynow, Mucins, Mucus, and Goblet Cells. *Chest* **154**, 169-176 (2018).

10. M. Kesimer *et al.*, Molecular organization of the mucins and glycocalyx underlying mucus transport over mucosal surfaces of the airways. *Mucosal Immunol* **6**, 379-392 (2013).

11. J. K. Sheehan, M. Howard, P. S. Richardson, T. Longwill, D. J. Thornton, Physical characterization of a low-charge glycoform of the MUC5B mucin comprising the gel-phase of an asthmatic respiratory mucous plug. *Biochem J* **338 (Pt 2)**, 507-513 (1999).

12. J. K. Sheehan *et al.*, Physical characterization of the MUC5AC mucin: a highly oligomeric glycoprotein whether isolated from cell culture or in vivo from respiratory mucous secretions. *Biochem J* **347 Pt 1**, 37-44 (2000).

13. D. J. Thornton, K. Rousseau, M. a. McGuckin, Structure and function of the polymeric mucins in airways mucus. *Annual review of physiology* **70**, 459-486 (2008).

14. B. A. Symmes, A. L. Stefanski, C. M. Magin, C. M. Evans, Role of mucins in lung homeostasis: regulated expression and biosynthesis in health and disease. *Biochem Soc Trans* **46**, 707-719 (2018).

15. L. E. Vinall *et al.*, Variable number tandem repeat polymorphism of the mucin genes located in the complex on 11p15.5. *Hum Genet* **102**, 357-366 (1998).

16. J. Fowler, L. Vinall, D. Swallow, Polymorphism of the human muc genes. *Front Biosci* **6**, D1207-1215 (2001).

17. S. Trillo-Muyo *et al.*, Granule-stored MUC5B mucins are packed by the non-covalent formation of N-terminal head-to-head tetramers. *J Biol Chem* **293**, 5746-5754 (2018).

18. D. Ambort *et al.*, Function of the CysD domain of the gel-forming MUC2 mucin. *Biochem J* **436**, 61-70 (2011).

19. J. Perez-Vilar, S. H. Randell, R. C. Boucher, C-Mannosylation of MUC5AC and MUC5B Cys subdomains. *Glycobiology* **14**, 325-337 (2004).

20. T. A. Gerken *et al.*, Emerging paradigms for the initiation of mucin-type protein O-glycosylation by the polypeptide GalNAc transferase family of glycosyltransferases. *J Biol Chem* **286**, 14493-14507 (2011).

21. T. Kiwamoto *et al.*, Endogenous airway mucins carry glycans that bind Siglec-F and induce eosinophil apoptosis. *J Allergy Clin Immunol* **135**, 1329-1340 e1329 (2015).

22. J. M. Larsson, H. Karlsson, H. Sjovall, G. C. Hansson, A complex, but uniform O-glycosylation of the human MUC2 mucin from colonic biopsies analyzed by nanoLC/MSn. *Glycobiology* **19**, 756-766 (2009).

23. Y. Zhu *et al.*, Munc13-2-/- baseline secretion defect reveals source of oligomeric mucins in mouse airways. *J. Physiol* **586**, 1977-1992 (2008).

24. Y. Maeda *et al.*, Airway epithelial transcription factor NK2 homeobox 1 inhibits mucous cell metaplasia and Th2 inflammation. *Am J Respir Crit Care Med* **184**, 421-429 (2011).

25. N. Jonckheere *et al.*, The mouse Muc5b mucin gene is transcriptionally regulated by thyroid transcription factor-1 (TTF-1) and GATA-6 transcription factors. *FEBS J* **278**, 282-294 (2011).

26. M. G. Roy *et al.*, Muc5b is required for airway defence. *Nature* **505**, 412-416 (2014).

27. B. R. Grubb *et al.*, Reduced mucociliary clearance in old mice is associated with a decrease in Muc5b mucin. *Am J Physiol Lung Cell Mol Physiol* **310**, L860-867 (2016).

28. M. A. Seibold *et al.*, A common MUC5B promoter polymorphism and pulmonary fibrosis. *N Engl J Med* **364**, 1503-1512 (2011).

29. F. B. Piel *et al.*, Global distribution of the sickle cell gene and geographical confirmation of the malaria hypothesis. *Nat Commun* **1**, 104 (2010).

30. B. F. Dickey, J. A. Whitsett, Understanding Interstitial Lung Disease: It's in the Mucus. *Am J Respir Cell Mol Biol* **57**, 12-14 (2017).

31. C. M. Evans *et al.*, Mucin is produced by clara cells in the proximal airways of antigen-challenged mice. *American Journal of Respiratory Cell and Molecular Biology* **31**, 382-394 (2004).

32. K. S. Song *et al.*, Interleukin-1 beta and tumor necrosis factor-alpha induce MUC5AC overexpression through a mechanism involving ERK/p38 mitogen-activated protein kinases-MSK1-CREB activation in human airway epithelial cells. *J Biol Chem* **278**, 23243-23250 (2003).

33. K. Takeyama *et al.*, Epidermal growth factor system regulates mucin production in airways. *Proc Natl Acad Sci U S A* **96**, 3081-3086 (1999).

34. S. W. Park *et al.*, Distinct roles of FOXA2 and FOXA3 in allergic airway disease and asthma. *Am J Respir Crit Care Med* **180**, 603-610 (2009).

35. K. S. Park *et al.*, SPDEF regulates goblet cell hyperplasia in the airway epithelium. *J Clin Invest* **117**, 978-988 (2007).

36. S. Z. Hasnain *et al.*, Muc5ac: a critical component mediating the rejection of enteric nematodes. *J Exp Med* **208**, 893-900 (2011).

37. B. F. Dickey, Exoskeletons and exhalation. *N.Engl.J.Med.* **357**, 2082-2084 (2007).

38. C. M. Evans *et al.*, The polymeric mucin Muc5ac is required for allergic airway hyperreactivity. *Nat Commun* **6**, 6281-6281 (2015).

39. C. W. Davis, M. L. Dowell, M. Lethem, M. Van Scott, Goblet cell degranulation in isolated canine tracheal epithelium: response to exogenous ATP, ADP, and adenosine. *The American journal of physiology* **262**, C1313-1323 (1992).

40. M. I. Lethem *et al.*, Nucleotide regulation of goblet cells in human airway epithelial explants: normal exocytosis in cystic fibrosis. *Am J Respir Cell Mol Biol* **9**, 315-322 (1993).

41. P. Verdugo, Supramolecular dynamics of mucus. *Cold Spring Harb. Perspect. Med* **2**, a009597 (2012).

42. J. B. Pereira-Leal, M. C. Seabra, The mammalian Rab family of small GTPases: definition of family and subfamily sequence motifs suggests a mechanism for functional specificity in the Ras superfamily. *J Mol Biol* **301**, 1077-1087 (2000).

43. A. Echard *et al.*, Interaction of a Golgi-associated kinesin-like protein with Rab6. *Science* **279**, 580-585 (1998).

44. J. R. Whyte, S. Munro, Vesicle tethering complexes in membrane traffic. *J Cell Sci* **115**, 2627-2637 (2002).

45. A. K. Gillingham, S. Munro, Long coiled-coil proteins and membrane traffic. *Biochim Biophys Acta* **1641**, 71-85 (2003).

46. T. Voets *et al.*, Munc18-1 promotes large dense-core vesicle docking. *Neuron* **31**, 581-591 (2001).

47. M. Zerial, H. McBride, Rab proteins as membrane organizers. *Nat Rev Mol Cell Biol* **2**, 107-117 (2001).

48. J. Rizo, C. Rosenmund, Synaptic vesicle fusion. *Nature Structural & Molecular Biology* **15**, 665-674 (2008).

49. T. C. Sudhof, J. E. Rothman, Membrane fusion: grappling with SNARE and SM proteins. *Science* **323**, 474-477 (2009).

50. T. Weber *et al.*, SNAREpins: minimal machinery for membrane fusion. *Cell* **92**, 759-772 (1998).

51. F. Parlati *et al.*, Rapid and efficient fusion of phospholipid vesicles by the alpha-helical core of a SNARE complex in the absence of an N-terminal regulatory domain. *Proc Natl Acad Sci U S A* **96**, 12565-12570 (1999).

52. J. A. McNew *et al.*, Compartmental specificity of cellular membrane fusion encoded in SNARE proteins. *Nature* **407**, 153-159 (2000).

53. Y. Hata, C. A. Slaughter, T. C. Sudhof, Synaptic vesicle fusion complex contains unc-18 homologue bound to syntaxin. *Nature* **366**, 347-351 (1993).

54. C. Rickman, R. R. Duncan, Munc18/Syntaxin interaction kinetics control secretory vesicle dynamics. *J Biol Chem* **285**, 3965-3972 (2010).

55. K. M. Misura, R. H. Scheller, W. I. Weis, Three-dimensional structure of the neuronal-Sec1-syntaxin 1a complex. *Nature* **404**, 355-362 (2000).

56. R. W. Baker *et al.*, A direct role for the Sec1/Munc18-family protein Vps33 as a template for SNARE assembly. *Science* **349**, 1111-1114 (2015).

57. S. Brenner, The genetics of Caenorhabditis elegans. *Genetics* **77**, 71-94 (1974).

58. P. Novick, C. Field, R. Schekman, Identification of 23 complementation groups required for post-translational events in the yeast secretory pathway. *Cell* **21**, 205-215 (1980).

59. S. D. Harrison, K. Broadie, J. van de Goor, G. M. Rubin, Mutations in the Drosophila Rop gene suggest a function in general secretion and synaptic transmission. *Neuron* **13**, 555-566 (1994).

60. M. Verhage *et al.*, Synaptic assembly of the brain in the absence of neurotransmitter secretion. *Science (New York, N.Y.)* **287**, 864-869 (2000).

61. L. Ma *et al.*, Munc18-1-regulated stage-wise SNARE assembly underlying synaptic exocytosis. *Elife* **4**, (2015).

62. A. T. Brunger, U. B. Choi, Y. Lai, J. Leitz, Q. Zhou, Molecular Mechanisms of Fast Neurotransmitter Release. *Annu Rev Biophys* **47**, 469-497 (2018).

63. L. C. Jones *et al.*, VAMP8 is a vesicle SNARE that regulates mucin secretion in airway goblet cells. *J. Physiol* **590**, 545-562 (2012).

64. B. Ren *et al.*, SNAP23 is selectively expressed in airway secretory cells and mediates baseline and stimulated mucin secretion. *Biosci Rep* **35**, (2015).

65. K. Kim *et al.*, Munc18b is an essential gene in mice whose expression is limiting for secretion by airway epithelial and mast cells. *Biochem J* **446**, 383-394 (2012).

66. M. J. Tuvim *et al.*, Synaptotagmin 2 couples mucin granule exocytosis to Ca2+ signaling from endoplasmic reticulum. *Journal of Biological Chemistry* **284**, 9781-9787 (2009).

67. B. N. Lambrecht, H. Hammad, The immunology of asthma. *Nature Immunology* **16**, 45-56 (2014).

68. D. J. Erle, D. Sheppard, The cell biology of asthma. *J Cell Biol* **205**, 621-631 (2014).

69. Q. Sha, A. Q. Truong-Tran, J. R. Plitt, L. A. Beck, R. P. Schleimer, Activation of airway epithelial cells by toll-like receptor agonists. *American Journal of Respiratory Cell and Molecular Biology* **31**, 358-364 (2004).

70. B. N. Lambrecht, H. Hammad. (2009), vol. 31, pp. 412-424.

71. P. G. Woodruff *et al.*, T-helper type 2-driven inflammation defines major subphenotypes of asthma. *Am J Respir Crit Care Med* **180**, 388-395 (2009).

72. B. N. Lambrecht, H. Hammad, The airway epithelium in asthma. *Nature Medicine* **18**, 684-692 (2012).

73. C. N. McBrien, A. Menzies-Gow, The Biology of Eosinophils and Their Role in Asthma. *Front Med (Lausanne)* **4**, 93 (2017).

74. H. Hammad *et al.*, House dust mite allergen induces asthma via Toll-like receptor 4 triggering of airway structural cells. *Nature medicine* **15**, 410-416 (2009).

75. J. a. Walker, J. L. Barlow, A. N. J. McKenzie, Innate lymphoid cells--how did we miss them? *Nature reviews. Immunology* **13**, 75-87 (2013).

76. R. G. J. K. Wolterink *et al.*, Pulmonary innate lymphoid cells are major producers of IL-5 and IL-13 in murine models of allergic asthma. *European Journal of Immunology* **42**, 1106-1116 (2012).

77. J. W. Messer, G. A. Peters, W. A. Bennett, Causes of death and pathologic findings in 304 cases of bronchial asthma. *Dis Chest* **38**, 616-624 (1960).

78. K. Takeyama, J. V. Fahy, J. A. Nadel, Relationship of epidermal growth factor receptors to goblet cell production in human bronchi. *Am J Respir Crit Care Med* **163**, 511-516 (2001).

79. <2015 Fishmans_ch06.pdf>.

80. K. G. Welsh *et al.*, MUC5AC and a Glycosylated Variant of MUC5B Alter Mucin Composition in Children With Acute Asthma. *Chest* **152**, 771-779 (2017).

81. A. L. Innes *et al.*, Ex vivo sputum analysis reveals impairment of protease-dependent mucus degradation by plasma proteins in acute asthma. *Am J Respir Crit Care Med* **180**, 203-210 (2009).

82. L. R. Bonser, L. Zlock, W. Finkbeiner, D. J. Erle, Epithelial tethering of MUC5AC-rich mucus impairs mucociliary transport in asthma. *J Clin Invest* **126**, 2367-2371 (2016).

83. V. J. Thanawala *et al.*, beta2-Adrenoceptor agonists are required for development of the asthma phenotype in a murine model. *Am J Respir Cell Mol Biol* **48**, 220-229 (2013).

84. M. E. Lachowicz-Scroggins *et al.*, Corticosteroid and long-acting ss-agonist therapy reduces epithelial goblet cell metaplasia. *Clin Exp Allergy* **47**, 1534-1545 (2017).

85. L. P. Nguyen *et al.*, Chronic exposure to beta-blockers attenuates inflammation and mucin content in a murine asthma model. *Am J Respir Cell Mol Biol* **38**, 256-262 (2008).

86. C. H. Fanta, Asthma. *The New England Journal of Medicine* **350**, 1002-1014 (2009).

87. E. Daviskas *et al.*, Inhalation of hypertonic saline aerosol enhances mucociliary clearance in asthmatic and healthy subjects. *Eur Respir J* **9**, 725-732 (1996).

88. M. R. Kosorok, W. H. Wei, P. M. Farrell, The incidence of cystic fibrosis. *Stat Med* **15**, 449-462 (1996).

89. R. J. Gregory *et al.*, Expression and characterization of the cystic fibrosis transmembrane conductance regulator. *Nature* **347**, 382-386 (1990).

90. R. C. Boucher, Cystic fibrosis: a disease of vulnerability to airway surface dehydration. *Trends Mol Med* **13**, 231-240 (2007).

91. C. Ferec, G. R. Cutting, Assessing the Disease-Liability of Mutations in CFTR. *Cold Spring Harb Perspect Med* **2**, a009480 (2012).

92. V. Kumar, A. K. Abbas, J. C. Aster, *Robbins and Cotran pathologic basis of disease*. (Elsevier/Saunders, Philadelphia, PA, ed. Ninth edition., 2015), pp. xvi, 1391 pages.

93. M. Mall, B. R. Grubb, J. R. Harkema, W. K. O'Neal, R. C. Boucher, Increased airway epithelial Na+ absorption produces cystic fibrosis-like lung disease in mice. *Nat Med* **10**, 487-493 (2004).

94. A. Livraghi-Butrico *et al.*, Mucus clearance, MyD88-dependent and MyD88-independent immunity modulate lung susceptibility to spontaneous bacterial infection and inflammation. *Mucosal Immunol* **5**, 397-408 (2012).

95. P. M. Quinton, Role of epithelial $HCO3^-$ transport in mucin secretion: lessons from cystic fibrosis. *American journal of physiology. Cell physiology* **299**, C1222-1233 (2010).

96. M. O. Henke, G. John, M. Germann, H. Lindemann, B. K. Rubin, MUC5AC and MUC5B mucins increase in cystic fibrosis airway secretions during pulmonary exacerbation. *Am J Respir Crit Care Med* **175**, 816-821 (2007).

97. P. R. Burgel, D. Montani, C. Danel, D. J. Dusser, J. A. Nadel, A morphometric study of mucins and small airway plugging in cystic fibrosis. *Thorax* **62**, 153-161 (2007).

98. A. Livraghi-Butrico *et al.*, Contribution of mucus concentration and secreted mucins Muc5ac and Muc5b to the pathogenesis of muco-obstructive lung disease. *Mucosal Immunol* **10**, 395-407 (2017).

99. C. E. Wainwright, Ivacaftor for patients with cystic fibrosis. *Expert Rev Respir Med* **8**, 533-538 (2014).

100. F. J. Accurso *et al.*, Effect of VX-770 in persons with cystic fibrosis and the G551D-CFTR mutation. *N Engl J Med* **363**, 1991-2003 (2010).

101. A. Rehman, N. U. Baloch, I. A. Janahi, Lumacaftor-Ivacaftor in Patients with Cystic Fibrosis Homozygous for Phe508del CFTR. *N Engl J Med* **373**, 1783 (2015).

102. H. J. Fuchs *et al.*, Effect of aerosolized recombinant human DNase on exacerbations of respiratory symptoms and on pulmonary function in patients with cystic fibrosis. The Pulmozyme Study Group. *N Engl J Med* **331**, 637-642 (1994).

103. M. R. Elkins *et al.*, A controlled trial of long-term inhaled hypertonic saline in patients with cystic fibrosis. *N Engl J Med* **354**, 229-240 (2006).

104. L. C. Jones *et al.*, VAMP8 is a vesicle SNARE that regulates mucin secretion in airway goblet cells. *J Physiol* **5903**, 545-561 (2012).

105. C. M. Evans *et al.*, Idiopathic Pulmonary Fibrosis: A Genetic Disease That Involves Mucociliary Dysfunction of the Peripheral Airways. *Physiol Rev* **96**, 1567-1591 (2016).

106. H. W. Young *et al.*, Central role of Muc5ac expression in mucous metaplasia and its regulation by conserved 5' elements. *Am.J.Respir.Cell Mol.Biol.* **37**, 273-290 (2007).

107. G. Zhen *et al.*, IL-13 and epidermal growth factor receptor have critical but distinct roles in epithelial cell mucin production. *Am.J.Respir.Cell Mol.Biol.* **36**, 244-253 (2007).

108. C. W. Davis, B. F. Dickey, Regulated airway goblet cell mucin secretion. *Annu.Rev.Physiol* **70**, 487-512 (2008).

109. Y. Zhu *et al.*, Baseline Goblet Cell Mucin Secretion in the Airways Exceeds Stimulated Secretion over Extended Time Periods, and Is Sensitive to Shear Stress and Intracellular Mucin Stores. *PLoS One* **10**, e0127267-e0127267 (2015).

110. B. Button, S. F. Okada, C. B. Frederick, W. R. Thelin, R. C. Boucher, Mechanosensitive ATP release maintains proper mucus hydration of airways. *Sci Signal* **6**, ra46 (2013).

111. H. W. Young, C. X. Sun, C. M. Evans, B. F. Dickey, M. R. Blackburn, A3 adenosine receptor signaling contributes to airway mucin secretion after allergen challenge. *Am J Respir Cell Mol Biol* **35**, 549-558 (2006).

112. J. Rizo, J. Xu, The Synaptic Vesicle Release Machinery. *Annu Rev Biophys* **44**, 339-367 (2015).

113. E. Oh, B. A. Spurlin, J. E. Pessin, D. C. Thurmond, Munc18c heterozygous knockout mice display increased susceptibility for severe glucose intolerance. *Diabetes* **54**, 638-647 (2005).

114. B. A. Gutierrez *et al.*, Munc18-2, but not Munc18-1 or Munc18-3, controls compound and single-vesicle-regulated exocytosis in mast cells. *J Biol Chem* **293**, 7148-7159 (2018).

115. J. H. Heeroma *et al.*, Trophic support delays but does not prevent cell-intrinsic degeneration of neurons deficient for munc18-1. *Eur J Neurosci* **20**, 623-634 (2004).

116. J. Liu *et al.*, ErbB2 Pathway Activation upon Smad4 Loss Promotes Lung Tumor Growth and Metastasis. *Cell Rep*, (2015).

117. E. L. Rawlins *et al.*, The role of Scgb1a1+ Clara cells in the long-term maintenance and repair of lung airway, but not alveolar, epithelium. *Cell Stem Cell* **4**, 525-534 (2009).

118. L. Piccotti, B. F. Dickey, C. M. Evans, Assessment of intracellular Mucin content in vivo. *Methods in Molecular Biology* **842**, 279-295 (2012).

119. D. A. Stoltz, D. K. Meyerholz, M. J. Welsh, Origins of cystic fibrosis lung disease. *N Engl J Med* **372**, 351-362 (2015).

120. A. G. Henderson *et al.*, Cystic fibrosis airway secretions exhibit mucin hyperconcentration and increased osmotic pressure. *J Clin Invest* **124**, 3047-3060 (2014).

121. S. M. Kreda, C. W. Davis, M. C. Rose, CFTR, mucins, and mucus obstruction in cystic fibrosis. *Cold Spring Harb Perspect Med* **2**, a009589 (2012).

122. K. Riento, M. Kauppi, S. Keranen, V. M. Olkkonen, Munc18-2, a functional partner of syntaxin 3, controls apical membrane trafficking in epithelial cells. *J Biol Chem* **275**, 13476-13483 (2000).

123. G. F. Vogel *et al.*, Cargo-selective apical exocytosis in epithelial cells is conducted by Myo5B, Slp4a, Vamp7, and Syntaxin 3. *J Cell Biol* **211**, 587-604 (2015).

124. I. Dulubova *et al.*, Munc18-1 binds directly to the neuronal SNARE complex. *Proc Natl Acad Sci U S A* **104**, 2697-2702 (2007).

125. F. Deak *et al.*, Munc18-1 binding to the neuronal SNARE complex controls synaptic vesicle priming. *J Cell Biol* **184**, 751-764 (2009).

126. D. van Breevoort *et al.*, STXBP1 promotes Weibel-Palade body exocytosis through its interaction with the Rab27A effector Slp4-a. *Blood* **123**, 3185-3194 (2014).

127. F. Rodriguez, M. N. Zanetti, L. S. Mayorga, C. N. Tomes, Munc18-1 controls SNARE protein complex assembly during human sperm acrosomal exocytosis. *J Biol Chem* **287**, 43825-43839 (2012).

128. A. P. Naren *et al.*, Regulation of CFTR chloride channels by syntaxin and Munc18 isoforms. *Nature* **390**, 302-305 (1997).

129. P. P. Lam *et al.*, Munc18b is a major mediator of insulin exocytosis in rat pancreatic beta-cells. *Diabetes* **62**, 2416-2428 (2013).

130. E. Oh, M. A. Kalwat, M. J. Kim, M. Verhage, D. C. Thurmond, Munc18-1 regulates first-phase insulin release by promoting granule docking to multiple syntaxin isoforms. *J Biol Chem* **287**, 25821-25833 (2012).

131. J. A. Lopez *et al.*, Bi-Allelic Mutations in STXBP2 Reveal a Complementary Role for STXBP1 in Cytotoxic Lymphocyte Killing. *Front Immunol* **9**, 529 (2018).

132. J. Torres, H. M. Funk, M. M. Zegers, M. B. ter Beest, The syntaxin 4 N terminus regulates its basolateral targeting by munc18c-dependent and -independent mechanisms. *J Biol Chem* **286**, 10834-10846 (2011).

133. S. Dolai *et al.*, Depletion of the membrane-fusion regulator Munc18c attenuates caerulein hyperstimulation-induced pancreatitis. *J Biol Chem* **293**, 2510-2522 (2018).

134. D. C. Thurmond, M. Kanzaki, A. H. Khan, J. E. Pessin, Munc18c function is required for insulin-stimulated plasma membrane fusion of GLUT4 and insulin-responsive amino peptidase storage vesicles. *Mol Cell Biol* **20**, 379-388 (2000).

135. J. Rink, E. Ghigo, Y. Kalaidzidis, M. Zerial, Rab conversion as a mechanism of progression from early to late endosomes. *Cell* **122**, 735-749 (2005).

136. M. Pakdel, J. von Blume, Exploring new routes for secretory protein export from the trans-Golgi network. *Mol Biol Cell* **29**, 235-240 (2018).

137. D. Shumilov *et al.*, Real-time imaging of exocytotic mucin release and swelling in Calu-3 cells using acridine orange. *Methods* **66**, 312-324 (2014).

138. A. Ermund *et al.*, The normal trachea is cleaned by MUC5B mucin bundles from the submucosal glands coated with the MUC5AC mucin. *Biochem Biophys Res Commun* **492**, 331-337 (2017).

139. L. S. Ostedgaard *et al.*, Gel-forming mucins form distinct morphologic structures in airways. *Proc Natl Acad Sci U S A* **114**, 6842-6847 (2017).

140. S. Y. Graeber *et al.*, Hypertonic saline is effective in the prevention and treatment of mucus obstruction, but not airway inflammation, in mice with chronic obstructive lung disease. *Am J Respir Cell Mol Biol* **49**, 410-417 (2013).

141. L. Silberstein *et al.*, Proximity-Based Differential Single-Cell Analysis of the Niche to Identify Stem/Progenitor Cell Regulators. *Cell Stem Cell* **19**, 530-543 (2016).

142. S. A. Tschanz, P. H. Burri, E. R. Weibel, A simple tool for stereological assessment of digital images: the STEPanizer. *J Microsc* **243**, 47-59 (2011).

143. T. D. Schmittgen, K. J. Livak, Analyzing real-time PCR data by the comparative C(T) method. *Nat Protoc* **3**, 1101-1108 (2008).

144. C. Human Microbiome Project, Structure, function and diversity of the healthy human microbiome. *Nature* **486**, 207-214 (2012).

145. C. Human Microbiome Project, A framework for human microbiome research. *Nature* **486**, 215-221 (2012).

146. M. T. Suzuki, L. T. Taylor, E. F. DeLong, Quantitative analysis of small-subunit rRNA genes in mixed microbial populations via 5'-nuclease assays. *Appl Environ Microbiol* **66**, 4605-4614 (2000).

147. J. G. Caporaso *et al.*, Ultra-high-throughput microbial community analysis on the Illumina HiSeq and MiSeq platforms. *ISME J* **6**, 1621-1624 (2012).

148. R. C. Edgar, Search and clustering orders of magnitude faster than BLAST. *Bioinformatics* **26**, 2460-2461 (2010).

149. R. C. Edgar, UPARSE: highly accurate OTU sequences from microbial amplicon reads. *Nat Methods* **10**, 996-998 (2013).

150. C. Quast *et al.*, The SILVA ribosomal RNA gene database project: improved data processing and web-based tools. *Nucleic Acids Res* **41**, D590-596 (2013).

151. R. E. Jacob *et al.*, Comparison of two quantitative methods of discerning airspace enlargement in smoke-exposed mice. *PLoS One* **4**, e6670 (2009).

152. B. Ren *et al.*, SNAP23 Is Selectively Expressed in Airway Secretory Cells and Mediates Baseline and Stimulated Mucin Secretion. *Bioscience Reports*, (2015).

153. M. D. Muzumdar, B. Tasic, K. Miyamichi, N. Li, L. Luo, A global double-fluorescent cre reporter mouse. *Genesis* **45**, 593-605 (2007).

154. V. E. Winkelmann *et al.*, Inflammation-induced upregulation of P2X4 expression augments mucin secretion in airway epithelia. *Am J Physiol Lung Cell Mol Physiol*, (2018).

155. J. D. Dickinson *et al.*, MyD88 controls airway epithelial Muc5ac expression during TLR activation conditions from agricultural organic dust exposure. *Am J Physiol Lung Cell Mol Physiol*, (2018).

156. S. Joshi *et al.*, Alterations in platelet secretion differentially affect thrombosis and hemostasis. *Blood Adv* **2**, 2187-2198 (2018).

157. I. R. Pulido, R. Jahn, V. Gerke, VAMP3 is associated with endothelial weibel-palade bodies and participates in their Ca(2+)-dependent exocytosis. *Biochim Biophys Acta* **1813**, 1038-1044 (2011).

158. M. E. Lachowicz-Scroggins *et al.*, Abnormalities in MUC5AC and MUC5B Protein in Airway Mucus in Asthma. *Am J Respir Crit Care Med* **194**, 1296-1299 (2016).

159. A. Rehman *et al.*, Reconciling the regulatory role of Munc18 proteins in SNARE-complex assembly. *IUCrJ* **1**, 505-513 (2014).

160. W. A. Spessott, M. L. Sanmillan, M. E. McCormick, V. V. Kulkarni, C. G. Giraudo, SM protein Munc18-2 facilitates transition of Syntaxin 11-mediated lipid mixing to complete fusion for T-lymphocyte cytotoxicity. *Proc Natl Acad Sci U S A* **114**, E2176-E2185 (2017).

161. R. F. Toonen, M. Verhage, Vesicle trafficking: pleasure and pain from SM genes. *Trends Cell Biol* **13**, 177-186 (2003).

162. E. Sieni *et al.*, Familial hemophagocytic lymphohistiocytosis: a model for understanding the human machinery of cellular cytotoxicity. *Cell Mol Life Sci* **69**, 29-40 (2012).

163. Y. Hackmann *et al.*, Syntaxin binding mechanism and disease-causing mutations in Munc18-2. *Proc Natl Acad Sci U S A* **110**, E4482-4491 (2013).

164. N. Sharma, S. H. Low, S. Misra, B. Pallavi, T. Weimbs, Apical targeting of syntaxin 3 is essential for epithelial cell polarity. *J Cell Biol* **173**, 937-948 (2006).

165. K. Riento *et al.*, Interaction of Munc-18-2 with syntaxin 3 controls the association of apical SNAREs in epithelial cells. *J Cell Sci* **111 (Pt 17)**, 2681-2688 (1998).

166. Y. Liu *et al.,* A mechanism of Munc18b-syntaxin 3-SNAP25 complex assembly in regulated epithelial secretion. *FEBS Lett* **581**, 4318-4324 (2007).

167. Y. Wang *et al.*, Epimorphin(-/-) mice have increased intestinal growth, decreased susceptibility to dextran sodium sulfate colitis, and impaired spermatogenesis. *J Clin Invest* **116**, 1535-1546 (2006).